Protein Interactions with Lipid Model Membranes

Xin Huang

B.E. in Applied Electrochemistry, 1986

M.E. in Environmental Chemistry, 1989

Shanghai Jiao Tong University, Shanghai, China

A thesis submitted to the faculty
of the Oregon Graduate Institute of Science & Technology
in partial fulfillment of the requirements for
Master of Science
in
Physical Chemistry

July, 1992

The thesis "Protein Interactions with Lipid Model Membranes" by Xin Huang has been examined and approved by the following Examination Committee:

David W. Grainger
Assistant Professor
Thesis Advisor

Joann Sanders-Loehr
Professor

David H. Thompson
Assistant Professor

Dedication

To my parents,

for their encouragement and care

To my husband,

for his support and help

Acknowledgements

I am deeply indebted to Dr. David W. Grainger, my advisor, for his guidance and instruction, for his patience and understanding throughout the course of this work. Without his broad knowledge in this and related fields and his helpful suggestions, I would have not been able to complete my thesis work successfully.

I gratefully acknowledge financial support from the Medical Research Foundation of Oregon and from the U.S. Department of Energy, Office of Basic Energy Sciences.
I owe my thanks to my thesis committee members, Dr. Joann Sanders-Loehr and Dr. David H. Thompson, for their time spent reviewing this document and for their helpful comments. I would like to thank Dr. Shankar B. Rananavare for his instructions in the X-ray experiments I performed and his helpful comments in the data analyses, Dr. Vlado Hlady at the University of Utah for his experimental assistance while I was conducting TIRF protein adsorption experiments, and Dr. Yabin Lei, Dr. Valerie Anderson and Dr. Jong-Mok Kim for their useful discussions and help with my work. I wish to express my thanks to the students, staff and faculty in both the Membrane Group and in Department of Chemical and Biological Sciences for their support during my two-year thesis work, especially Nancy Christie and Jennifer Peterson. Finally, I deeply thank to Lorin L. Ye, my husband, for his special support and understanding.

Table of Contents

Abstract

Myelin basic protein C-1 charge isomer, the most cationic component of myelin basic protein, is indicated to have a specific role in organizing lipids and stabilizing multilayer membrane lamellae in the myelin sheath. Monolayer hysteresis studies show that it can interact both with zwitterionic (DMPC) and anionic (DMPA, DHP and GM1) lipids, indicating that both hydrophobic and electrostatic interactions exist. Poly-l-lysine, a commonly used model for cationic extrinsic proteins, can only interact with negatively charged lipids, DMPA, DHP and GM1. Monolayer hysteresis and small-angle X-ray scattering show no detectable interaction of the cationic polypeptides with the zwitterionic lipid, DMPC. Ionic strength dependency of interaction indicates the influence of intermolecular hydrogen bonding in the lipid head group region between polypeptide and lipid. Both "salting-out" and double layer screening effects of the salt compete with each other in the interaction mechanism. Additionally, a new technique-Total Internal Reflection Fluorescence (TIRF) is used to probe model lipid membrane-protein interactions at surfaces. Adsorption and desorption kinetics of the serum albumin are investigated on supported bilayers of acidic and zwitterionic lipids.

Chapter 1

Introduction

1.1 The Myelin Sheath

The myelin sheath exists in both the central and peripheral nervous systems as a multilayer membrane structure surrounding nerve cell axons. Schwann cells create the sheath by actively wrapping layer upon layer of their own plasma membrane into a tight spiral around each axon. Fig. 1.1 shows how an axon becomes myelinated [1]. During neural development, Schwann cells first envelop the axon. These cells then grow in a spiral fashion, wrapping many layers around the axon. As shown in Table 1.1 [2], these membranes are unusually low in protein and high in lipid contents, allowing them to act as excellent insulators. Schwann cells are spaced regularly along the axon but are separated by the nodes of Ranvier -- the only points in a myelinated axon at which exchange of ions with the surrounding environment can occur.

The development of an electrical insulation system for the axon, in the form of a myelin sheath, is a crucial step in the course of evolution since a myelinated axon can transmit signals much faster and more efficiently, and make more room for a great number of other axons because of its compact multilayer structure. The sheath structure is described as being composed of concentrically wrapped layers of mixed lipids alternating with thin layers of protein (Fig. 1.2). Within each layer, the lipid hydrocarbon chains extend radially into lipid bilayers and the polar head groups are exposed to the aqueous interfaces between adjacent bilayers, loosely binding to protein in these interstices [3].

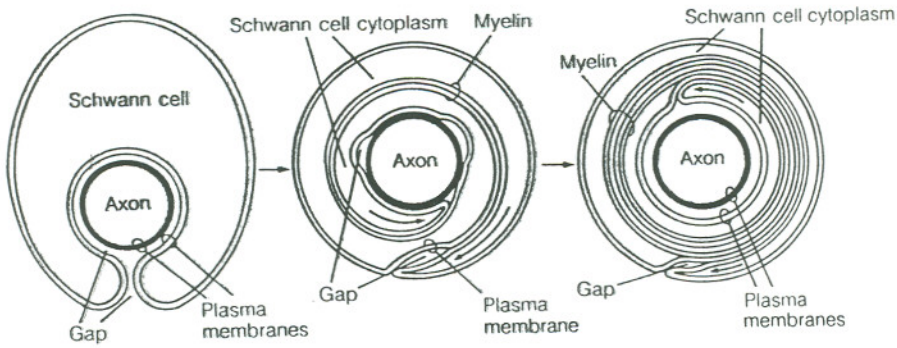

Fig. 1.1 Nerve axon myelination by Schwann cells [1].

Table 1.1 Composition of Normal Human Myelin [2]

	% Dry Weight
Protein	24.0
Basic protein	5.4
Proteolipid	
Lipophilin	7.2
Other LH-20 fractions	4.2
Thioethanol soluble	0.6
Others (Wolfgram, DM20, glycoproteins)	6.6
Lipid	Mol % Total Lipid
Cholesterol	40.9
Cerebroside	15.6
Cerebroside sulfate	4.1
Phosphatidylcholine	10.9
Phosphatidylethanolamine	13.6
Phosphatidylserine	5.1
Sphingomyelin	4.7
Others	5.1

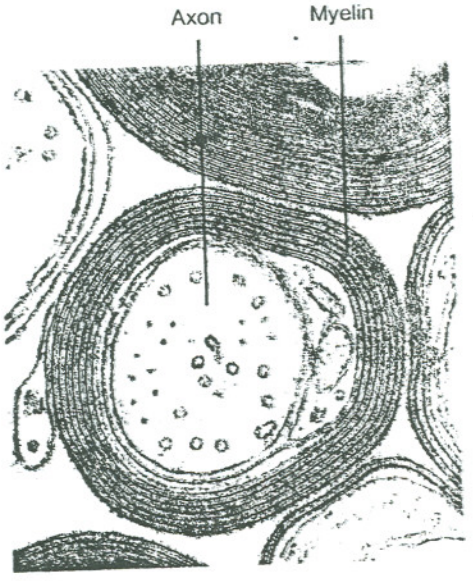

Fig. 1.2 Electron micrograph of a myelinated axon from the spinal cord [1].

The myelin sheath is a fluid membrane that maintains normal membrane-membrane contacts within the sheath multilayers even when the axons are swelling [4]. This unique, biological lamellar structure has attracted much attention, both chemically and biologically. The main research questions focus on the specific chemical structures which are responsible for the compact layering of the myelin lamellae and the myelin structure's relationship to demyelinating diseases [5]. Answers to these questions rely on a complete understanding of myelin's chemical composition and relationship to its physical properties.

1.2 Lipid Composition of the Myelin Sheath

The myelin sheath is the most lipid-rich of any biological membranes, containing approximately 80 mol% lipid and 20 mol% protein. The main lipid components are cholesterol, sphingolipids, phospholipids and gangliosides shown in Table 1.1.

1.2.1 Cholesterol

Cholesterol (Fig. 1.3a) comprises 40 mol% of the total lipid content of myelin membranes. This is very unusual for a biological membrane as most plasma membranes contain nearly 25 mol% of cholesterol [1].

Cholesterol has a specific and complex effect on membrane fluidity. It does not influence the transition temperature markedly, but broadens the transition and blurs the distinction between the membrane gel and fluid states [2]. The specific role for the high concentration of cholesterol in myelin is still unknown. Some evidence shows that cholesterol-rich lipoproteins are responsible for nerve development [6]. The physiological role of cholesterol is speculated to be a dampening agent or a stabilizing force which is needed for the overall integrity of the cell plasma membrane [7]. The synthesis of cholesterol is regulated by lipoproteins [8].

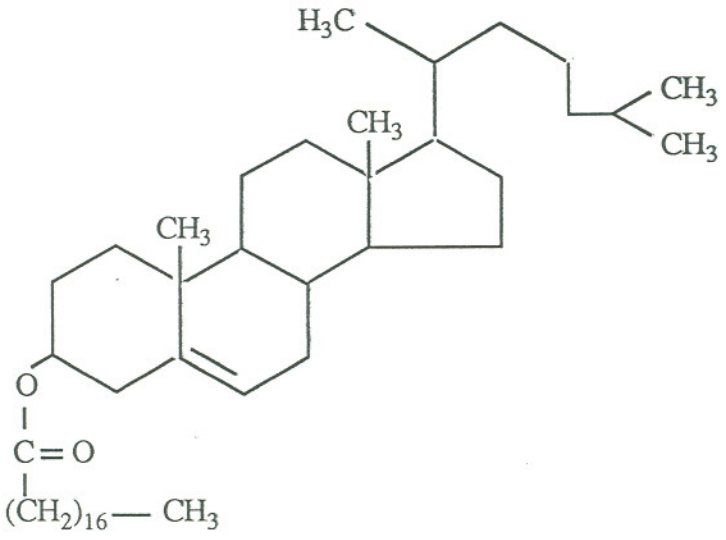

a.

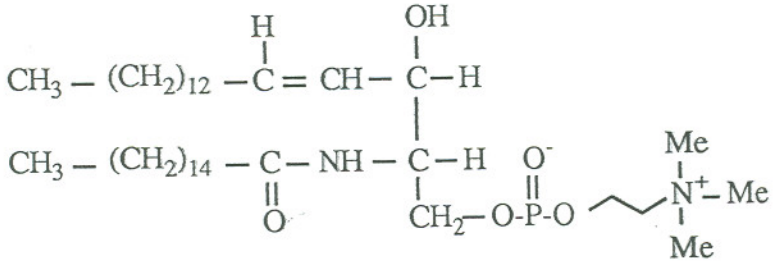

b.

Fig. 1.3 Structure of the myelin lipid: a. cholesteryl stearate b. sphingomyelin c. phospholipids d. ganglioside GM1.

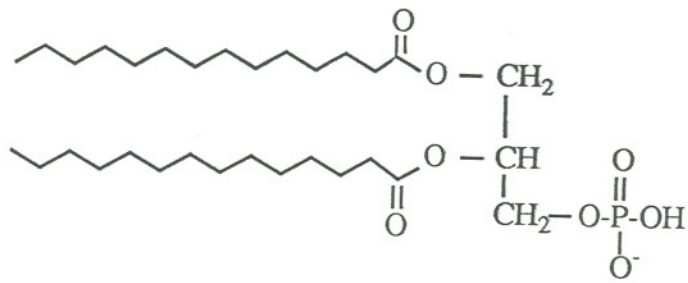

(PA)

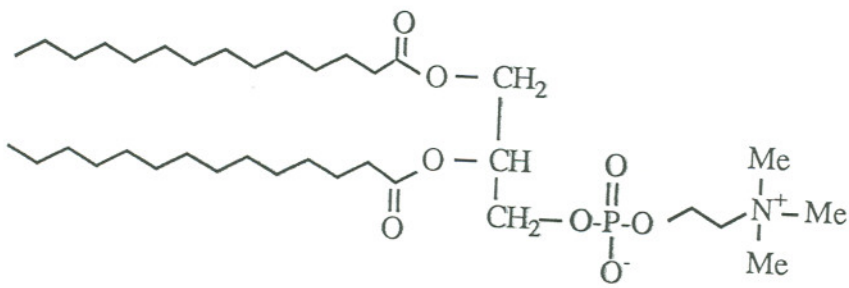

(PC)

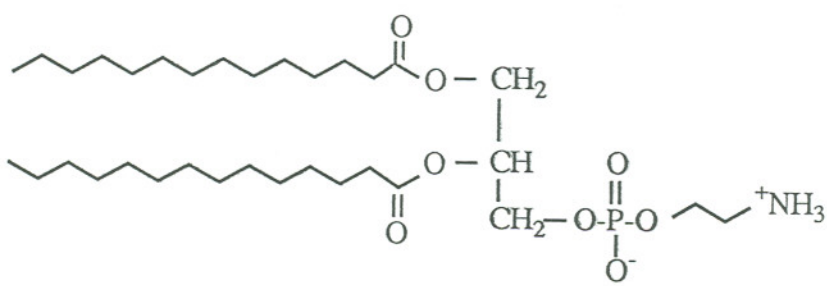

(PE)

c.

Fig. 1.3 Structure of the myelin lipid: a. cholesteryl stearate b. sphingomyelin c. phospholipids d. ganglioside GM1.

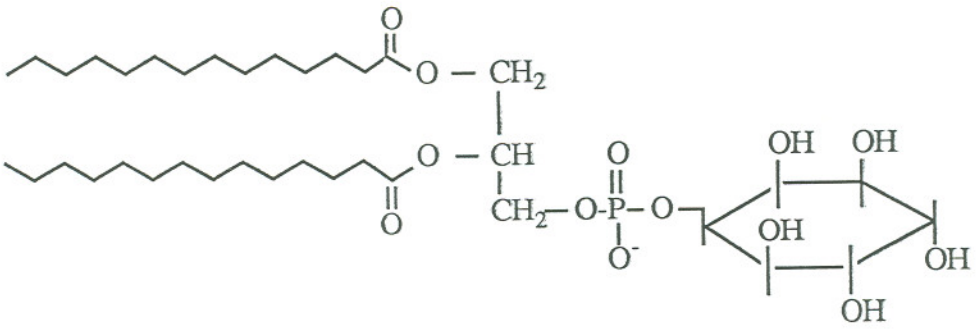

(PI)

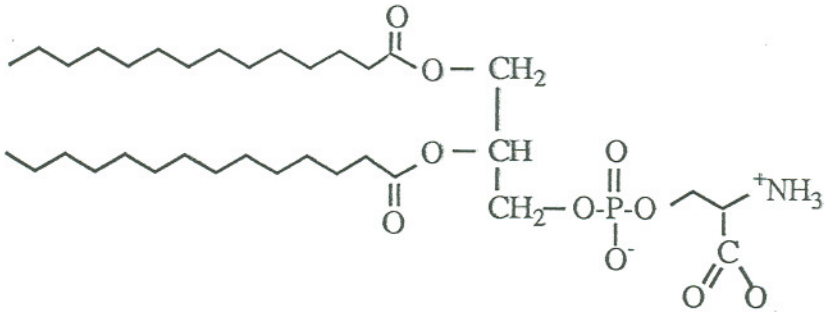

(PS)

c.

Fig. 1.3 Structure of the myelin lipid: a. cholesteryl stearate b. sphingomyelin c. phospholipids d. ganglioside GM1.

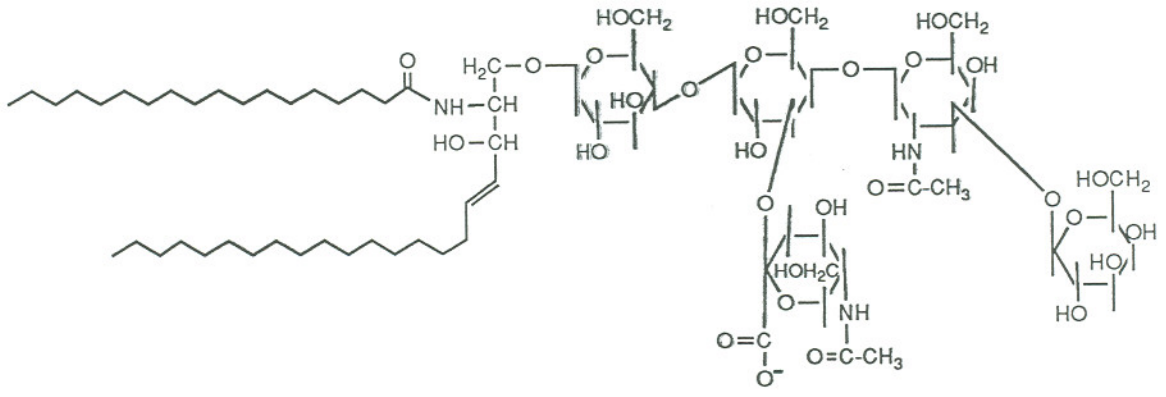

d.

Fig. 1.3 Structure of the myelin lipid: a. cholesteryl stearate b. sphingomyelin c. phospholipids d. ganglioside GM1.

1.2.2 Sphingolipids

Sphingolipids, especially sphingomyelin, are abundant components of the myelin sheath, constituting up to 4.7mol% of the total myelin lipids. The lipids are in a continuous state of metabolic turnover which includes both biosynthesis and degradation.

Sphingomyelin (Fig. 1.3b) has a zwitterionic phosphatidylcholine (PC) head group and ceramide backbone. The amide bond present in the ceramide backbone allows lateral association with other lipid phosphoglycerol backbones via hydrogen bonding. Association of sphingomyelin with other membrane lipids depends on the hydrophobic region of the molecule [9]. The hydrophobic portions of sphingomyelin are made up of extremely long fatty acids ranging from C18 (steric acid) to C24 (lignoceric acid). These long hydrophobic chains and other lipid chains readily form the lipid bilayer compartments which can host membrane proteins in certain orientations. Recent research [10] has found that sphingomyelin hydrocarbon chains maintain mixed interdigitated chain packing across bilayer membranes which is more ordered than the usual hydrated noninterdigitated bilayer phase. If this mixed interdigitation does occur in biological membranes, the penetration of long asymmetric lipid hydrocarbon chains across the entire hydrocarbon width of the bilayer would afford a transmembrane linkage that could play an important role in the transmission of information across these membranes.

1.2.3 Phospholipids

Another significant fraction of lipids found in myelin are phospholipids, including phosphatidylcholine (PC), phosphatidylethanolamine (PE), phosphatidylinositol(di)phosphate (PI), and phosphatidylserine (PS) (Fig. 1.3c).

Phospholipids are the essential components of most biological membranes. The long hydrophobic carbon chains coupled with hydrophilic head groups comprise the

amphiphiles which spontaneously form well-organized lamellar structures -- the basic architecture of membrane bilayers. Because of the important role of phospholipids in biomembrane systems, many basic studies have been performed on model membranes to address the physical and biological properties of phospholipids [11-16]. Compared to their hydrocarbon chains, phospholipid head groups hold greater biological and physiological significance [17]. Surface polarity and interfacial hydration of phospholipid head groups determine the characteristics of the lipid membranes and their interactions with the exterior environment. The large polar head groups of phospholipids, all carrying some charge, with head groups of other lipids (cholesterol, sphingolipid), play an important role in the compact structure of the myelin sheath. This will be discussed later in more detail. The specific role for certain phospholipids in the myelin sheath, like PI, remains unknown [5].

1.2.4 Gangliosides

Gangliosides are sialic acid-bearing sphingoglycolipids which are ubiquitous components of mammalian cell surface membranes. They are present as trace lipids in the myelin membrane. Among them, GM1 (galactosyl-N-acetylgalactosaminyl(N-acetyl-neuraminyl) galactosylglucosylceramide) is the most abundant sphingoglycolipid in the myelin membrane of the central and peripheral nervous systems (Fig. 1.3d). Little is known about the specific biochemical functions of gangliosides, but their presence in the outer surface of plasma membranes, especially in the myelin sheath, provides some interesting clues. They are prominent in nerve cell membranes of all vertebrates, implying their involvement in neuronal functions. The functional roles of gangliosides are thought mainly to be cell-cell recognition, modulators for cell membrane receptors and membrane ion pumps and ion channels.

In order to fully understand and characterize the properties of gangliosides, investigations on artificial membranes including vesicles and monolayers have been

performed by many research groups [18-21].

Although the hydrophobic portion of gangliosides is on average highly conserved, the presence of successive charged or uncharged carbohydrate residues in the polar head group modify their interfacial conformation, molecular packing and phase stability in biomembranes. An interesting point is that, despite many variations in head group sugar structure which lead to different molecular packing properties, monolayer studies have shown that surface potentials of different gangliosides are quite similar [5]. This implies that while the number of charges per ganglioside head group can vary from one to three (GM1-GD_{1a}-GT_{1b}), the membrane can maintain the similar apparent potential drop across the head group region [18] .

In general, the polar head groups of gangliosides and other glycosphingolipids appear to be one of the major determinants of their phase behaviors. Compared to phospholipids, the presence of the carbohydrate rather than phosphorylcholine in the polar head group reduces the effect of the number of methylene groups in the amide-linked fatty acyl chains on the transition temperature [22]. Hydrophobic chain length therefore has a relatively minor effect on the membrane phase transition temperature.

Gangliosides themselves cannot form bilayers in excess water unless some kind of stabilization is provided by other bilayer-forming lipids, such as phospholipids [23]. Thus, the interaction between phospholipid and GM1 becomes an important factor for GM1's existence in biomembranes. However, few studies have been directed to elucidate the interactions between ganglioside and phospholipid. It has been reported that when gangliosides are incorporated into dipalmitoylphosphatidylcholine (DPPC) bilayers, GM1 increases the gel-liquid crystalline transition temperature of DPPC because it shields phospholipid polar head groups to reduce repulsive interactions. In mixed PC and GM1 large unilamellar vesicles, the thermotropic lipid phase behavior is related to the ganglioside chain length in presence of Ca^{2+}, suggesting that the driving force for ganglioside phase separation is due to a passive ganglioside exclusion from

Ca^{2+}-perturbed phosphatidylcholine-rich regions within the bilayer [24]. This implies that because Ca^{2+} has no effect on PC phase behavior, chain length plays a possible role in the modulation of ganglioside function. Also, due to electrostatic repulsions, large water-structuring effects and steric constraints in their polar head groups, gangliosides appear to be stabilized by interactions with proteins [19]. This will be discussed in further detail later in this dissertation.

1.3 Myelin Proteins

Unlike the cell plasma membrane where proteins can comprise up to 76wt% of the membrane mass [25], myelin membranes contain relatively little protein (20mol%). Several types of proteins exist in myelin, differing in size, shape, and amino acid composition. The main protein is proteolipid (PLP), comprising 50% of the total protein in myelin. It is an integral membrane protein whose interactions with negatively charged myelin lipids (e.g., PA, PS) are dependent on pH and salt concentration [26]. An important but only trace protein found in myelin is myelin-associated glycoprotein, or MAG, a complex of protein and carbohydrate that is four times larger than PLP. MAG is found between the myelin and the axon and is one of the first components to disappear when myelin break-down begins during demyelinating syndromes [27]. It may also play an important role in the formation of new myelin.

Myelin basic protein (MBP) comprises 30% of total myelin protein. It is a relatively small protein (18.4 kDa), containing about 170 amino acids with 12 lysine and 19 arginine residues which make MBP a highly positively charged protein. This protein has received intensive biological and chemical studies in recent years because of its relation to demyelinating diseases, like multiple sclerosis, and its unique features in formation and stabilization of the myelin sheath [28-30].

1.3.1 MBP-Lipid Interactions: Previous Studies

MBP shows all the characteristics of a peripheral protein and predominantly binds to negatively charged lipids electrostatically to alter membrane properties. ESR (electron spin resonance) spectroscopy has shown that, in mixtures of neutral and anionic phospholipids, e.g., DMPC/DMPG, MBP prefers to bind to anionic lipids, and that this electrostatic interaction decreases as the percentage of neutral phospholipid increased [31-32]. Specific charge-charge interactions may be very crucial for organizing the myelin sheath in nervous tissue. While MBP is incorporated into unilamellar PG vesicles, the motion of PG head groups in the gel phase is restricted by intermolecular interaction caused by the addition of MBP, creating a new protein-induced "domain" [29, 33]. Similar results are also found in phosphatidic acid (PA), an acidic phospholipid which lacks a head group other than the negatively charged phosphate moiety [34]. These MBP-induced perturbations have also been shown to cause a thermotropic profile change in the lipids [21]. After binding to membranes, the motion of the protein increases upon heating and is sensitive to the lipid phase transition [35]. The association of MBP with PG suspensions results in a broadening of the lipid phase transition [36].

Measurements of tryptophan fluorescence of MBP in the presence and absence of sodium dodecylsulfate (SDS) indicate that the tryptophan, which is in a hydrophobic segment of the protein, moves into a less polar environment when the protein is bound to SDS [3]. Monolayer studies show that MBP can penetrate into the ganglioside monolayers [37].

Phosphatidylethanolamine (PE) naturally adopts a non-bilayer hexagonal cylinder structure (H_{II}) in pure form under certain hydration, pH, and temperature conditions. In the myelin sheath, however, the lipid exists as bilayer or multilayer structures. X-ray and NMR studies show that MBP has the ability to convert PE H_{II} structures into lamellar (L_{α}) structures [28]. MBP may, therefore, not only cause the

compact structure of the myelin sheath, but also stabilize this structure through protein-lipid interactions.

Relatively large amounts of zwitterionic PC lipids are found in the myelin sheath. The specific role of PC lipids in the formation and stabilization of the myelin sheath is still puzzling. Current ESR and NMR results are consistent in showing that addition of MBP does not influence the membrane structure or morphology of PC vesicles [35]. Lipid thermostudies showed that MBP had little effect on the transition temperature of PC in aqueous dispersions, but could increase the phase transition temperature of ganglioside dispersions [38]. However, in mixtures of gangliosides and DPPC, MBP changes the properties of both lipids, indicating that MBP does not interact exclusively with one lipid type, but with the lipid matrix as a whole.

^{1}H-NMR study shows that the resonance of Met-20, an MBP amino acid residue, loses approximately 40% of its original intensity while Met-167 of MBP exhibits no significant change upon addition of lyso PC lipid to a final concentration of 25 mM (above the critical micelle concentration of the lipid). This implies that the Met-20 side chain may penetrate into the hydrophobic lipid matrix region [39]. It confirms the intrinsic capacity of MBP to interact strongly with neutral lipids, perhaps via a combination of both protein/protein and protein/lipid bridges.

1.3.2 Possible Membrane Interactions for MBP

Although EPR and NMR studies show that all these interactions occur in the polar head group region [31,33,35], the abilities of MBP to influence phospholipid phase transitions, induce phase separation of acidic phospholipids and distort the packing of lipid chains near the head group region suggest the presence of other types of interactions in addition to protein binding via electrostatic attraction to acidic lipid head groups [40-42]. Large portions of hydrophobic segments found in MBP (52% apolar amino acids) make it possible to interact with the lipid acyl chains either by partially

penetrating into the bilayer as shown in Fig. 1.4 or by deforming and expanding the bilayer so that the acyl chains are exposed to the hydrophobic regions of the protein as drawn in Fig. 1.5. Less detectable evidence for incorporation of some MBP hydrophobic sequences into the membrane acyl region by EPR and NMR may be due to a broadened resonance which is beyond detection [35].

Much evidence demonstrates the existence of hydrophobic and electrostatic interactions between MBP and phospholipids. However, this interaction does not induce drastic conformational changes in the lipid phosphate moiety. This suggests that the binding between phospholipid head groups and MBP is relatively loose. The interaction is mostly of a polar nature with no strong bonding between specific groups [36]. This may explain the observed rapid exchange of PG lipid molecules between the bulk and protein-associated phases [43].

Although the interaction between MBP and lipids has received intensive study, recent reports of MBP microheterogeneity have prompted questions regarding the specific roles for various MBP isomers in organizing lipids in the myelin sheath. Further studies are therefore useful in order to fully understand the function of MBP in the myelin sheath.

1.4. The Biomembrane and Relevant Model Systems

1.4.1 Biomembrane Models

Though scientists knew of the existence of cells before they could observe them directly with the assistance of a microscope, only recently has an acceptable model for the structure of biological membranes been proposed. In 1972, Singer and Nicholson forwarded what has now been proven to the most-widely accepted model for the structure of the biological membrane, called the "fluid mosaic model" (Fig. 1.6) [44-46]. In this model proteins are assumed to be either superficially or integrally

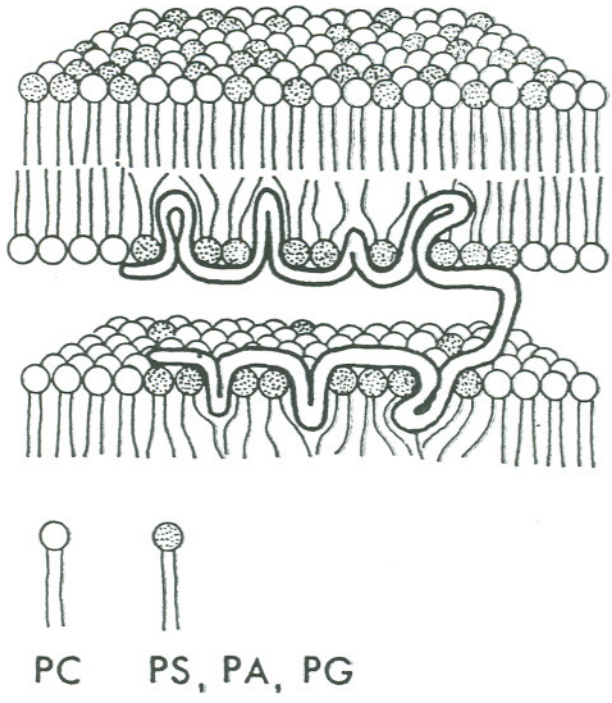

Fig. 1.4 Schematic representation of myelin basic protein bound to lipid bilayers [2].

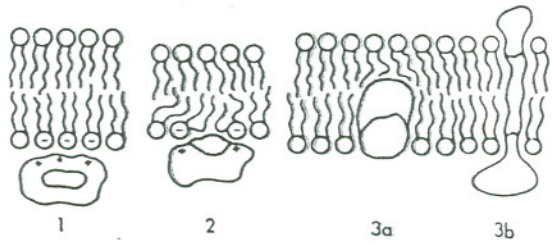

Fig. 1.5 Schematic representation of different types lipid-protein interaction: (1) electrostatic only, (2) electrostatic plus hydrophobic resulting in deformation of the bilayer, (3a,b) hydrophobic interaction. The interaction of basic protein with lipid may be of type 2 while lipophilin may be type 3 [2].

associated with lipids in a fluid bilayer membrane which has an asymmetric structure. Membrane asymmetry has been proposed to account for specific lipid-protein interaction and unidirectional transport functions of the cell membrane [47]. Lipids are assumed to be distributed homogeneously within each bilayer leaflet and all components are freely diffusing. Membrane fluidity is very essential as many membrane properties are dependent upon it (e.g., lateral diffusion of lipids and proteins in the membrane). Although it is now known that many integral proteins do not diffuse freely and that lipids exhibit density fluctuations and non-random domain microstructures, important elements of fluid mosaic model remain valid today. With respect to myelin sheath formation, recruitment of lipids into domains and induction of highly curved multilamellar membrane structures rely on membrane properties consistent with those proposed in the Singer-Nicholson model.

1.4.2 The Significance of Model Membranes

The biological cell is an extremely complicated microcompartment. Fully understanding and describing the specific functions and dynamics of the biomembrane (e.g. "ion pump" function, endocytosis, signal transduction, mitosis) including the interactions between lipids, membrane proteins and lipids, membrane proteins with each other, and peripheral soluble macromolecules with membranes has proven impossibly complex. In order to understand even the simplest cell structure-function relationship one must rely on simple membrane models. A model membrane may be constructed by using only lipids or a mixture of lipids and proteins. Using these systems to separate variables, the properties and functions of relevant lipid and protein and their interactions can be chemically and biologically understood.

Four model membrane systems are widely used to model biological membrane structure and function [48]. Brief details of these four systems follow, although reference is made to more comprehensive reviews of these systems for further details.

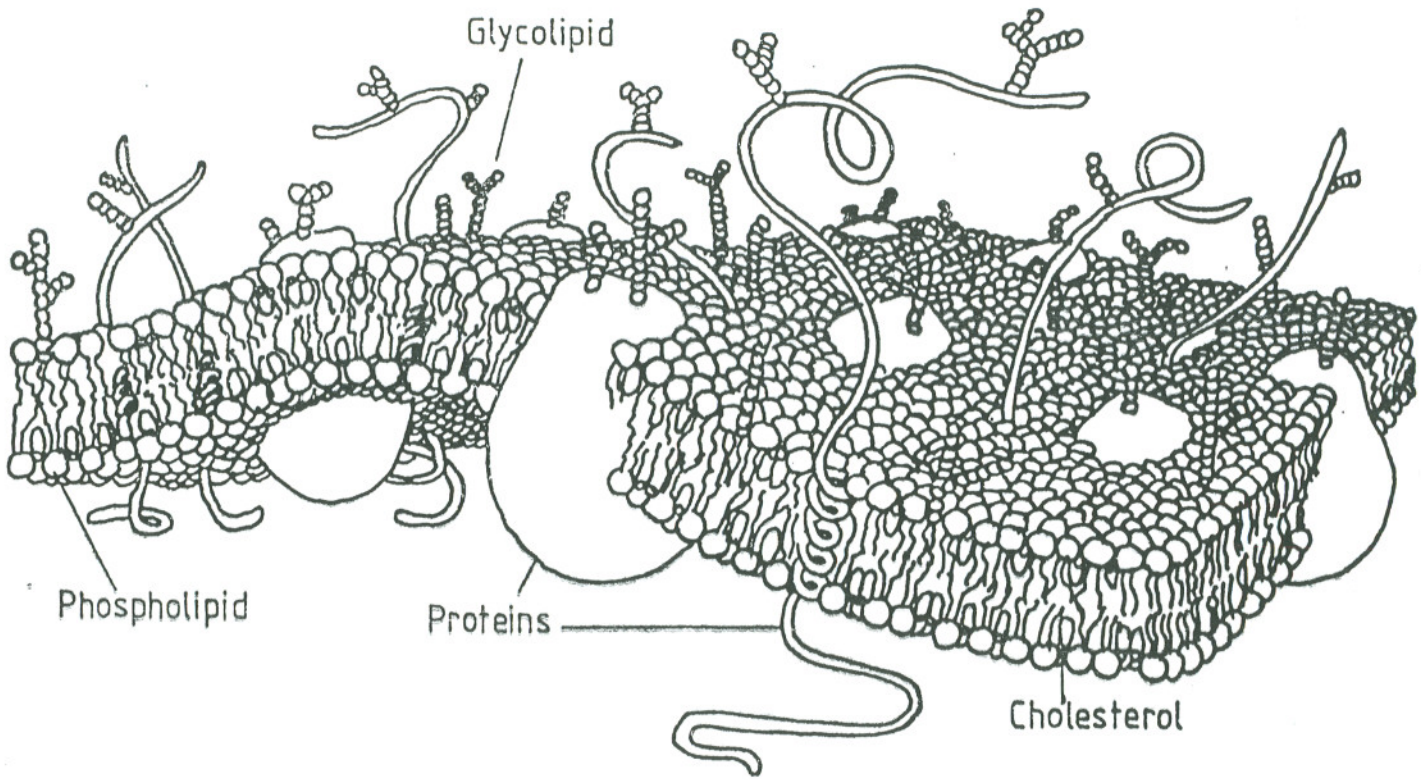

Fig. 1.6 Schematic representation of the Fluid Mosaic Model proposed by Singer and Nicolson (1972) [46].

A. Liposomes and Vesicles

Phospholipids dispersed into aqueous solution aggregate spontaneously once hydrated to form closed spherical lipid structures called liposomes (Fig. 1.7a). Liposomes have been classified by size: small unilamellar vesicles (SUV, 200-500Å diameter), large unilamellar vesicles (LUV, 0.1-10μ diameter) and multilamellar vesicles (MLV, 1000-8000Å) [49]. These structures are, in many regards, similar to actual cell membranes. Because of their stability and easy fabrication, liposomes have been intensively studied and applied as model systems to the topics of biomembrane transport, protein interfacial recognition, reconstruction of integral membranes proteins, pharmaceuticals, biomembrane interfacial chemistry and biophysical properties of lipid supramolecular assembly [50-54].

B. Black Lipid Membranes

Black lipid membranes are planar lipid bilayers which, by covering a hole in a polymer support, separate into two aqueous phases (Fig. 1.7b). Lipids are generally "painted" in an organic solution across a pinhole under water. The painted lipid film spontaneously thins to form a lipid bilayer supported on its polymer-anchored circumferential edge by a lipid-solvent pool (the torus). This model is very convenient for transport studies since the aqueous compartments on both sides of the membrane are accessible. The system can be easily controlled and monitored within the limits of their lifetime and durability [49].

C. Lipid Monolayers

When a lipid solution is spread onto a subphase, it will organize spontaneously to form a continuous monomolecular film (Fig. 1.7c). The lipid monolayer can also be manipulated by compressing the surface film with a movable floating barrier. This changes the packing density and organization of the lipid film. Although organized

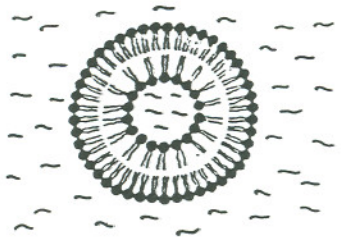

a. liposome

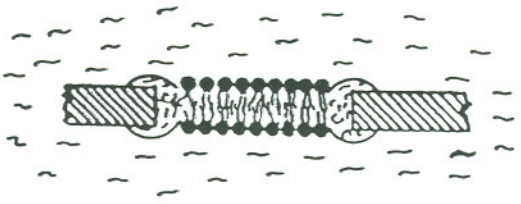

b. black planar lipid membrane

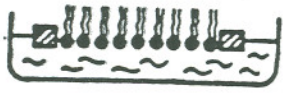

c. monolayer

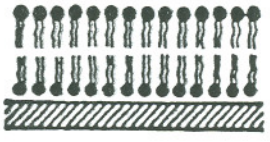

d. Langmuir-Blodgett film

Fig. 1.7 Schematic representation of four widely used model membranes.
a. liposome b. black planar lipid membrane c. monolayer d. Langmuir-Blodgett film

lipid monolayers only represent one leaflet half of a cell membrane, monolayer studies can provide precise information on molecular packing and orientation not readily obtained from other model systems. The hydrophobic components of the lipid are directed uniformly outwards the air and the hydrophilic head groups associate with the subphase. Many investigations have used monolayers to study biomembrane properties by measuring surface pressure-area diagrams [48,55]. This will be further discussed in the next section.

D. The Supported Bilayer and Langmuir-Blodgett Films

A supported bilayer is formed by transferring lipid monolayers successively onto solid substrates (Fig. 1.7d). This method produces juxtaposedly ordered lipid arrays to represent a lipid bilayer, or alternatively with multiple transfers, multilayer (Langmuir-Blodgett) lipid films. Solid substrates could be either hydrophobic or hydrophilic so that different substrate surface properties direct the order of lipid film deposition to serve various research purposes. The hydrocarbon chains of lipids will face the substrate if a hydrophobic substrate is applied, and vice versa for hydrophilic substrates [56]. The interaction of molecules (antibodies, proteins, hormones) from solution with cell surface membranes can be modeled by both supported bilayers [56] and Langmuir-Blodgett films [57] to characterize the physical and chemical properties of cell membranes.

1.4.3 Mimicking Biomembrane Processes -- Lipid Monolayers as Simple Models

1. Phase Behavior of Lipid Monolayers

When a lipid solution in a volatile solvent is spread at the air-water interface, the self-organizing properties of the lipid aggregates will result in a two-dimensional lipid phase having several distinct physical regimes. This phase can exist as a two-

dimensional gas, liquid, or solid depending on the amount of lipid on the surface and its packing state. When the air-water interface occurs within a Langmuir-Blodgett film balance [58], a movable barrier can sweep the surface to change the surface area available to the lipid film. Changes in interfacial tension resulting from lateral lipid associations are measured (surface pressure) (Fig. 1.8). Two-dimensional monolayer molecular density can be strictly regulated by changing the average area available to each molecule in the film. Surface pressure resulting from monolayer compression is plotted as a function of monolayer area at constant temperature to yield diagrams called "surface pressure-area isotherms". Each lipid isotherm is extremely reproducible if done correctly and "fingerprints" the interfacial characteristic of each lipid.

Changes in the interfacial tension are usually denoted by the term "surface pressure". If γ_o is the interfacial tension of the clean interface of a pure liquid and γ is the interfacial tension after adsorption of a solute, then the surface pressure π is defined by [59],

$$\pi = \gamma_o - \gamma$$

which has units of mN/m. A typical surface pressure-area diagram is depicted schematically in Fig. 1.9.

In the gas-analog phase, there is extensive disorder of the lipid molecules resulting from large molecular area and sub-monolayer surface concentrations of lipids. A reduction of the molecular area by compression induces a first-order phase transition leading to the formation of a liquid-analog phase. This phase represents a full and coherent lipid monolayer where the interactions exist primarily between lipid head groups and the acyl chain orientations are largely disordered (gauche). Further compression often results in another first-order phase transition which produces a liquid/solid coexistence phase. This phase is characterized by the presence of highly ordered, crystalline domains of solid phase lipids within a matrix of relatively disordered liquid phase lipid. Finally, added compression will result in a second-order

order transition yielding the solid-analog phase, the most organized and dense lipid phase for this two-dimensional system. Lipid acyl chains here have assumed all-trans, quasi-crystalline configurations and head groups are tightly associated. Often, there are defect regions (grain boundaries) between adjacent lipid crystalline domains which have grown to confluence in two-dimensions. Diffraction studies on monolayers have shown that these lipid phases assume a space grouping very similar to that seen in bulk lipid crystalline phases. Further compression will force this phase to collapse to bulk lipid phase formation.

2. Protein-Lipid Interactions Studies in Monolayers

The lipid monolayer system yields significant benefits in the study of protein-lipid interactions when the protein(s) readily dissolve(s) in the aqueous subphase. Proteins can be introduced into membrane systems where the lipid packing, organization, and lateral surface pressure are readily defined and controlled. Other methods of observing protein-lipid membrane interactions, including lipid bilayer vesicles, planar lipid membranes, and lipid-surfactant micelles, allow no control or adjustment of lipid interfacial properties except for lipid headgroup chemistry. Lateral surface pressure in membrane bilayers remains a significant experimental uncertainty and is not variable in these systems. Lipid monolayers, therefore, have inherent advantages in controlling interfacial properties to observe influences on protein binding. Protein interaction can be either selective or non-specific. Interactions can be hydrophobically driven, electrostatic, or combinations of other weaker forces (van der Waals, hydrogen bonding). Any interaction between lipid and protein will change the properties of the lipid membrane, which in turn can be monitored at constant pressure (yielding changes in monolayer area) or constant area (yielding changes in monolayer pressure). Protein binding to the lipid interface, incorporation of protein into the lipid membrane and the influence of protein on the lipid phase behavior can be easily monitored and investigated. Two methods are commonly used for these investigations:

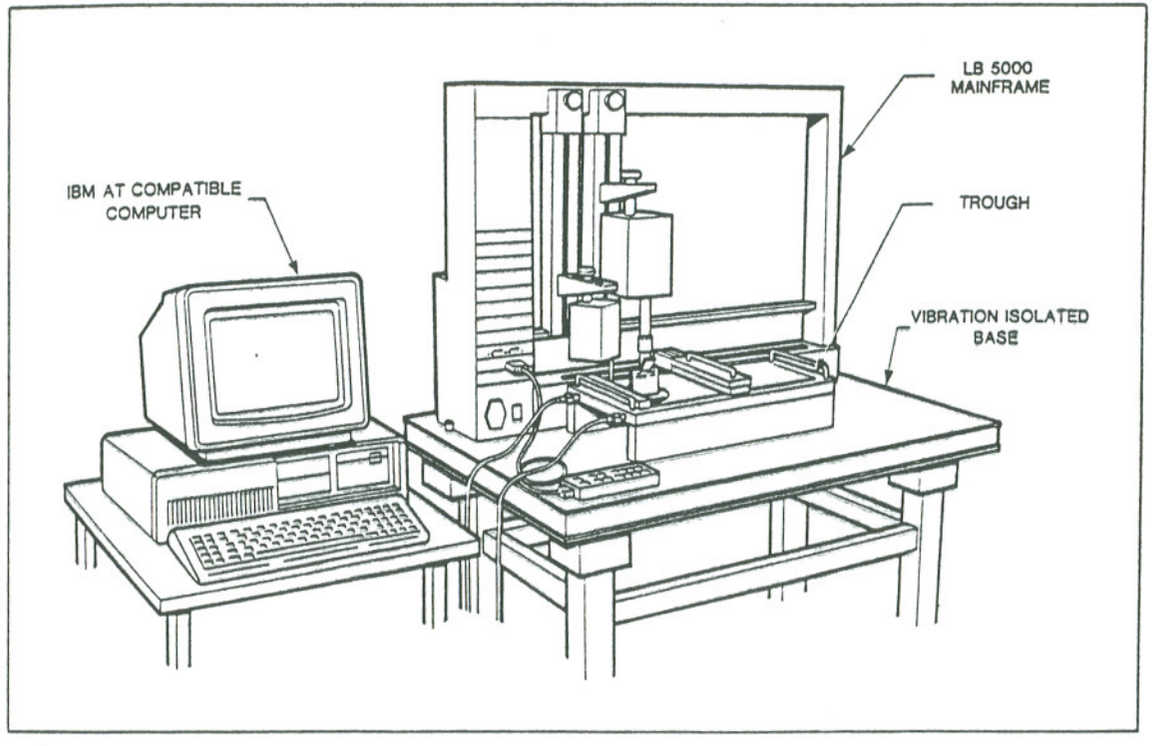

Fig. 1.8 Schematic representation of the Langmuir film balance (KSV, LB5000)

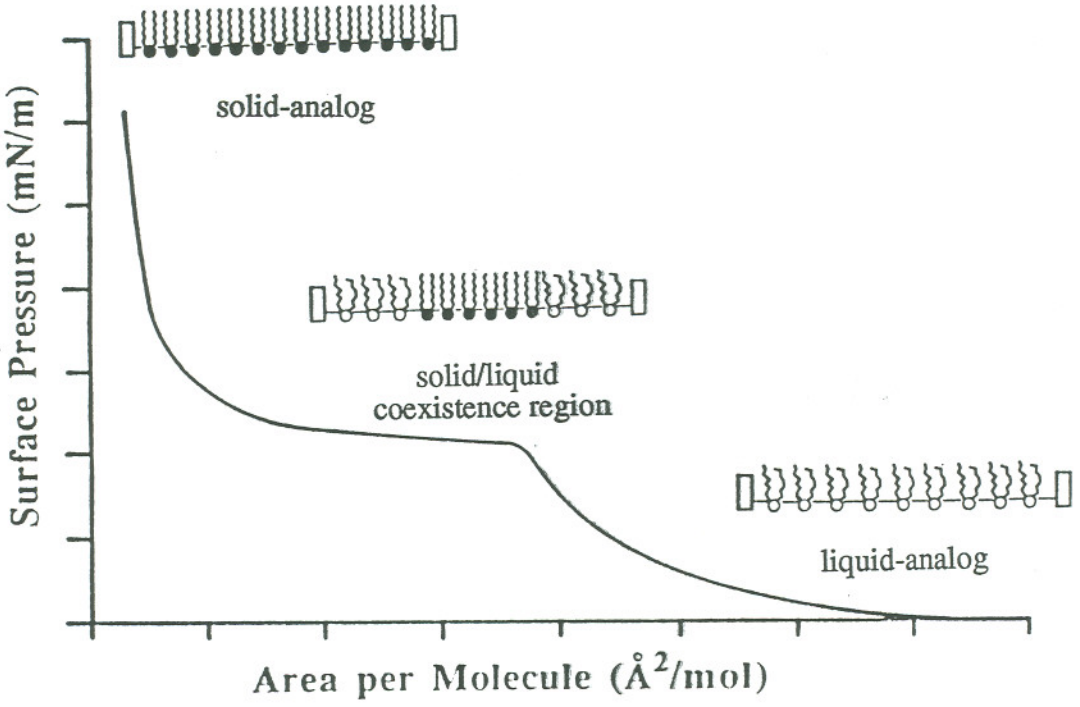

Fig. 1.9 Surface pressure-molecular area diagram for a lipid monolayer: representation of the compression behavior and molecular packing in the gas, liquid and solid-analog phases.

a. Protein-Lipid Monolayer Hysteresis Studies

Proteins are injected under the lipid monolayer at the desired lipid phase. The monolayer is then compressed to a certain higher surface pressure or smaller molecular area and expanded to the maximum molecular area immediately. Interactions between the proteins and lipids differ between expanded and condensed states, resulting in a feature of hysteresis which can provide insight into the interaction process (Fig. 1.10) [60-61].

b. General Monolayer Kinetics Experiments

Binding kinetics of proteins onto lipid membranes can be studied by injecting protein of interest under lipid films at a known surface pressure. Due to the interaction or specific recognition of the protein with the lipid, the lipid phase will be influenced. Changes in surface pressure at constant temperature (isotherms) can be monitored at constant molecular area (Fig. 1.11) or changes in molecular area at constant temperature can be monitored at constant pressure (isobars). Because protein surface concentration under the lipid membrane cannot be accurately controlled or determined, the information gained from this technique is limited to relative comparisons.

1.5 Experimental Strategy for Lipid Monolayer Studies : Interactions between Myelin Basic Protein and Phospholipids

1.5.1 Myelin Basic Protein and the C-1 Charge Isomer

Myelin basic protein has received intensive studies in recent years because of its biological and chemical importance, particularly with regard to the etiology of demyelinating syndromes including multiple sclerosis. Nearly all reported studies which have addressed MBP-lipid interactions utilize MBP as extracted and isolated from nervous tissue. Although purified MBP isolated from human brain white matter migrates as a single band, on alkaline gels it has been resolved into 6 bands

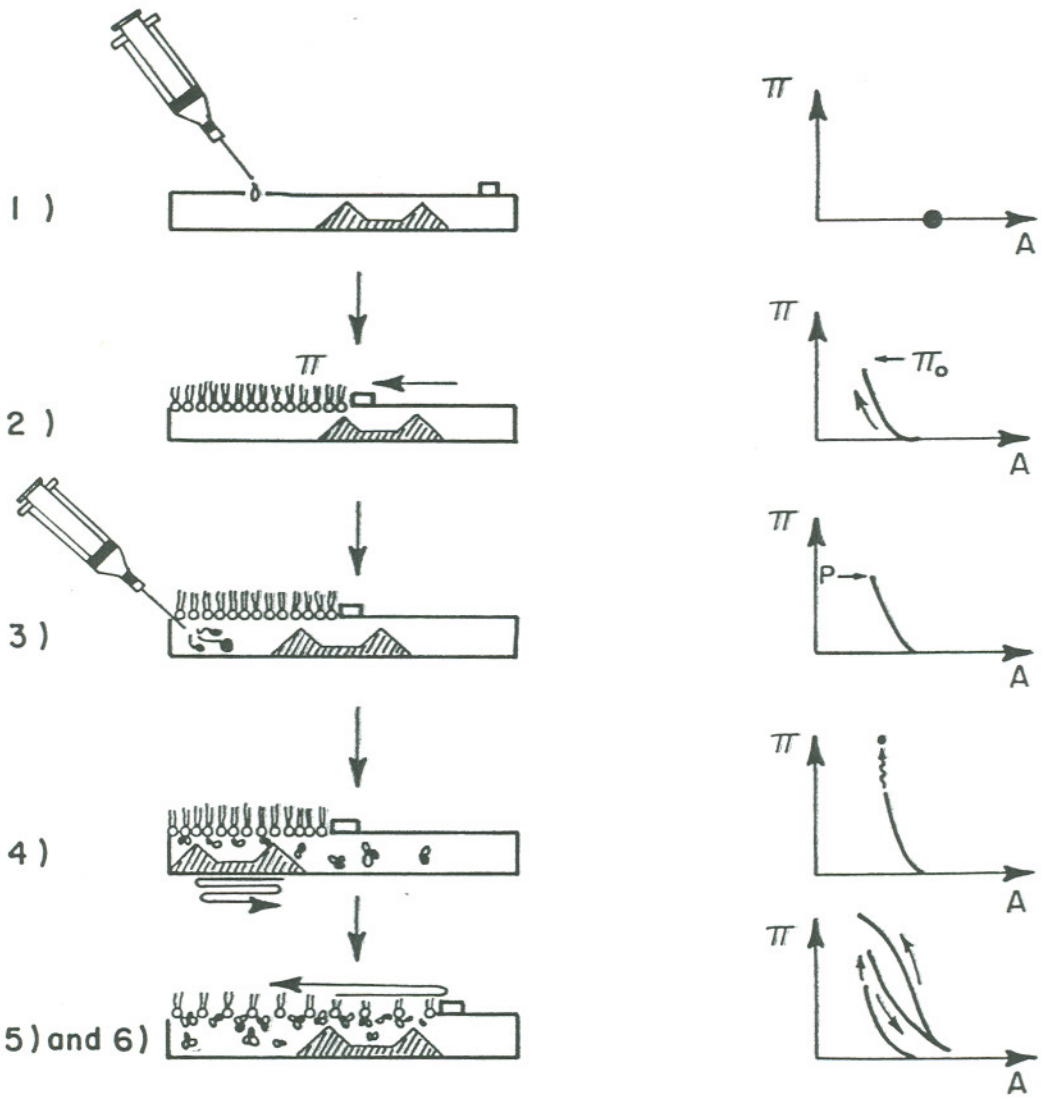

Fig. 1.10 Schematic representation of protein-lipid monolayer hysteresis studies [61].

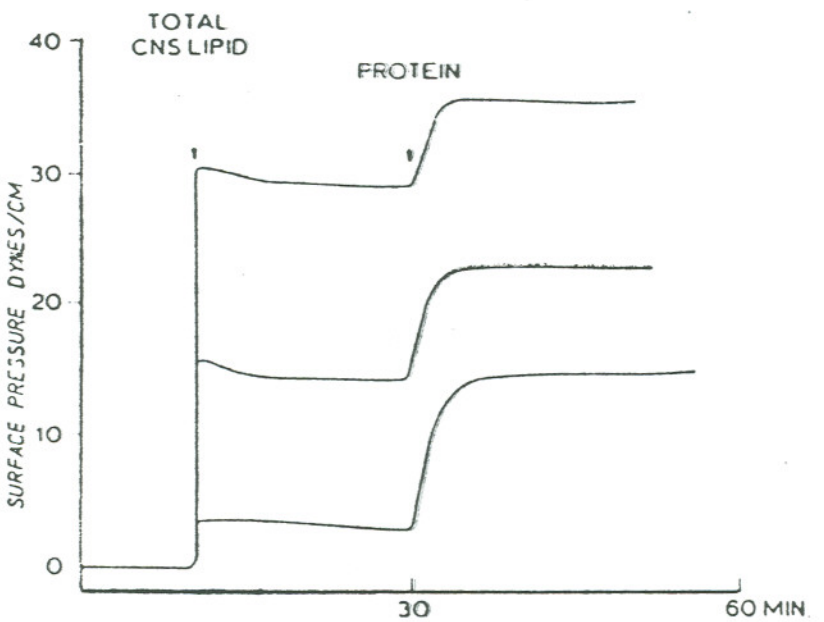

Fig. 1.11 Schematic representation of general monolayer kinetics experiments [32].

(components) on the basis of charge. Each band is referred to as a charge isomer and differs from the others by a single charge. Each charge isomer is thought to have different roles in the interaction of MBP with myelin lipids. The charge isomer, C-1, is the most cationic component and is most effective in inducing the multilamellar structures [62].

The source of MBP charge microheterogeneity is generally considered to arise from the loss of a C-terminal arginine, deamidation of glutamine or asparagine, and protein phosphorylation. However, this charge microheterogeneity has not yet been well-defined, so that any combination of the above mentioned factors may result in the formation of large numbers of charge isomers observed in alkaline gels [63]. Since all studies consistently show that the dominant effect between MBP and lipids is electrostatic interaction, and other work has shown that the MBP C-1 charge isomer is the most cationic of all the MBP charge isomers, it will be most useful to further study the properties and possible physiological functions of these charge isomers in forming the myelin sheath.

1.5.2 Electrostatic Interactions between Lipid Membranes and Poly-l-Lysine

Most studies of the molecular interactions between lipids and proteins have been performed on model systems composed of well-defined lipid and protein components. Poly-l-lysine (PLL) is one of the most interesting and commonly used models of extrinsic proteins because of its basic character. This synthetic polypeptide is available in a wide range of molecular weights from commercial sources. Each lysine bears a positive charge at physiological pH so that lysine monomer can interact readily with acidic lipid membranes. Since the interaction between PLL and lipids is nearly exclusively electrostatic, PLL can be used as a model compound to compare with interactions observed between myelin basic protein and lipid membranes [64].

1.5.3 Acidic and Zwitterionic Phospholipids as Lipid Model Membranes

Protein-lipid interactions can be divided into two components, hydrophobic and electrostatic. Since these two interactions mainly occur in the lipid head group region it is important to choose lipids with both charged and neutral head groups in order to sort out each interaction. In this regard, both anionic and zwitterionic head groups have been selected for this work. In light of the specific function of gangliosides in the central nervous system [1], GM1 is also chosen as a relevant model lipid system.

1.5.4 Physical Significance of Hysteresis Experiments

Monolayer hysteresis diagrams are composed of three separate isothermal curves: the first compression, subsequent monolayer expansion, and second compression to collapse (Fig. 1.10). Hysteresis shows the influence of protein(s) on the lipid molecular packing and the process of repeated adsorption-desorption of protein on the lipid monolayer. The lipid monolayer undergoes phase changes upon compression. If the lipid molecular packing can be fully restored within the kinetics limits of the monolayer expansion, there will be no hysteresis. With the injection of protein under the lipid monolayer, absence of hysteresis signifies no interaction between the lipid membrane and protein since pure lipid monolayers generally recover quickly during the compression and expansion process. If, during the sequential process of compressing the monolayer to a certain elevated surface pressure and expanding immediately to the maximum molecular area, the expansion curve does not overlap with the first compression curve, then the monolayer undergoes a slower recovery during the expansion period than in the original compression period.

During monolayer compression, increasing lipid monolayer packing density (decreased molecular area) forces bound proteins to conform to the changing lipid membranes. Two dynamic processes are possible in varying degrees. One is adsorbed protein reconfiguration/reorganization and the another is the desorption of the protein

from the monolayer interface. During the subsequent membrane expansion process, the protein in the subphase may attempt to regain its most-favorable interaction with the membrane and try to bind to the monolayer again while at the same time the lipid molecules try to return to their original unconfined, loosely packed state. After the barrier expands to maximum molecular area, the experiment arbitrarily allows 40 minutes for the proteins and lipids to repeat their interaction before recompressing the monolayer again to its collapse point.

Protein adsorption to the monolayer is a diffusion-controlled process so that protein adsorption-desorption process is considered slower than the restoration of the lipid molecular packing state. Ideally, the slower step can be considered to be an irreversible process and the restoration of the molecule packing can be considered to be a reversible step. Four results are possible:

1. If the second compression curve overlaps with the first compression curve, this indicates that the monolayer has completely restored itself and that all desorbed protein has recombined or integrated into the monolayer during the expansion and waiting period.

2. If the second compression curve overlaps with the expansion curve, then this indicates that the protein cannot recombine with the lipid monolayer during the time scale of the expansion and subsequent incubation. This indicates an irreversible event occurs where protein-lipid interactions present during the initial compression are eliminated by compression-induced desorption.

3. If the second compression curve locates between the first compression curve and the expansion curve, then both processes occur, but neither occurs to completion.

4. If the onset area of second compression curve is greater than that of the first compression and expansion curve, it indicates that protein exhibits larger surface activity while binding to the lipid monolayers.

1.6 Protein Adsorption onto Lipid Model Membranes

Adsorption of proteins from aqueous sytems onto surfaces is a very important problem in biomedical and industrial areas. Protein adsorption can be totally irreversible, partially reversible, or completely reversible, depending on adsorption time. Most proteins on surfaces are found to be irreversibly adsorbed at longer adsorption times, indicating that proteins undergo surface-induced conformational changes after adsorprtion [65,66]. Prevention of biofouling and protein denaturation on surfaces has been an intensive research interest for years.

Biomembranes serve many functions as integral components of cell walls in governing cell function, controlling permeation of essential substances, rejecting toxins, and compatmentalizing cell machinery. These membranes also demonstrate only specific interactions with the wide array of proteins found in physiological milieu. Interest has been focused recently on the use of cell membrane materials and membrane mimics as new materials and surfaces for prevention of biofouling and protein adsorption. We are interested in methods to study interaction mechanisms between soluble proteins and lipid surfaces and to further apply them in biomedical devices and biosensors. Artificial model membranes (polymer surfaces, Langmuir-Blodgett films, lipid monolayers) have been used for this purpose [67-68].

One novel approach to study protein adsorption onto model lipid membranes is Total Internal Reflection Florescence (TIRF) technique. TIRF is a spectroscopic method for interrogating surfaces based on surface-bound evanescent waves produced by internal reflection within a medium which extend from the surface and decay into the external medium. The local evanescent field can be used as a probe in the surface region to selectively excite fluorescence of adsorbed proteins (Fig. 1.12). An optical signal is reflected through a medium under conditions which allow total internal reflection. At each reflection point at the medium phase boundary, a standing wave is produced when the refractive indices satisfy the condition, $n_1 > n_2$. Because of

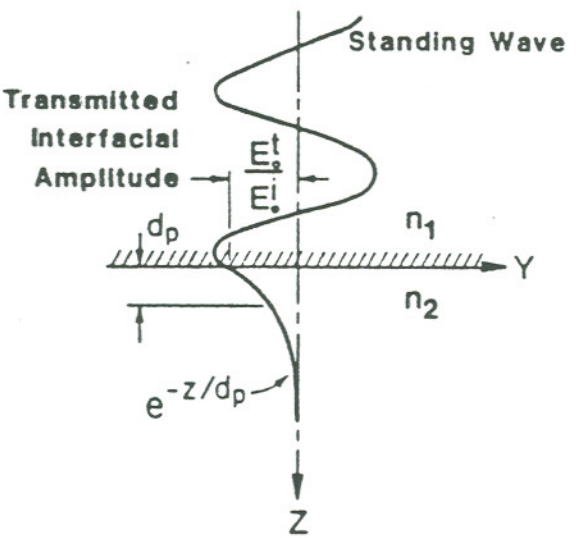

Fig. 1.12 Shematics of the surface wave in the y-z plane showing the standing wave pattern and exponential decay of the transmitted electric field amplitued into the rarer medium 2 [69].

boundary conditions for the electromagnetic wave, the wave amplitude in the external medium 2 is nonzero and can excite fluorescence of adsorbed proteins within the vicinity of the interface. The evanescent field in this region is bound to the surface and decays into the external medium exponentially [69].

1.7 Research Objectives

Research described in this thesis uses model lipid membranes to study protein interactions. Monolayer hysteresis methods are used to elucidate lipid-polypeptide (MBP C-1 and PLL) interactions as a function of lipid monolayer physical states. Lipid membrane charge and head group chemistry are both investigated. Subphase ionic strength is changed to monitor binding contributions from both intermolecular hydrogen bonds and charge-charge effects on lipid-protein interactions. Lyotropic liquid crystalline lipid lamellar phases are characterized by small-angle X-ray diffraction to model the myelin sheath structure. Supported lipid membranes are used to study adsorption of albumin from solution onto membrane surfaces using the TIRF method.

Chapter 2

Experimental Methods

Experimental methods and components are described in the following sections. Lipid monolayer hysteresis experiments have been used to study the interactions between polypeptides (MBP C-1 and PLL) and lipids (DMPA, DMPC, DHP and GM1). Salt effects on these interactions were further approached by this method. Because of the multilayer structure of myelin sheath, lipid liquid crystal multilamellar gel phases are made and the structures are characterized by small-angle X-ray scattering. Polypeptide secondary structure before and after interactions were examined by circular dichroism. Protein adsorption studies were performed using the Total Internal Reflection Fluorescence technique.

2.1 Chemicals

1. The following chemical components were used without further purification (numbers in parentheses represent respective molecular weights).

Dimyristoylphosphatidylcholine (DMPC, Avanti Polar Lipids, 677.76).

Dimyristoylphosphatidic acid (DMPA, Sigma, 614.8).

Dimyristoylphosphoglycerol (DMPG, Avanti Polar Lipids, 688.85)

Ganglioside GM1 (Matreya Biochemical, 1547).

Dihexadecylphosphate (DHP, Aldrich Chemical Company, 546.86).

Tris(hydroxymethyl)aminomethane (Tris, Aldrich Chemical Company, 121.14).

Sodium chloride (NaCl, Aldrich Chemical Company, 58.44).

Sodium phosphate dibasic (Na_2HPO_4, Aldrich Chemical Company, 141.96)

Potassium phosphate monobasic (KH_2PO_4, Aldrich Chemical Company, 136.09)

Fluorescein isothiocyanate (FITC, Sigma, 389.4)

2. Lead stearate (Pfaltz&Bauer, Inc., mol.wt. 774, 98% purity) was further purified according to the following procedure:

   a. Mix 10-20 mg lead stearate with 3 ml $CHCl_3$.

   b. Heat the solution to boil.

   c. Filter the solution immediately through a pre-warmed funnel.

   d. Evaporate the solvent to recover the purified solid.

2.2 Polypeptides

1. Poly-l-lysine (PLL, Sigma, mol. wt. 21,700) was dissolved in 5mM Tris buffer and stored at 4°C.

2. Myelin basic protein C-1 charge isomer (MBP C-1)

   MBP C-1 charge isomer was kindly provided by Dr. Mario A. Moscarello, Hospital for Sick Children, Toronto, Canada. It was isolated from human brain white matter as described previously [70]. Microheteromer isoform components of MBP were prepared by the method of Chou and coworkers [71] with slight modifications [70]. MBP was dissolved in a urea-glycine buffer, pH 9.6, and applied to a CM52 cellulose cation exchange column equilibrated in a urea-glycine buffer, pH 10.6. The components were eluted from the column using a NaCl gradient (0- 0.2M), and then desalted on a Bio-Gel P-2 column in 0.01 N HCl. The desalted components were dialyzed, lyophilized and stored at -20°C prior to experiments. MBP C-1 was reconstituted in 5mM Tris buffer at pH 7.4 and stored at 4°C.

3. Labelled albumin

   Bovine albumin (from ICN ImmunoBiological, crystallized, 60 kDa) was dissolved

in a carbonate buffer to give a protein concentration of 1-20 mg/ml. The final volume should be less than 3ml for purification on the Sephadex column described. Protein was labelled by the following procedure:

a. Prepare a solution of fluorescein isothiocyanate (FITC) in a carbonate buffer to give a concentration of approximately 1 mg/ml.

b. Add FITC immediately into the protein solution and react for 2-3 hours in the dark (or wrapped by a foil) at room temperature (mixing ratio: 1 mg FITC/100mg protein)

c. Apply the mixture to a Sephadex column and elute with PBS buffer.

d. Degree of labelling is calculated according to the following formula:

$$C_{FITC} = A_{294} / \varepsilon_{494,FITC}$$

$$C_{Albumin} = (A_{280} - 0.154 * A_{294}) / \varepsilon_{278,Albumin}$$

$$\text{Degree of labelling} = C_{FITC} / C_{Albumin}$$

2.3 Buffer Systems

2.3.1 Buffer for Monolayer Hysteresis Studies

Tris buffers of different ionic strengths were used as subphases in the monolayer experiments. Each Tris buffer was adjusted to pH 7.4 (± 0.1) by adding HCl. Ionic strengths were adjusted with NaCl according to the following recipes, (I = calculated ionic strength):

Buffer 1: 5mM Tris buffer, I=0

Buffer 2: 5mM Tris + 0.02M NaCl, I=0.02

Buffer 3: 5mM Tris + 0.1M NaCl, I=0.1

Buffer 4: 5mM Tris + 0.3M NaCl, I=0.3

Buffer 5: 5mM Tris + 0.5M NaCl, I=0.5

Buffer 6: 5mM Tris + 1.5M NaCl, I=1.5

2.3.2 Buffer for Protein Adsorption Studies

0.379 g Na_2HPO_4 and 0.073 g KH_2PO_4 were dissolved into 1l distilled water to form 50 mM PBS buffer.

2.4 Monolayer Film Balance Studies

Monolayer hysteresis studies were performed on a thermostatted Teflon trough of dimensions 150mm × 475mm (1100 ml volume capacity, KSV Instruments, Helsinki, Finland) (Fig. 2.1). Constant temperature (20°C ± 0.2°C) was maintained by running a water/ethylene glycol mixture through a coil in the Teflon trough base, regulated by a constant-temperature circulation bath (RC6 Lauda, Brinkmann). Surface pressures were measured using the Wilhelmy plate method [59]. A carefully sandblasted platinum plate was cleaned by alternate ethanol rinsing and flaming and was suspended from the KSV electrobalance into the aqueous subphase where surface pressure was recorded as mN/m. A hydrophilic barrier was cleaned with chloroform prior to each experiment. The barrier position was controlled by a microstep-driving stepping motor and was measured using an optical encoder. The buffer surface was cleaned by sweeping the barrier while aspirating the surface with a stainless steel nozzle. Lipid monolayers were formed by applying 80 µl lipid solutions in $CHCl_3$ or $CHCl_3$:EtOH mixture (volume ratio $CHCl_3$:EtOH=9:1) to the surface of the buffer. MBP C-1 or PLL was introduced under lipid monolayers at 0mN/m or 5mN/m by injecting 3 ml polypeptide buffer solution through the surface of the monolayer while traversing the monolayer surface. After injection of the polypeptide (lipid:polypeptide mole ratio = 20:1, diluted to 3ml by the buffer used in the aqueous subphase) under the lipid monolayer and waiting for an incubation period of two hours, the monolayer was compressed at a speed of 0.2 $Å^2$ /molecule/min to 37 mN/m, and then immediately expanded to the maximum molecular area. After waiting for another 40 minutes, the monolayer was compressed again to the monolayer collapse pressure.

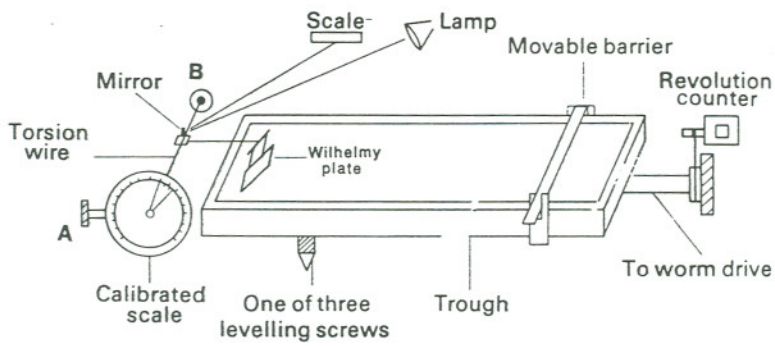

Fig. 2.1 Basic film balance arrangement for monolayer measurements with the Wilhelmy plate [59].

2.5 Circular Dichroism of Polypeptides

Appropriate amounts of DHP (8mM) were sonicated in Tris buffer (pH=8.4) using a 0.5 inch flat titanium tip on a conventional horn energized by a Heat Systems-Ultrasonics W185 sonicator for 10 minutes. The lipid suspension was filtered through 0.22 μm pore size cellulose nitrate membrane filters and centrifuged at 20°C in a TY65 rotor at 36,000 rpm (approx. 100,000g) on a Beckman L5-65 centrifuge for 90 minutes to remove multilamellar vesicles or undispersed lipid, and titanium particles from the sonication horn. The supernatant containing small unilamellar vesicles was carefully decanted and used within 12 hr. Vesicles and polypeptide (vesicles:polypeptide molar ratio=1:0.006) were mixed and diluted to 2 ml with Tris buffer (pH=7.4) and analyzed immediately using a Jasco J-40 instrument.

2.6 Small-Angle X-ray Scattering of Lipid Lamellar L_α Phases

2.6.1 Lipid Lyotropic Liquid Crystal Preparations

A certain amount of lipid (approx. 70 mg) was mixed with water (lipid:water approx. 75:25 w/w) in a glass tube. The tube was flame-sealed and inverted to centrifuge on a bench-top centrifuge (2000 rpm) for 5-10 minutes. This inversion-centrifugation procedure was repeated several times until the lipid sample was fully hydrated. The glass tube was placed in a water bath where the temperature was controlled above the lipid phase transition temperature. Normally, the mixture required 1-2 month(s) to form its respective liquid crystal.

The following lipid or lipid/polypeptide mixtures were prepared for liquid crystal studies. The lipid/water ratios were chosen according to the DMPC phase diagram published by Janiak and coworkers [72].

1. DMPC:H_2O = 70:30 w/w
2. DMPC:DMPA:H_2O = 71.4:3.6:25 w/w/w

3. DMPC:PLL:H_2O = 70.1:5.4:24.5 w/w/w

4. DMPC:DMPA:PLL:H_2O = 67.7:3.4:5.2:24.9 w/w/w/w

2.6.2 Small-Angle X-ray Scattering

Small angle X-ray diffraction studies were carried out using a Phillips XRG-2500 generator, operating at 35 kV and 20 mA, using a sealed, fine-focus copper tube. The X-ray beam was monochromatized using a ß-nickel filter and collimated using a pin-hole collimator. Liquid crystal samples were transfered from glass tubes to Mark capillaries (1mm OD). Diffraction patterns were collected with a linear position sensitive detector (spatial resolution 92 microns) interfaced to a personal computer through a Nuclear Data multichannel analyzer [73]. Sample-to-detector distance (12cm) was adjusted to enable simultaneous detection of small angle diffraction peaks. The d-spacing was calibrated using lead stearate.

The X-ray wavelength is 1.54 Å and the known d-spacing of lead stearate is 50.2 Å [74]. The distance between detector and sample can, therefore, be accurately obtained. A calibration scan was performed whenever the sample-to-detector distance was changed. A DMPC powder sample was performed (Fig. 2.2) after the lead stearate calibration and compared very well with previously published data [75]. The d-spacing of sample liquid crystals can be calculated according to Bragg's Law [76].

2.7 Total Internal Reflection Fluorescence (TIRF) Experiments

2.7.1 Quartz Silanization.

The quartz slides were cleaned by ultrasonication in concentrated sulfuric acid for 1 hour and followed by EtOH and chloroform rinsing. The cleaned slides were then immersed in a solution containing 1% octadecyltrichlorosilane-8% chloroform-12% carbon tetrachloride-76%hexadecane (volume ratio) for 15 minutes while sonicating at

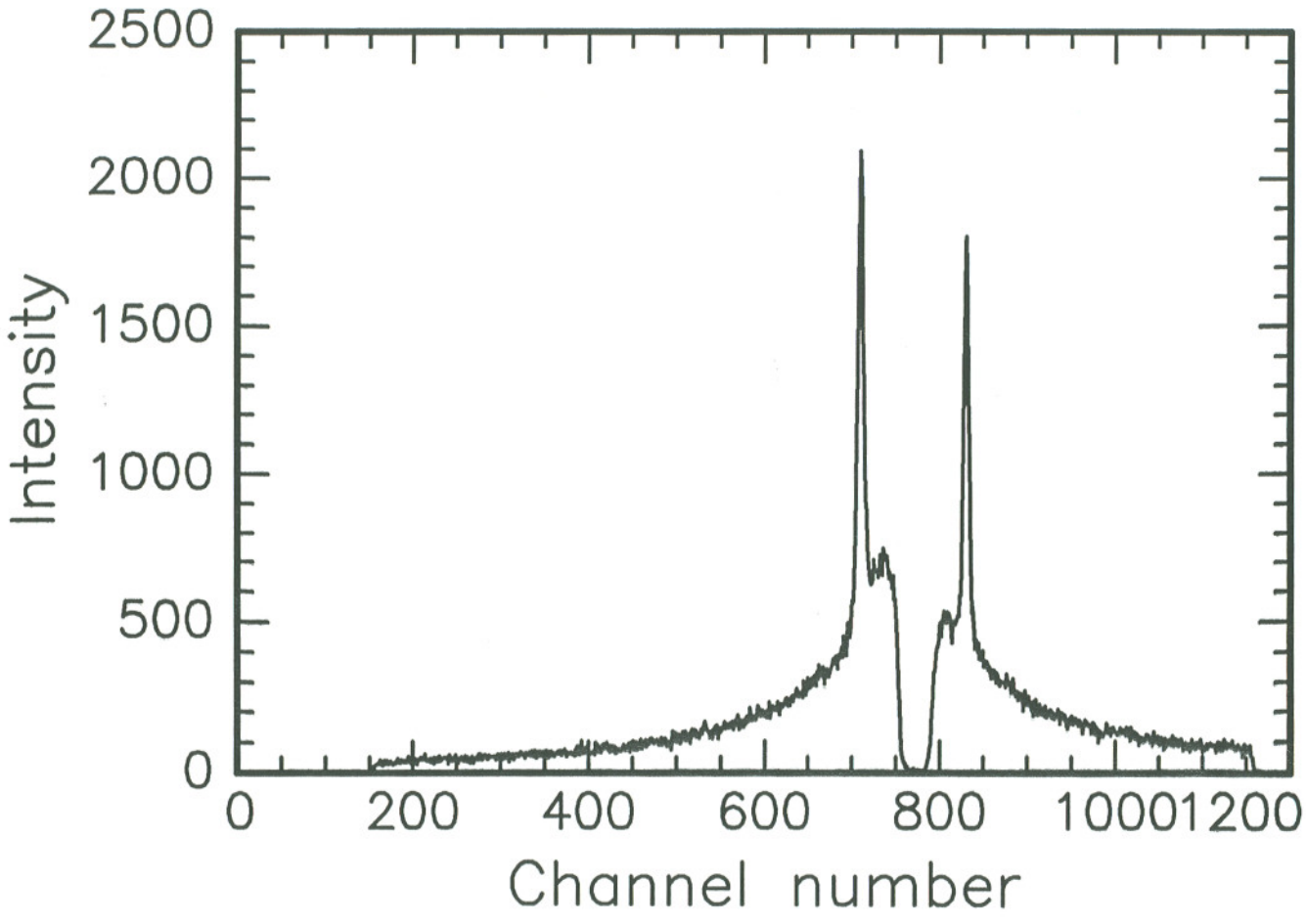

Fig. 2.2 Small-angle X-ray diffraction diagram for DMPC powder at 25°C.

same time [77]. The silanized surface was rinsed with chloroform three times and stored in chloroform solution until used.

2.7.2 Supported Lipid Films

Lipid-chloroform solutions were spread onto the KSV film balance surface, compressed to the desired surface pressure (in the liquid-condensed phase) and held until the surface pressure was stable (roughly 10 minutes) before dipping. For supported DMPC bilayers, the best dipping pressure was 40 mN/m and that for DMPG was 50 mN/m. The silanized quartz slides were dipped vertically from air through the lipid monolayer into the subphase at a speed of 2 mm/min. After film transfering, the supported lipid films on quartz were kept under water in vials until used.

2.7.3 TIRF-CCD Apparatus and Protein Adsorption Experiments

The TIRF apparatus consisted of an Ar^+ ion laser (Model 95, Lexel), laser beam manipulation optics, a TIRF flow cell, fluorescence collection optics, a monochromator (1681C, Spex) with 300 grooves/mm grating and a charge-coupled device camera [Thompson CFS TH7882CDA CCD with UV response coating, a CC200 camera controller, a CH220 liquid cooled camera head, a LC200 liquid-circulation unit, a CE200 camera electronics unit with 50 kHz 140-bit A/D converter, and a RS1770 video option (Photometrics)]. The CCD detector was cooled to -46°C to minimize dark current. The CCD camera controller was connected to a computer (MacII, Apple) via a DMA board (National Instrument, NBDMA-8) for data processing and display. The schematics of the apparatus optics was given in Fig. 2.3. The 488-nm laser beam was collimated with a 10-cm-f.l. lens (2 cm diameter) and passed through a rectangular beam mask (3×10mm). The beam was directed by the mirror normal to the face of the 70°-cut dovetail fused-silica prism, which served as an internal reflection element. The quartz with supported lipid film on it was optically coupled to the largest face of the

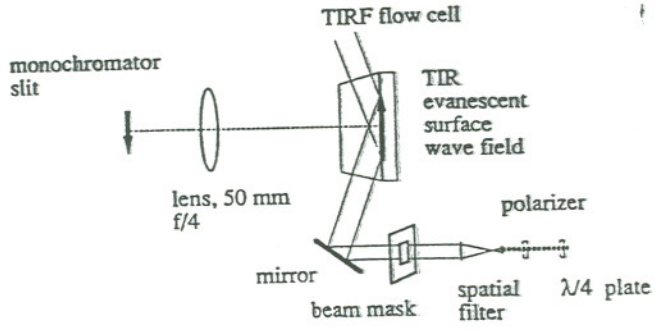

Fig. 2.3 Schematic representation of the TIRF apparatus optics [78].

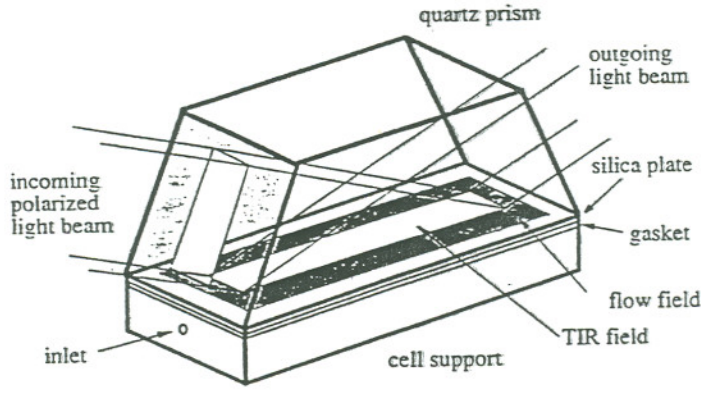

Fig. 2.4 Schematic representation of the TIRF flow cell [78].

prism with the use of glycerol. The beam was totally reflected at the interface between the the quartz and buffer solution. The area illuminated by the beam undergoing total internal reflection was in the middle of the TIRF flow field and has the size of 3×30 mm. The dimensions of the flow field were $0.5 \times 5 \times 60$ mm and were determined by the size of silicone rubber gasket. Fig. 2.4 shows the schematic set-up of the TIRF flow cell and the total internal reflection area inside the flow field. The flow cell for the TIRF experiment was designed to avoid the depletion of bulk adsorbate concentration, or to avoid transport-limited adsorption process. The area illuminated by the total internal reflection was focused with a 50-mm, f/4 macro lens (Pentax, Asahi Co.) on the entrance slit of the monochromator. The width of the slit was 2mm. The CCD camera was placed at the exit plane of the monochromator and oriented with its short axis along the slit axis and with its long axis with the dispersion axis of the monochromator. The total wavelength coverage was approximately 120 nm. The grating was adjusted so that the scattered 488-nm excitation light did not fall on the face of the CCD array ($\lambda_{central} = 572$ nm). An exposure of 1s was imaged onto the middle part of CCD array. An exposure of 1s was used in combination with the sequence CCD command. Three hundred exposures of 1s duration were made in a sequence. Total elapsed time for completion of these operations was 300s. Four of these "adsorption" images were collected one after another: during the first two 300-s intervals the labelled albumin solution was directed at a speed of 0.49 ml/min through the TIRF cell and during the other two 300-s intervals the flow was switched to the buffer solution at a speed of 1.5 ml/min in order to follow the desorption of adsorbed protein. After subtracting the background noise, these four images were combined into a 384×1200 pixels "adsorption-desorption" image, and this image was then transferred to the computer and saved for further processing. Altogether protein was adsorbed for 10 min from a flowing protein solution and subsequently desorbed for 10 min from a flowing buffer solution [78].

Chapter 3

Results and Discussion: Comparisons of Myelin Basic Protein Charge Isomer C-1 and Poly-l-Lysine Interactions with Lipid Monolayers

3.1 Interactions of Dimyristoylphosphatidic Acid (DMPA) with PLL and MBP C-1.

Phosphatidic acid (PA) does not exist in the myelin sheath, however, comparison of different polar head group structures between PA and other acidic phospholipids is useful in the study of its interaction with MBP [7]. The application of dimyristoylphosphatidic acid (DMPA) in this research has proven helpful to further approach the mechanism of the interaction between MBP and acidic phospholipid and understand the influence of intermolecular hydrogen bonding in the head group region.

3.1.1 Monolayer Isotherms of Dimystoylphosphatidic Acid (DMPA) on Subphases of Varying Ionic Strength

The surface pressure-area (π-A) curves for DMPA at various salt concentrations are depicted in Fig. 3.1. The isotherm at 0.1M NaCl compares well with that published by Demel and coworkers [55]. The DMPA monolayer undergoes a two-dimensional first-order phase transition from the liquid-expanded state to the liquid-condensed state at all salt concentrations studied. For salt concentrations below 0.3 M, the onset of the liquid expanded phase is 92.4 $Å^2$/molecule, and for concentrations above 0.5M, the onset of /molecular area moves to 98.3 $Å^2$/molecule. The phase transition pressures (liquid expanded to liquid condensed) differ from each other as shown in Table 3.1. The phase transition onset pressure for 0.1M salt subphase is 11.8 mN/m. Increasing

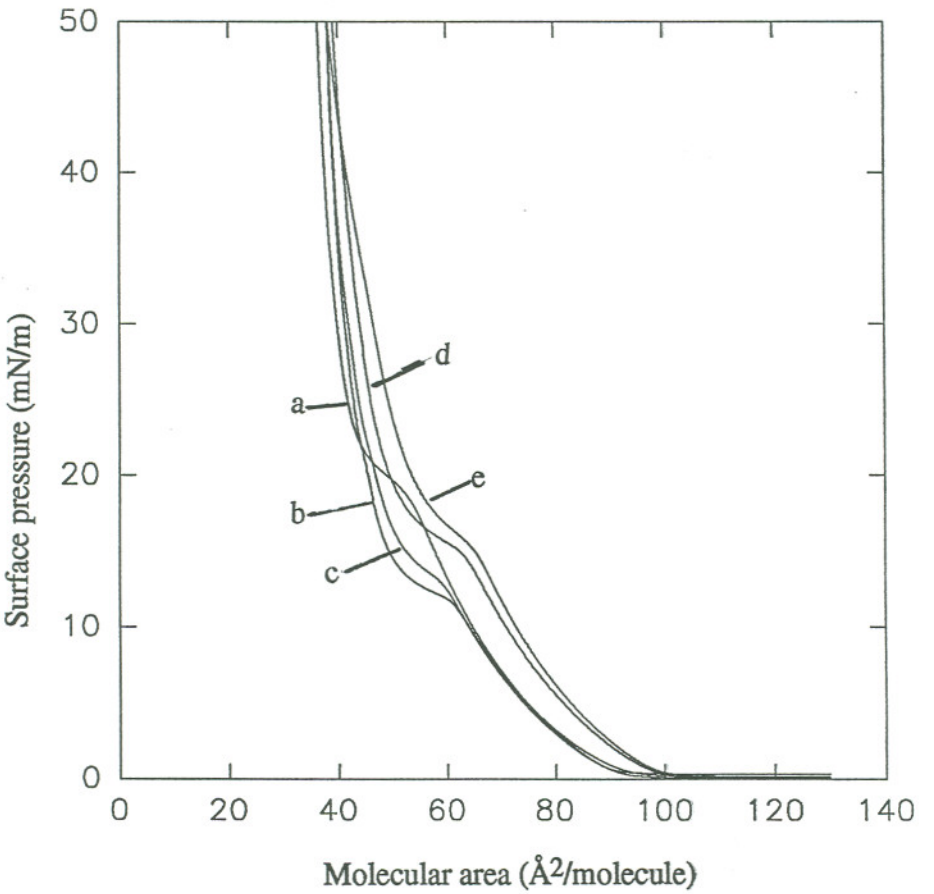

Fig. 3.1 Surface pressure-area isotherm of DMPA on subphases (pH=7.4 ± 0.1) of varying ionic strength: a. 5mM Tris b. 5mM Tris + 0.1M NaCl c. 5mM Tris + 0.3M NaCl d. 5mM Tris + 0.5M NaCl e. 5mM Tris + 1.5M NaCl

Table 3.1 Comparison of Isotherm of Varying Ionic Strength

salt concentration (M)	onset molecule area ($Å^2$/molecule)	phase transition pressure (mN/m)
0.0	92.4	18.3
0.1	92.4	11.8
0.3	92.4	12.7
0.5	98.3	14.7
1.5	98.3	15.2

the salt concentration also increases the onset pressure. In the absense of salt, however, the phase transition pressure of DMPA reaches 18.3 mN/m, as the ionization state of the phosphate group plays a role in all these differences among the isotherms [55,79]. Although intermolecular hydrogen bonding can compensate for some head group charge, the electrostatic repulsion between neighboring head groups becomes stronger as the monolayer is compressed. This induces a high phase transition pressure between LE and LC states. Addition of salt can decrease this repulsion and consequently lower the phase transition pressure. However, increasing the salt concentration from 0 to 0.5M NaCl lowers the pK_{a2} of PA from 9.0 to 7.5 by shielding the charge and lowering the surface potential [70,80]. This changes the ionization state of the PA head group, from $DMPA^{-1}$ to $DMPA^{-2}$. $DMPA^{-2}$ has higher energy in the gel phase than $DMPA^{-1}$ because of $DMPA^{-2}$ tiltings in the gel phase as well as of the loss of intermolecular interaction, therefore the phase transition pressure increases again [81-82]. Since Na^+ ions break the intermolecular hydrogen bonding, the lipid molecule occupies more area without the bonding than with the bonding.

3.1.2 DMPA Interactions with PLL in Lipid Monolayers

Fig. 3.2 shows the interaction between DMPA and PLL in monolayers. The binding of PLL to DMPA dramatically condenses the DMPA monolayer, resulting in a 34 $Å^2$/molecular area reduction at the onset of surface pressure. Such a significant change is brought about by charge neutralization of anionic DMPA molecules by adsorbing cationic PLL.

The characteristic transition from the liquid-expanded to liquid-condensed phases for DMPA is removed as a result of PLL binding to DMPA monolayers. A small but detectable hysteresis is observed, indicating some PLL is removed by the compression-expansion process. The second compression curve shows nearly the same take-off point as the first compression curve, but does not overlap upon further

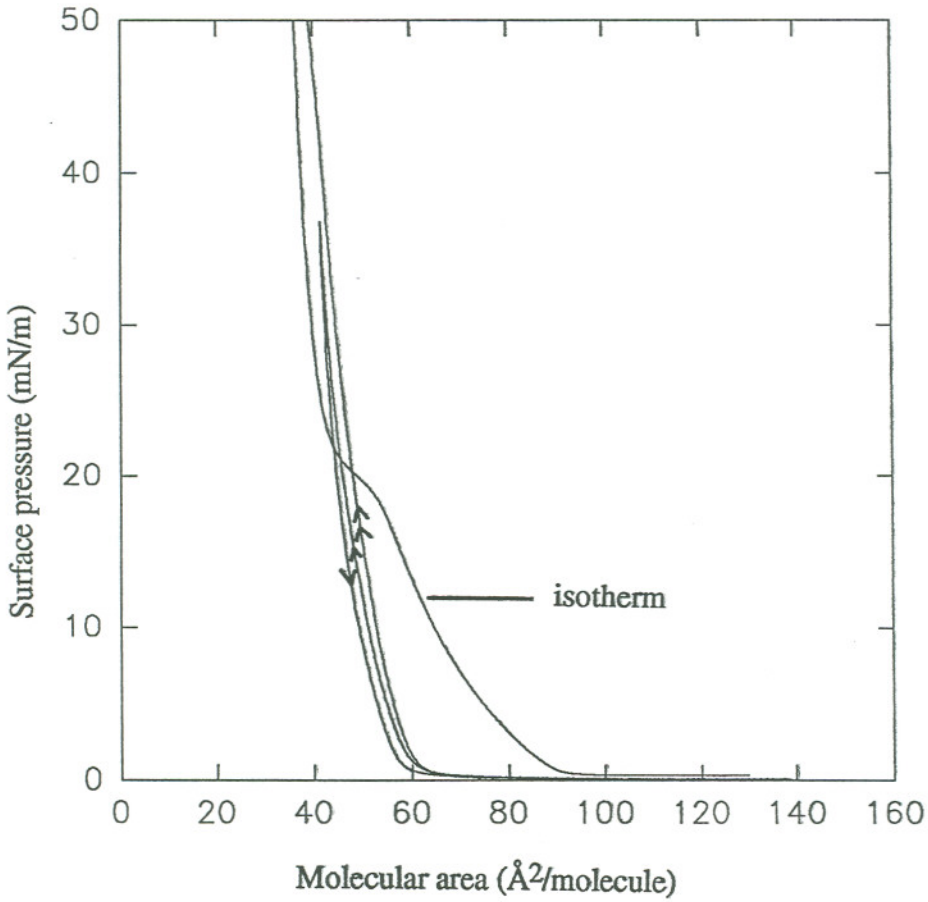

Fig. 3.2 Monolayer hysteresis of DMPA with PLL on 5mM Tris (pH=7.4 ± 0.1) buffer subphase.

compression, indicating that the monolayer packing properties have changed, and that some irreversible conformation change of lipid has occurred, although almost all the lost protein has recombined onto the DMPA monolayer again with subsequent expansion and a 40 minute waiting time.

Salt studies show that a larger hysteresis is obtained after the addition of NaCl into the monolayer subphase. Fig. 3.3 graphs molecular area differences for DMPA monolayers on subphases of various ionic strength at 4 mN/m and 25 mN/m. At 4 mN/m, the monolayer is in the liquid-expanded phase and at 25 mN/m is in the liquid-condensed phase. These surface pressures are chosen to best express the interaction differences before and after the phase transition. As pointed out above, the stronger the interaction, the larger the observed hysteresis or the more significant area reduction. Molecular area reduction in the liquid-expanded phase increases up to a salt concentration of 0.3 M, and decreases when more salt is added to the subphase. This area loss, however, is still larger than that in the absense of salt. It appears that the addition of NaCl promotes the interaction between DMPA and PLL.

Since the pK_{a1} of DMPA is 3.5 and pK_{a2} is 9, the DMPA head group has one negative charge at physiological pH. When DMPA chloroform solution is spread onto a Tris buffer subphase (pH=7.4), it tends to bind water strongly because of the direct, quantum-mechanical interaction [83] or the hydrogen bonds between the water molecules and the head group. This membrane hydration depends on the net surface charge density and the membrane surface electrostatic properties. Fig. 3.4 shows the possible intermolecular hydrogen bondings between adjacent head groups in addition to their hydrogen bonds with water. Hydrogen bonding disperses the charge of the head groups and as a result, the net apparent charge of the lipid is reduced. This lowers the interaction energy between PLL and DMPA and costs cationic PLL more energy to bind the DMPA head group, indicated as a small hysteresis obtained in the experiment.

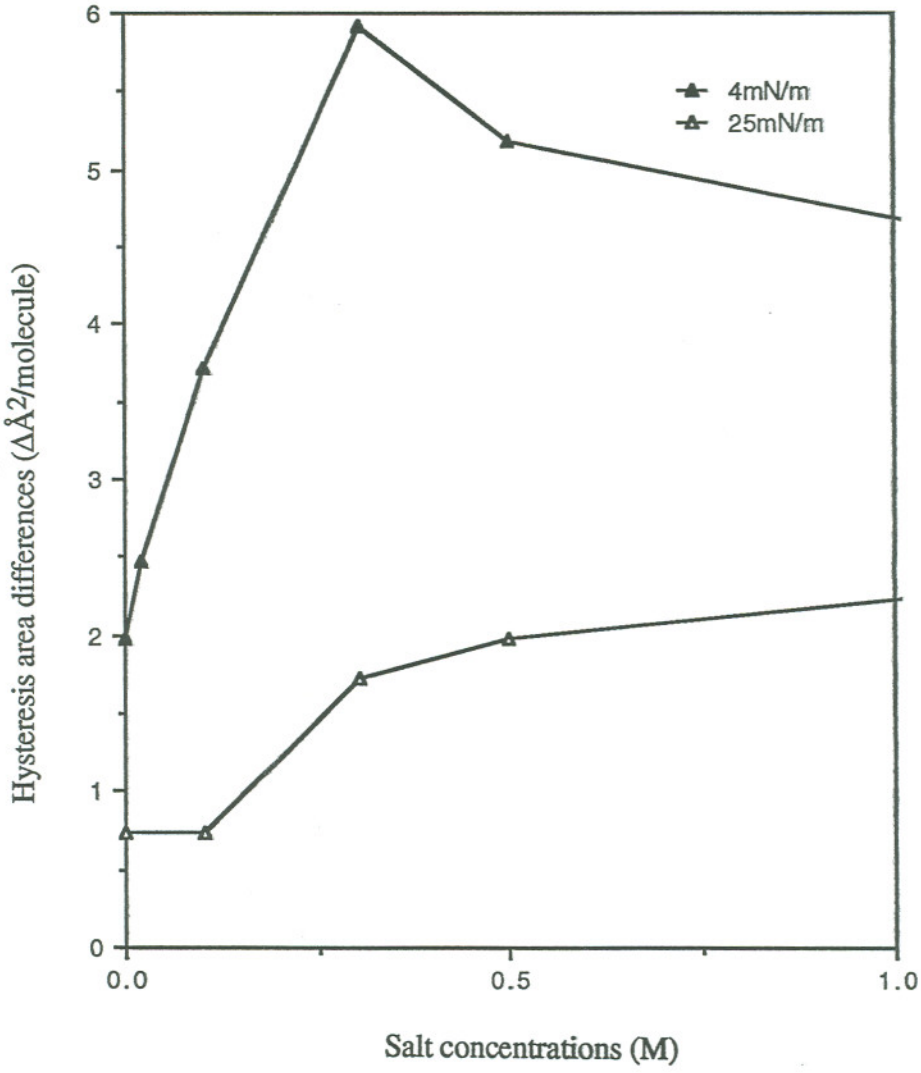

Fig. 3.3 Molecular area differences for DMPA monolayers with PLL on subphases of various ionic strength at 4 mN/m and 25 mN/m. Subphases: 5mM Tris buffer + various salt concentrations (pH=7.4 ± 0.1).

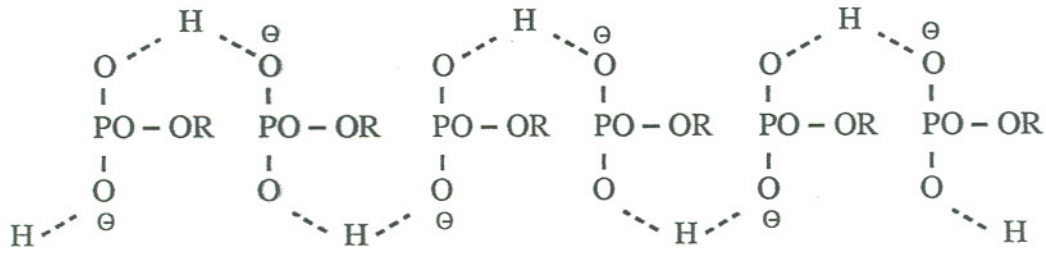

Fig. 3.4 Schematic representation of DMPA intermolecular hydrogen bonding between adjacent lipid head groups [51].

Addition of Na^+ ions changes the structure of the surface double layer. Although the majority of ions in the double layer are only weakly associated with the membrane surface, relatively few Na^+ ions that bind intimately to the membrane components will affect the membrane function and structure significantly. This yields two effects. On the one hand, tightly bound Na^+ ions will shield the negatively charged head groups to prevent PLL from attaching to anionic head groups. On the other hand, the existence of Na^+ ions breaks intermolecular hydrogen bonds in the head group region and consequently increases the apparent charge of each DMPA head group. This increases the interaction between the cationic polypeptide and DMPA. A larger hysteresis, therefore, is observed when more Na^+ ions are added.

By comparing the salt effects on the interaction of PLL with DMPA, one can determine how hydrogen bonding changes in DMPA affect PLL adsorption onto the DMPA monolayer. With increasing salt, DMPA demonstrates an increased interaction with PLL. Comparing the isotherms at different salt concentrations (Fig. 3.1), one can find that the take-off molecular area increases at 0.5 M, indicating that the breaking of hydrogen bonds occurs between 0.3M-0.5M. The greatest apparent negative charge of the DMPA monolayers found on the subphase makes lipid interact strongly with the PLL, and the largest hysteresis is observed under these conditions. At higher concentrations, charge screening effects dominate and this interaction decreases. This effect may also be due to the dehydration of PLL at high salt concentrations [64].

Although the interaction decreases on a 1.5M salt subphase, it is still stronger than that without salt. In the absence of salt, the Helmholtz layer surrounding the head group is composed solely of water. It is difficult for PLL to approach the anionic interface under these conditions because of the high resistance of displacing bound water. After adding salt, water molecules are replaced by Na^+ ions. Small size of Na^+ ion and the thin double layer enhances PLL's approaching and binding. On the other hand, the positively charged NH_3^+ group in PLL and the Cl^- counterion in subphase

can also form a loosely-bound ion pair which help it approach the DMPA head group.

3.1.3 Interaction of DMPA with MBP C-1 in Lipid Monolayers

Fig. 3.5 shows the interaction between DMPA and MBP C-1 in monolayers. Compared to the interaction of PLL with DMPA, the hysteresis curve shows condensation of molecular area from 90.9 $Å^2$/molecule to 71.6 $Å^2$/molecule. The plateau phase transition region in the pure DMPA isotherm is replaced by two inflections at 12 mN/m and 17 mN/m. A small hysteresis is observed, indicating a certain amount of protein is lost during the compression-expansion process. The take-off point of the second compression curve is even smaller than the expansion curve, and shows a different behavior from the hysteresis curve, suggesting that lost protein does not rebind to the DMPA monolayer during the 40 minutes relaxation time and also that remaining MBP C-1 has rearranged its binding to DMPA.

Similar to PLL, the addition of NaCl increases the interaction between MBP-1 and DMPA. The molecular area difference versus salt concentration plot shows similar behavior as that for PLL in a range up to 0.5M (Fig. 3.6). However, at 1.5M, instead of exhibiting a drop in area loss as for PLL with DMPA, MBP C-1 shows strong interaction with DMPA, indicating the differences between MBP C-1 and PLL. According to the Gouy-Chapman theory, the thickness of the ionic cloud depends strongly on the ion concentration and the charge type of the electrolyte. At high salt concentration, the diffuse layer is very thin, and the protein can approach quite close to interface before the electrostatic repulsion becomes significant. By that time the van der Waals attraction is already quite significant, allowing initial polypeptide binding (see section 3.8) [83]. This effect holds for both PLL and MBP C-1. However, the hydrophobic sequences intrinsic to MBP C-1 allows this protein to penetrate the monolayer after this initially interfacial binding event. The hydrophobic interaction between MBP C-1 and DMPA becomes obvious.

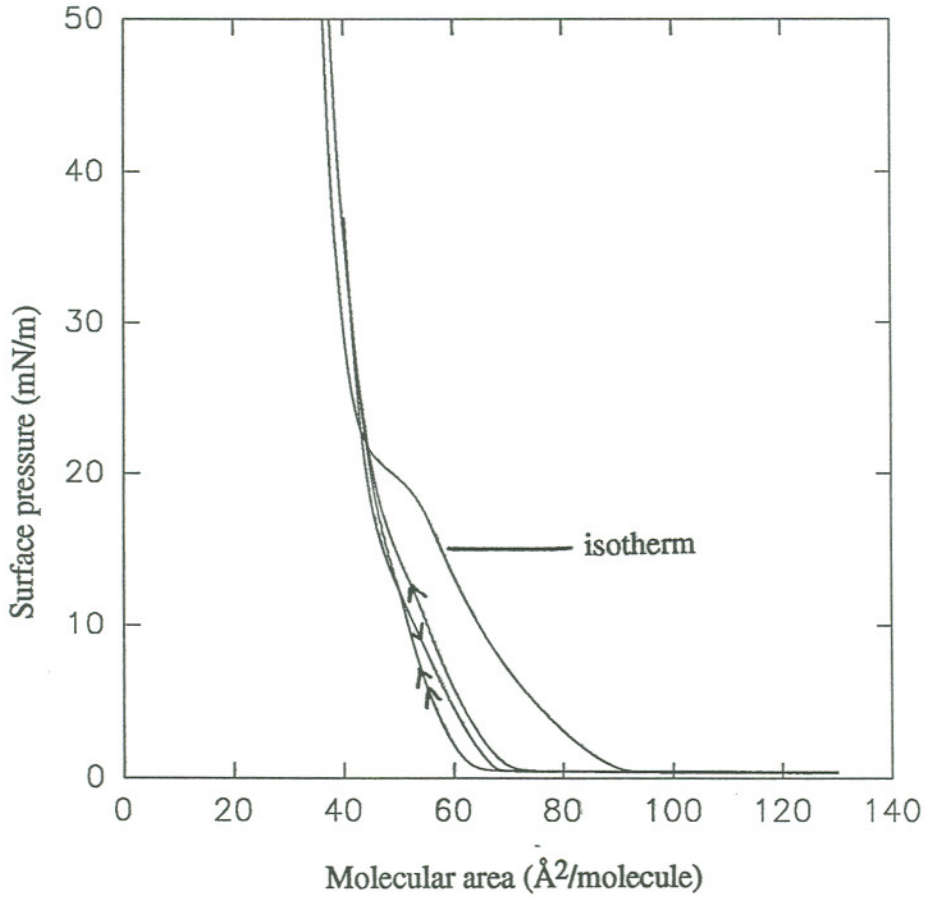

Fig. 3.5 Monolayer hysteresis of DMPA with MBP C-1 on 5mM Tris (pH=7.4 ± 0.1) buffer subphase.

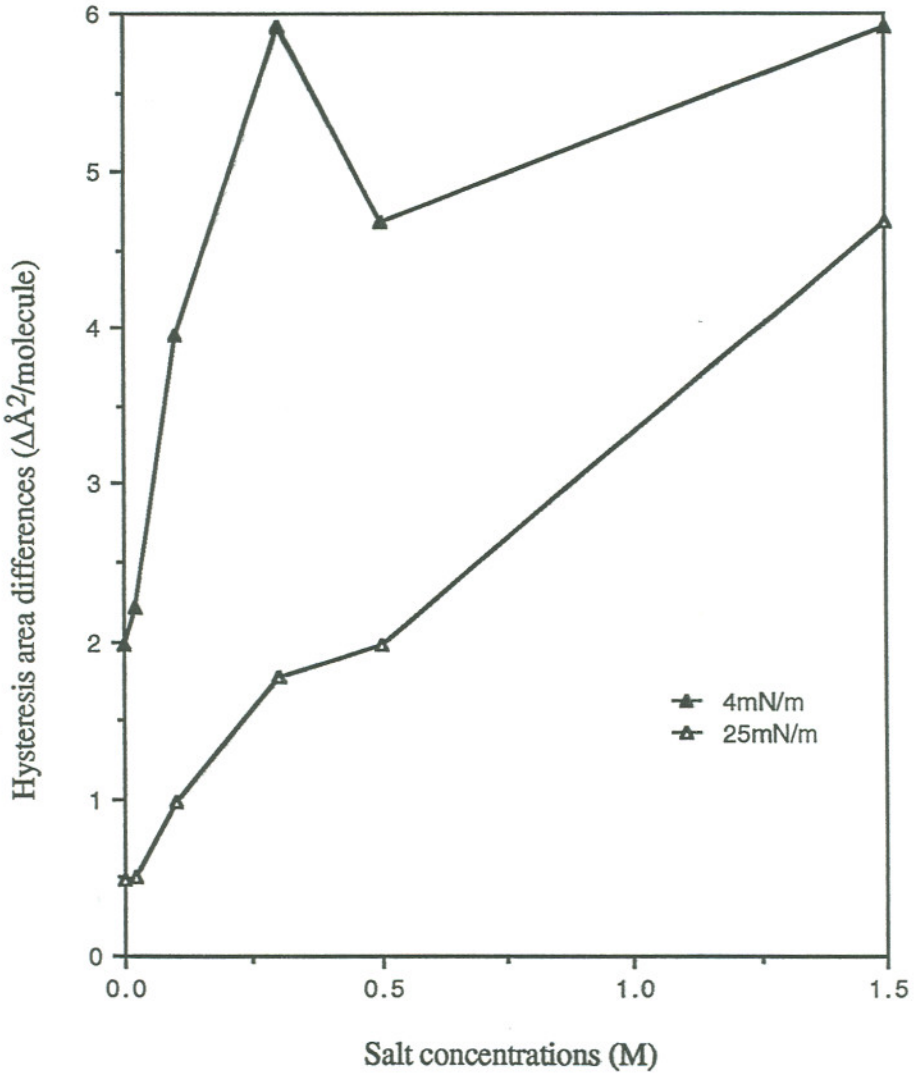

Fig. 3.6 Molecular area differences for DMPA monolayers with MBP C-1 on subphases of various ionic strength at 4 mN/m and 25 mN/m. Subphases: 5mM Tris buffer + various salt concentration (pH=7.4 ± 0.1).

3.1.4 Polypeptides Condensing and Expanding Effects on Monolayers

By plotting the molecular area difference between DMPA pure lipid isotherms and hysteresis curves at the onset pressure versus salt concentration (Fig. 3.7), we find that at low salt concentrations (< 0.1M), the monolayer molecular area differences of DMPA exceed 20Å^2 due to the existence of polypeptides under the DMPA monolayer. This condensing effect is observed until 0.1M and then exhibits a consistent decrease with increasing ionic strength. As mentioned in sections 3.1.2 and 3.1.3, at relatively high salt concentrations (>0.1M), the polypeptides still maintain strong interactions with DMPA. This condensing effect demonstrates that the interaction mechanism at higher salt concentrations is different from those at lower salt concentrations.

3.2 Interaction of Ganglioside GM1 Monolayers with PLL and MBP C-1

3.2.1 Monolayer Isotherms of Ganglioside GM1 on Subphases of Varying Ionic Strength

The surface pressure-area isotherms of GM1 lipid on subphases varying in salt concentration are shown in Fig. 3.8. The differences among these curves on different subphases are qualitatively quite similar and the main features are comparable to each other. The molecular area differences of onset surface pressure are due to differences in the magnitudes of intermolecular hydrogen bonding in the large head groups [23].

3.2.2 Interaction between Monolayers of Ganglioside GM1 and PLL

Hysteresis isotherms for monolayers of ganglioside GM1 on 5mM Tris subphases containing PLL are shown in Fig. 3.9. GM1 is negatively charged due to a single sialic acid moiety and contains a significantly larger bulky polar head group compared to most other lipids. Injection of PLL induces the condensation of GM1

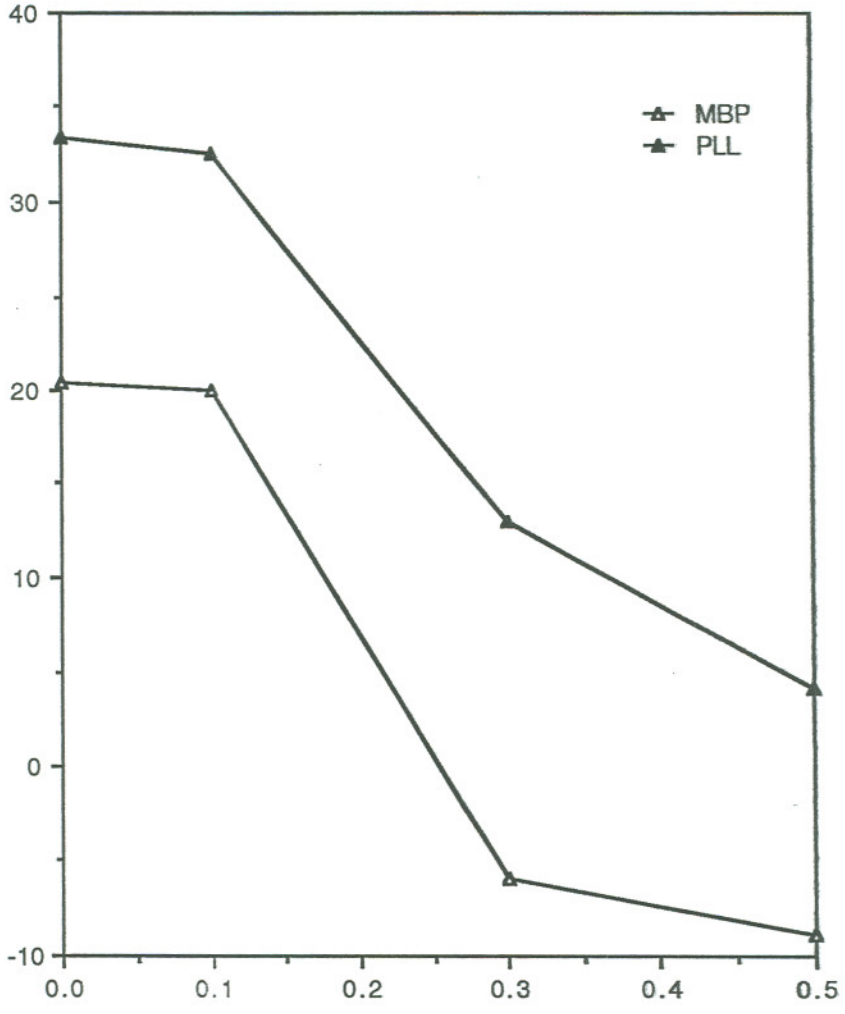

Fig. 3.7 MBP C-1 and PLL condensing and expanding effects on DMPA monolayers. Subphase: 5mM Tris buffer + various salt concentration (pH=7.4 ± 0.1).

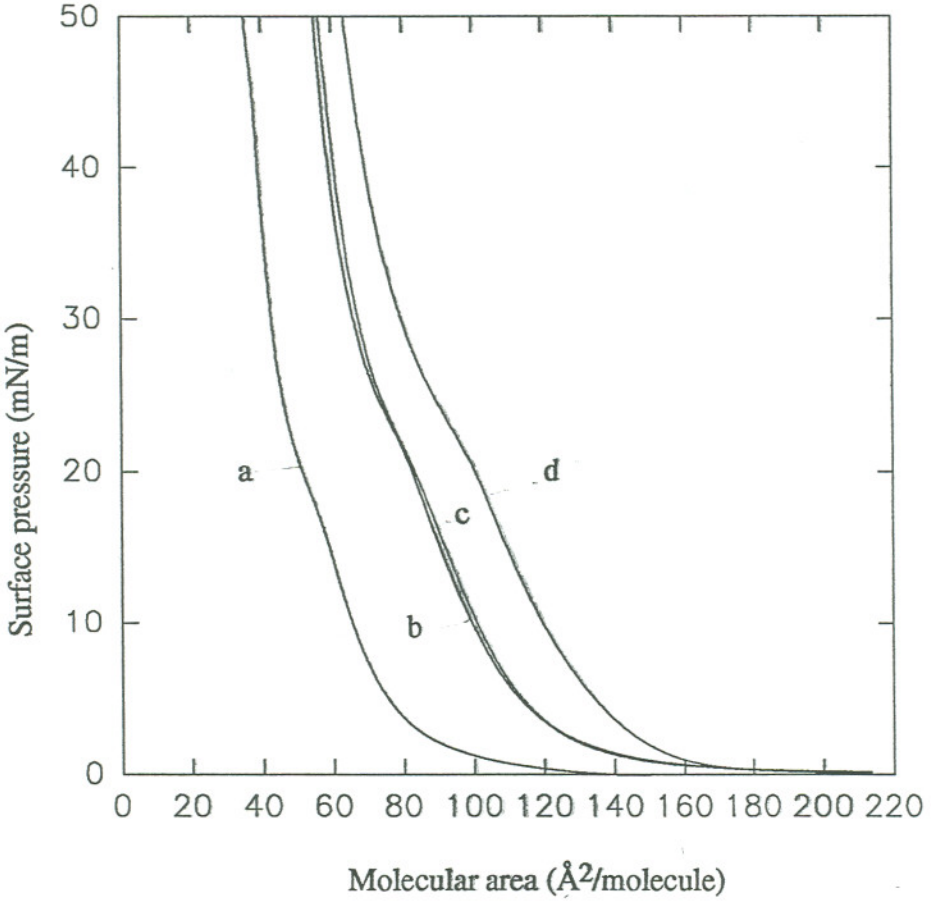

Fig. 3.8 Surface pressure-area isotherm of GM1 on subphases varying ionic strength (pH=7.4 ± 0.1). a. 5mM Tris b. 5mM Tris + 0.3M NaCl c. 5mM Tris + 0.5M NaCl d. 5mM Tris + 1.5M NaCl

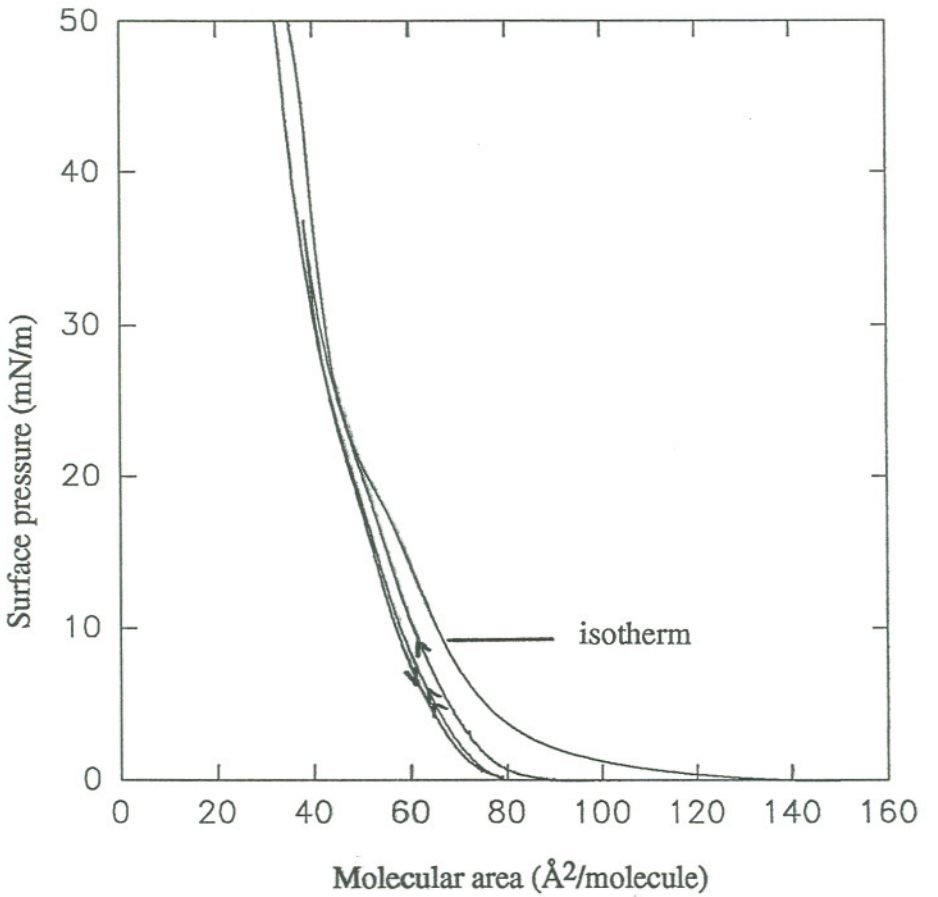

Fig. 3.9 Monolayer hysteresis of GM1 with PLL on 5mM Tris subphase (pH=7.4 ± 0.1).

monolayers, causing the LE onset to shift from 140 Å^2/molecule to 86 Å^2/molecule, nearly a 50% reduction in molecular area. Moreover, the addition of PLL erases the LE/LC phase transition seen at nearly 19 mN/m in the pure isotherm. This behavior is similar to that observed in DMPA. After 40 minutes' reincubation time after expansion, the second hysteresis compression curve nearly overlaps the previous expansion curve, indicating that PLL which ejects from the lipid interface during the compresion-expansion process does not readily recombine with the GM1 monolayer. The process of PLL desorption appears to be irreversible.

Addition of NaCl to the Tris subphase dramatically increases the interaction between GM1 and PLL. Fig. 3.10 shows the hysteresis molecular area differences between the first compression and expansion at various surface pressures as a function of subphase salt concentration. At 4 mN/m, the GM1 monolayer is in the liquid-expanded phase, and at 21 mN/m it is in the liquid-condensed phase. Much larger hysteresis is obtained in the liquid-expanded phase, indicating that PLL prefers to interact with GM1 at the liquid-expanded phase region at the same salt concentration. The increasing trend at two surface pressures is the same, suggesting a similar interaction mechanism among these lipid phase regions.

Hysteresis area differences increase as subphase salt concentration increases, even at 1.5M. Addition of Na^+ ions screens the negative charge of the GM1 head group. However, this effect does not become dominant in the GM1-PLL interaction. Na^+ ions appear to promote the interaction between GM1 and PLL. The existence of Na^+ breaks the intermolecular hydrogen bonding in the GM1 head group, perhaps exposing the sialic acid residue more to the subphase. At high ionic strength PLL is dehydrated. All these may be the factors for increasing interaction. GM1-PLL and DMPA-PLL interactions are distinctly different from each other. Despite the differences in the hydrocarbon chains between these two, the size of head group region must play the dominant role in this effect.

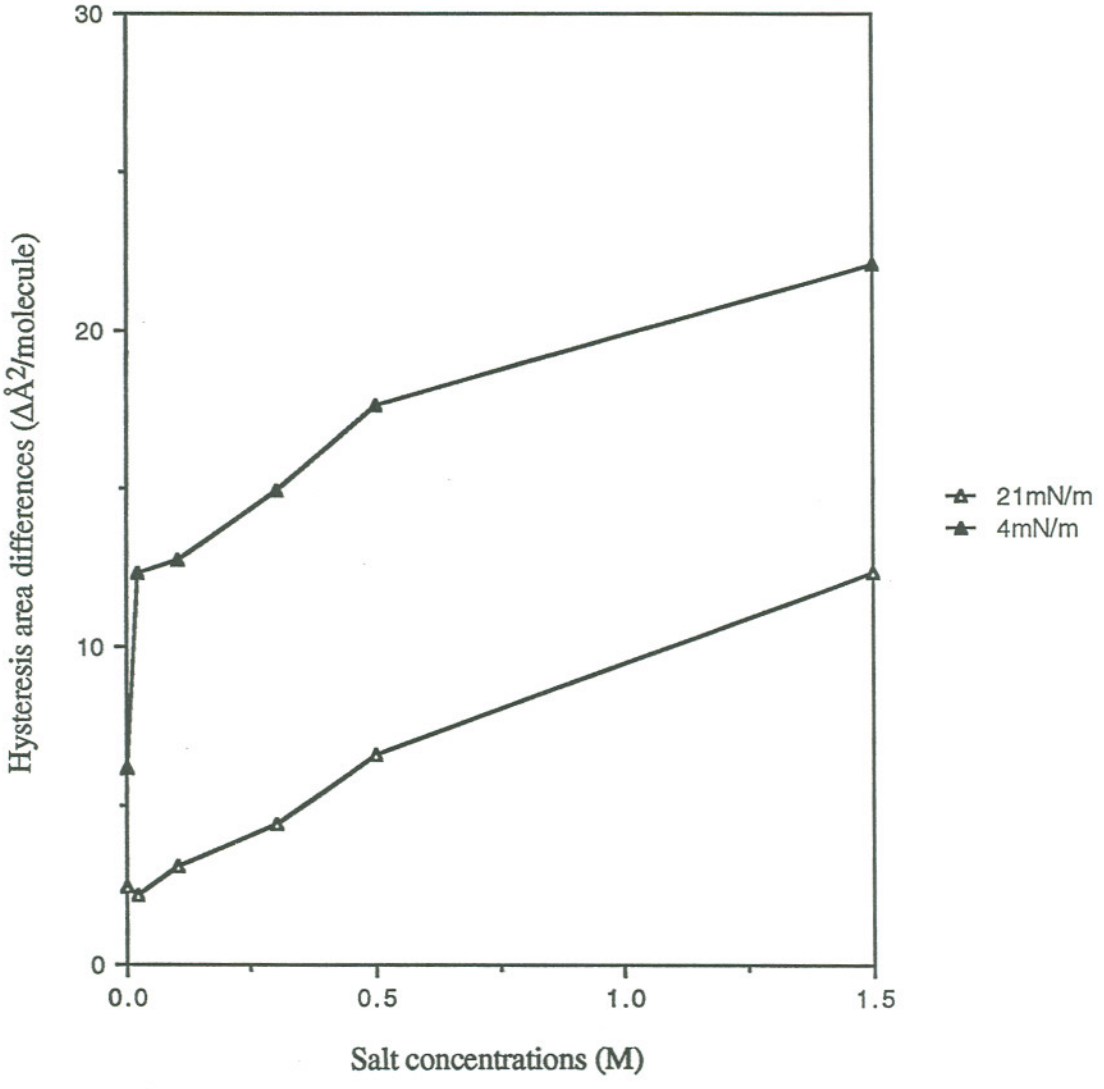

Fig. 3.10 Molecular area differences for GM1 monolayers with PLL on subphases of various ionic strength at 4 mN/m and 21 mN/m. Subphases: 5mM Tris buffer + various salt concentration (pH=7.4 ± 0.1).

3.2.3 Interactions of Ganglioside GM1 Monolayers with MBP C-1

Contrary to PLL, GM1 monolayer interaction with MBP C-1 consistently induces expansion of monolayer molecular area, although the expansion is only 35 Å^2/molecule (Fig. 3.11). This interaction results in a relatively larger hysteresis than observed in GM1 with PLL, suggesting that a strong interaction occurs between GM1 and MBP. Because of the existence of MBP, the GM1-MBP C-1 monolayer has a higher surface pressure at same molecular area than the pure GM1 monolayer. At an area of 100 Å^2/molecule, surface pressure for GM1-MBP C-1 increases to 3.4 mN/m compared to only 1.2 mN/m for GM1, indicating that MBP C-1 strongly perturbs the GM1 head group and that the additional penetration of sequences parts of the protein gives rise to a high lateral surface pressure.

After monolayer expansion and relaxation for 40 minutes, the protein expelled during compression does not recombine into the lipid membrane since surface pressure onset of the second compression curve overlaps the expansion curve at surface pressures below 8 mN/m. However, the remaining of MBP C-1 adsorbed to the lipid interface is observed to influence the structure of GM1-MBP C-1 monolayer. At surface pressures above 8 mN/m, the second recompression curve has a much smaller molecular area than the expansion curve -- even smaller than pure isotherm at same surface pressure. More MBP C-1 proteins are removed from the monolayer and the molecular packing changes under the influence of MBP C-1 adsorbing and significant MBP C-1 penetrating the lipid interface.

The molecular area differences at lateral surface pressures of 4.1 mN/m, and 20.8 mN/m as a function of salt concentration are shown in Fig. 3.12. Similar to PLL, MBP C-1 interacts strongly with GM1 in the liquid-expanded phase (4.1 mN/m). At surface pressures higher than the phase transition pressure (20.8 mN/m), the molecular area remains constant until 0.5 M. In the liquid-expanded phase, the interaction shows a slight decrease after 0.3 M, suggesting that increasing ionic strength has more effects

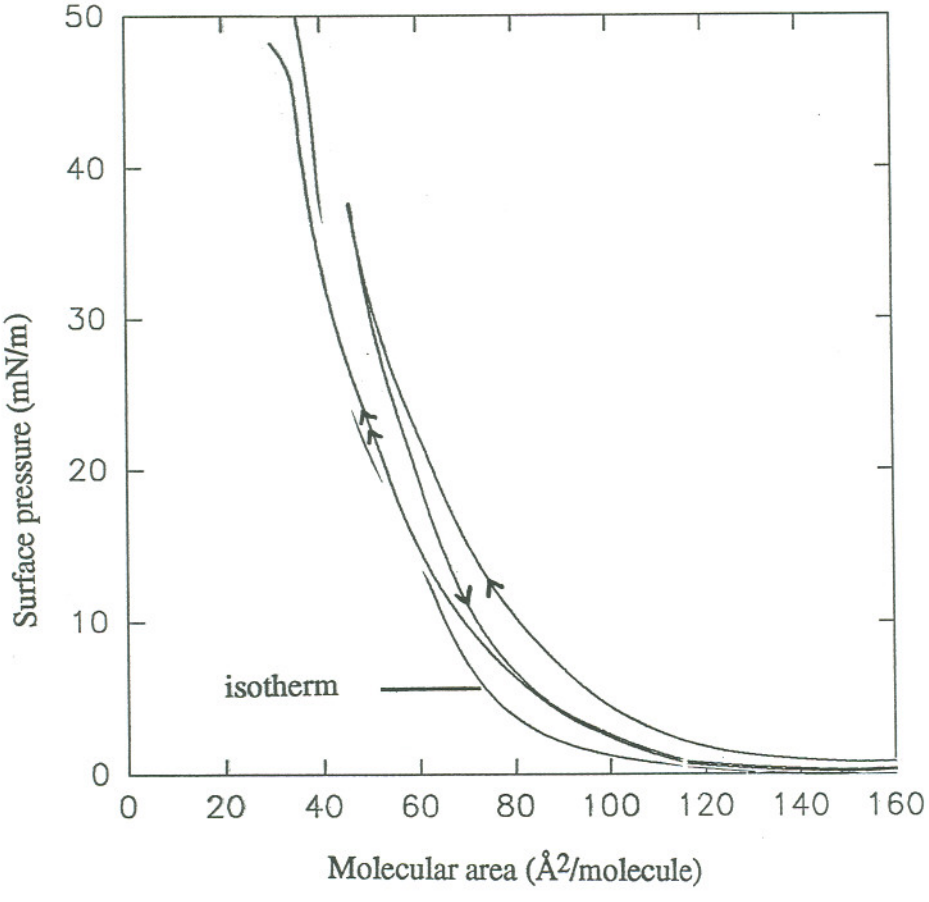

Fig. 3.11 Monolayer hysteresis of GM1 with MBP C-1 on 5mM Tris buffer (pH= 7.4 ± 0.1).

on the lipid liquid-expanded phase than on the liquid-condensed phase. Comparing Fig. 3.11 with Fig. 3.12, the trends of the curves are different, indicating that two different mechanisms exist in these two interactions. The GM1-MBP C-1 interaction is stronger than the GM1-PLL interaction at the same salt concentration. One explanation is that the large head group of GM1 can provide more opportunities for MBP C-1 to interact hydrophobically.

3.3 Interactions between DMPC Monolayers and PLL and MBP C-1

The electrostatic dependence of PLL interaction with zwitterionic DMPC lipid membranes is demonstrated in Fig. 3.13. PLL interaction with DMPC monolayers shows no detectable hysteresis. The second compression curve overlaps the first compression curve. Although the hysteresis isotherm containing PLL shows a slight condensation of the monolayer at gas and liquid-expanded phase, there is very little evidence for any significant interactions between the components in this system. The small condensation effect may be due to a small perturbation on the DMPC head group by PLL adsorption.

Interaction of MBP C-1 with DMPC monolayers shows a slight hysteresis at surface pressures below 10 mN/m (Fig. 3.14). After the monolayer is expanded to the maximum molecular area, surface pressure remains at 2.3 mN/m, indicating there are some significant associations between DMPC and MBP C-1 in the liquid-expanded phase to produce this finite surface pressure. When the monolayer is recompressed after 40 minutes, it immediately enters the liquid-expanded phase. The surface pressure of the expansion curve is greater than that of the first compression curve. It is evident that expansion allows more proteins to penetrate into the monolayer at large molecular areas. During the reincubation period some MBP C-1 associate with DMPC monolayers again. Comparing the pure isotherm of DMPC and the hysteresis of DMPC-MBP C-1, the monolayer is expanded by 14.1 $Å^2$ in the presence of MBP C-1.

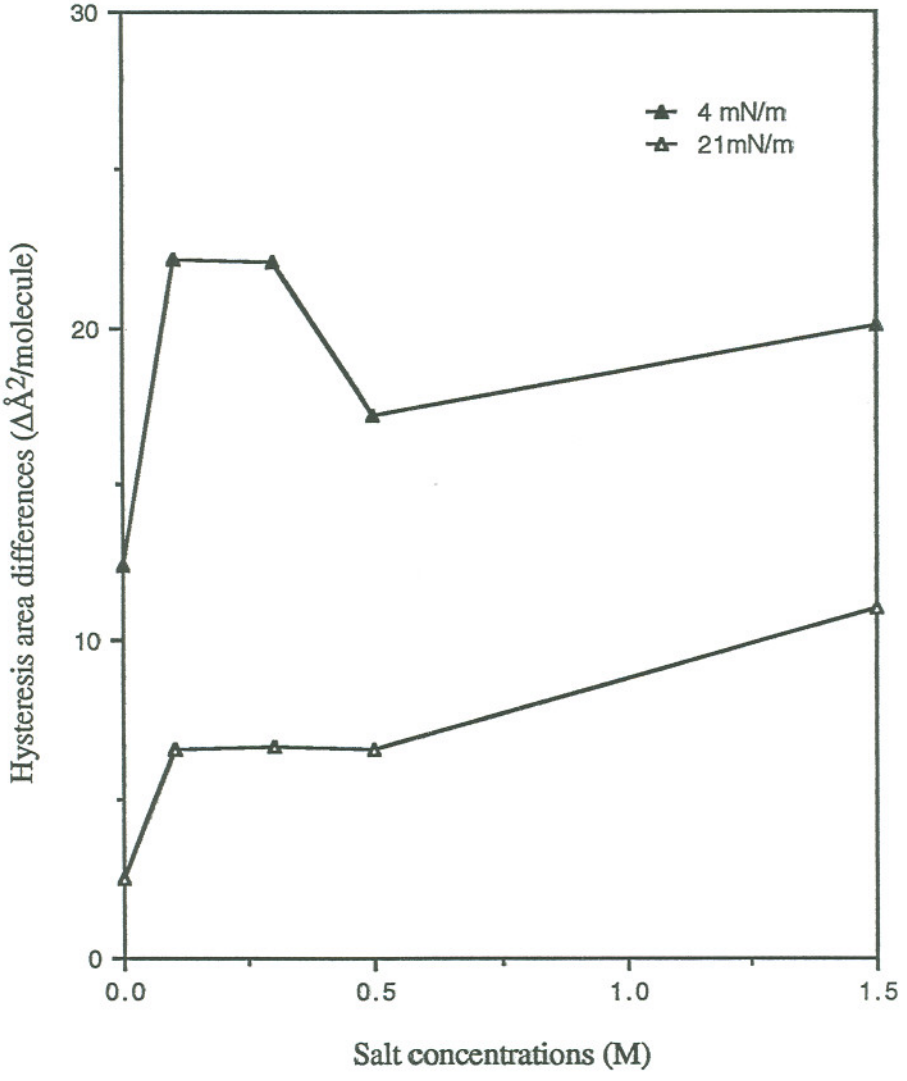

Fig. 3.12 Molecular area differences for GM1 monolayers with MBP C-1 on subphases of various ionic strength at 4 mN/m and 21 mN/m. Subphases: 5mM Tris buffer + various salt concentration (pH=7.4 ± 0.1).

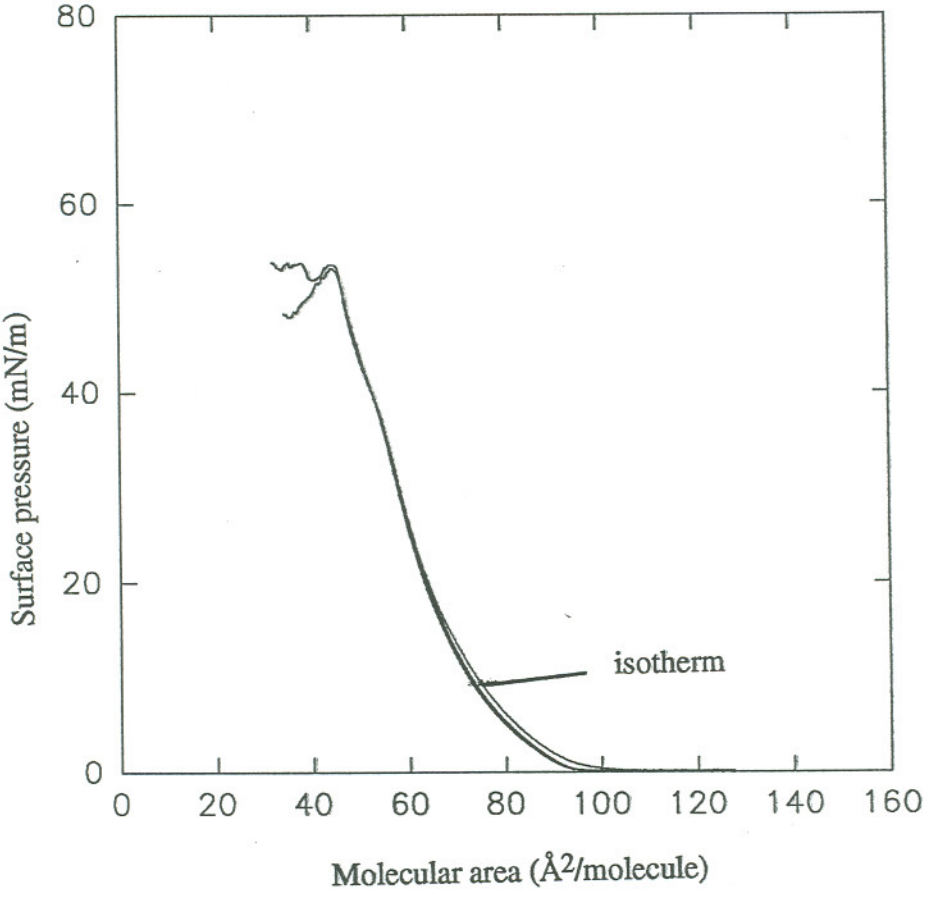

Fig. 3.13 Monolayer hysteresis of DMPC with PLL on 5mM Tris subphase (pH=7.4 ± 0.1).

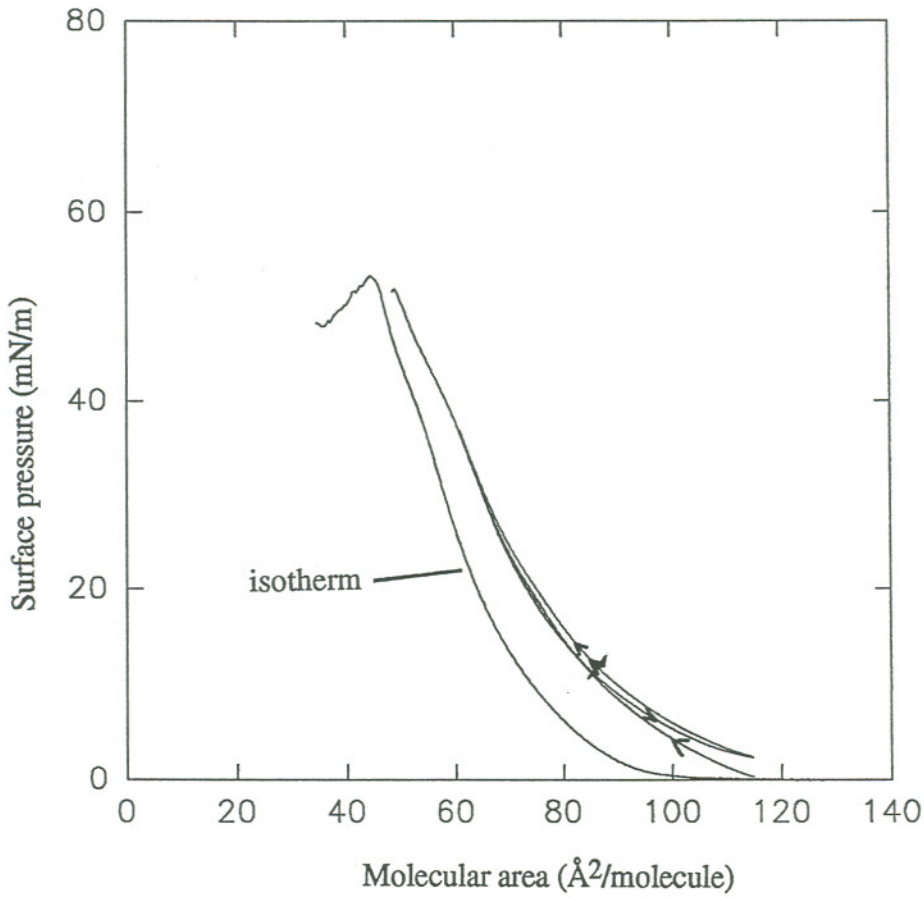

Fig. 3.14 Monolayer hysteresis of DMPC with MBP C-1 on 5mM Tris subphase (pH=7.4 ± 0.1).

Since DMPC is net neutral, the only interaction involved is the hydrophobic insertion of the protein's hydrophobic segments into the lipid membranes. Absence of this effect between PLL and DMPC is strong support for this assertion.

3.4 Liquid Crystalline Lamellar Lipid Phases as Models for Myelin Multilayers

3.4.1 Small-Angle X-ray Diffraction of DMPC and DMPC/Poly-l-lysine Liquid Crystalline Phases

Fig. 3.15 shows the small-angle X-ray diffraction pattern for 70wt% DMPC-30wt% H_2O lyotropic liquid crystal. The d-spacing of these lamellar samples is 64.46 Å, which compares well with previously published data (d=64.9 Å) [72]. In contrast to DMPC powder patterns, higher order scatterings up to three orders are observed, indicating that a ordered multilamellar structure has formed. Addition of PLL (70.1wt%DMPC-5.4%PLL-24.5%H_2O) does not change the scattering pattern of DMPC liquid crystal and its d-spacing (Fig. 3.16). This demonstrates that DMPC has no interaction with PLL, particularly in multilamellar preparations. PLL does not incorporate into the DMPC multilayer.

3.4.2 Small-Angle X-ray Diffraction of DMPC/DMPA and DMPC/DMPA/Poly-l-lysine Liquid Crystalline Phases

The small-angle X-ray diffraction pattern for a 71.4 wt% DMPC-3.6% DMPA-25% H_2O lyotropics at room temperature is shown in Fig. 3.17. Second order scattering peaks are observed, confirming again the L_α lamellar phase formation in the PC:PA lipid mixture. The d-spacing of the mixed liquid crystals is 62.48 Å, slightly expanded from that of DMPC probably due to repulsive interlayer interactions between anionic DMPA in adjacent multilayers.

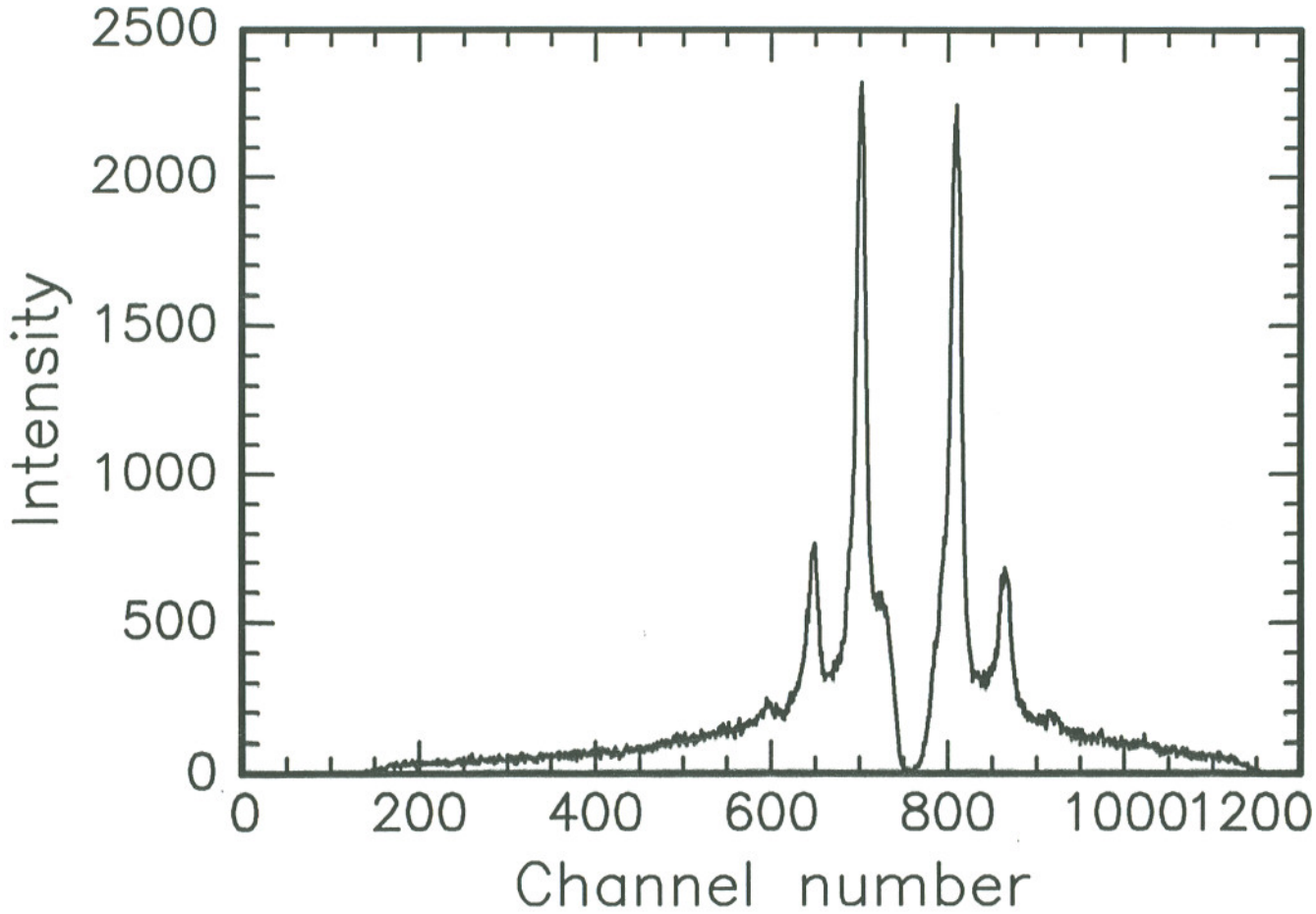

Fig. 3.15 Diagram of small-angle X-ray diffraction for 70% DMPC-30% (wt) H_2O lyotropic liquid crystalline lamellar phase at 25 °C.

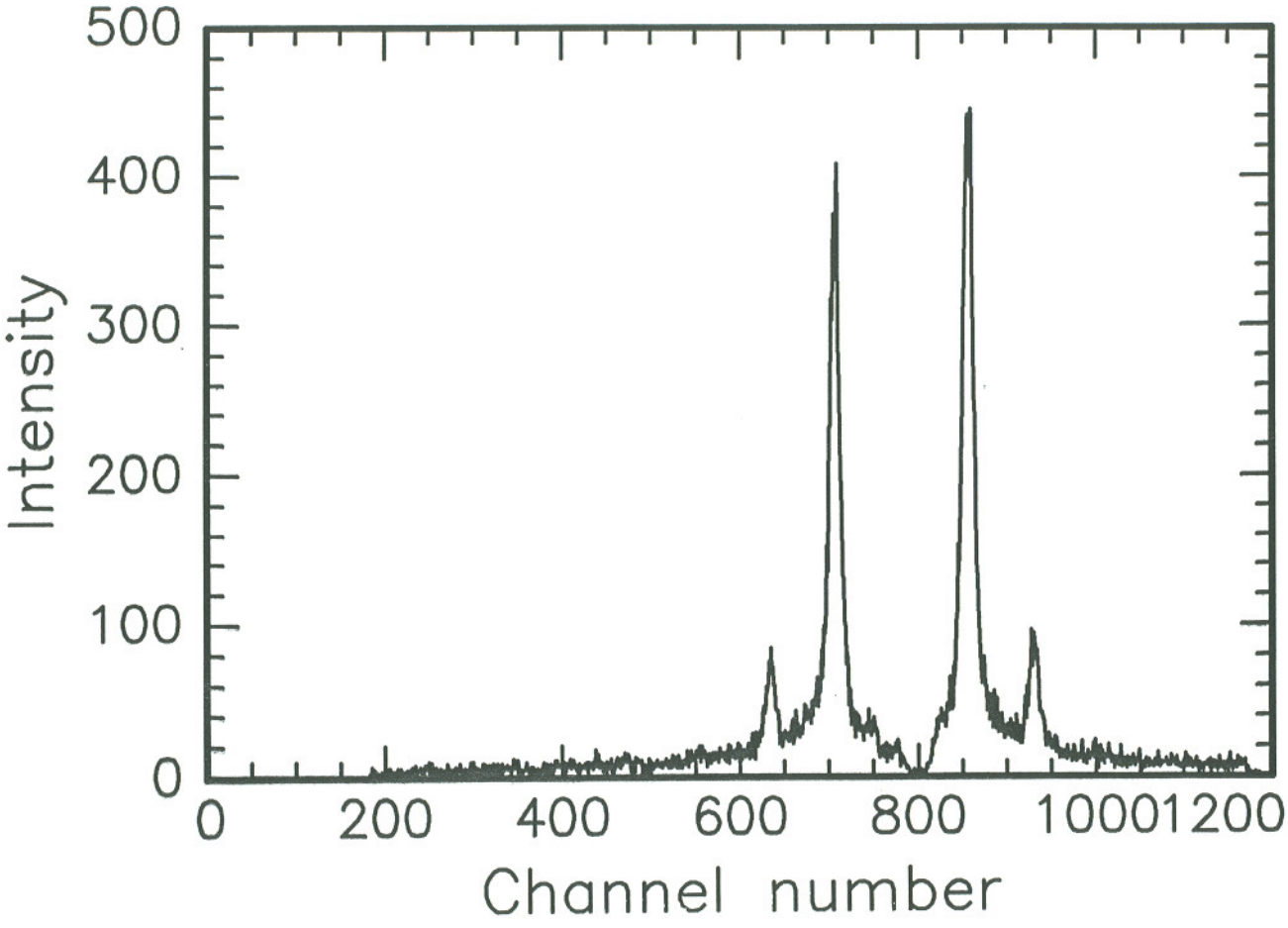

Fig. 3.16 Diagram of small-angle X-ray diffraction for 70.1% DMPC-5.4% PLL-24.5% (wt) H_2O lyotropic liquid crystalline lamellar phase at 25 °C.

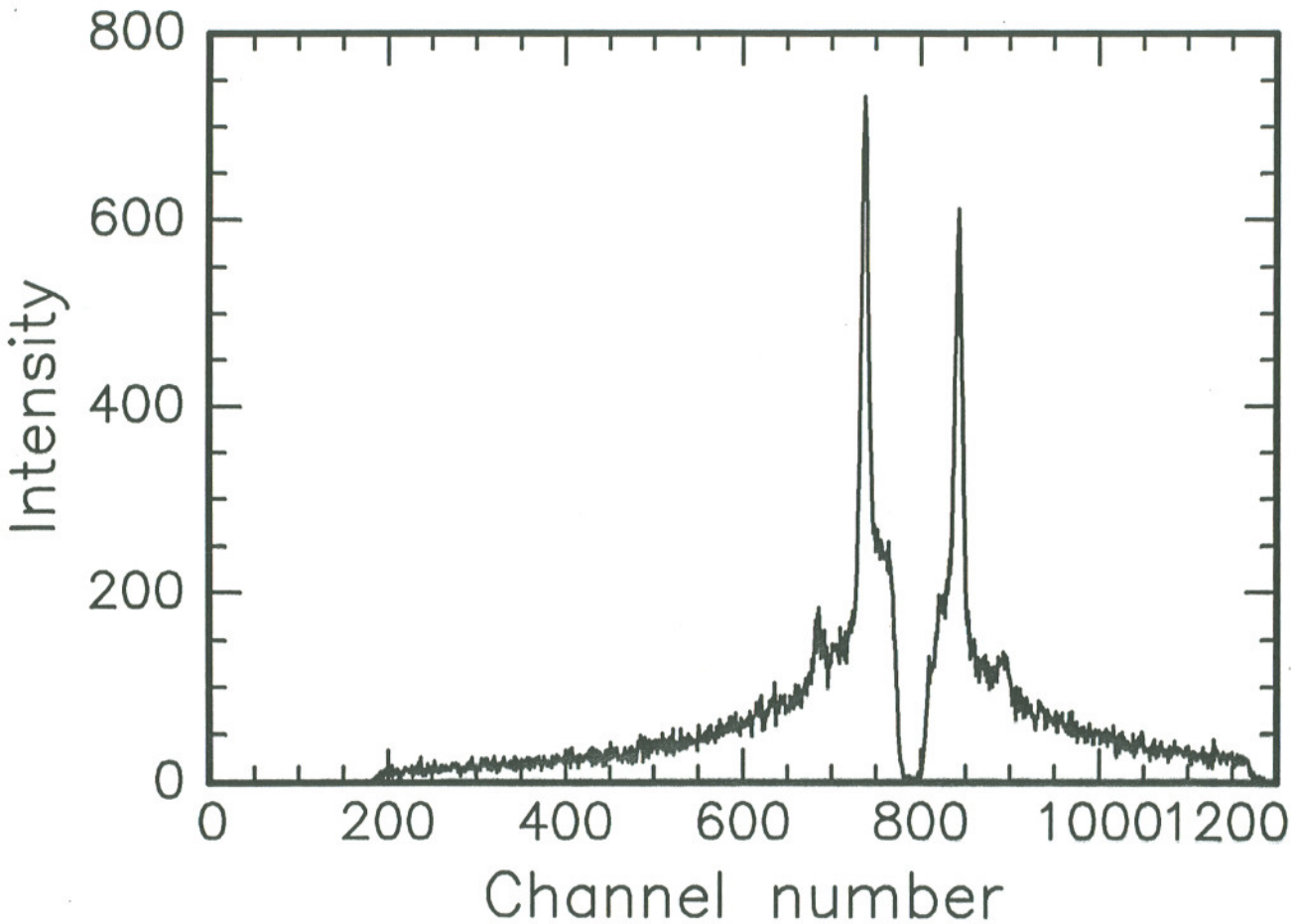

Fig. 3.17 Diagram of the small-angle X-ray diffraction for 71.4% DMPC-3.6% DMPA-25% (wt) H_2O lyotropic liquid crystalline lamellar phase at 25 °C.

Unlike PLL in 70.1wt% DMPC-5.4% PLL-24.5% H_2O lipid lyotropic where PLL has no influence on the d-spacing, addition of PLL into PC-PA liquid crystal (67.7wt% DMPC-3.4% DMPA-5.2% PLL-24.9% H_2O) increases the d-spacing to 67 Å, indicating that PLL has incorporated into the lipid multilayer (Fig. 3.18). This effect must reflect a combination of PLL-DMPA electrostatic interactions which decrease the d-spacing as well as PLL steric and occupied volume factors serving to increase interlamellar distances. This approach offers some insight into the structure-function relationships in native myelin sheath. Further studies, including experiments with MBP, will assist in understanding the features of the myelin sheath and may provide information for clarifying pathogenesis of demyelinating diseases.

3.5 Dihexadecylphosphate Monolayer Hysteresis Studies with MBP C-1 and PLL

Fig. 3.19 shows hysteresis curves for the negatively charged lipid, dihexadecylphosphate (DHP), on a subphase of Tris buffer, pH 8.4 at 20°C containing PLL. The subphase pH is increased to 8.4 in this case because the pKa of DHP's phosphate is approximately 7 and monolayer studies performed near the pKa are not reproducible. The monolayer is in this case compressed first to 5 mN/m before injection of PLL. Upon dispersing PLL under this DHP monolayer, lateral surface pressure decreases immediately to 0.5-0.7 mN/m. Like DMPA, this is due to head group charge neutralization by the binding of PLL to the monolayer. The hysteresis curve demonstrates two inflections not found on the pure DHP isotherm: one at 10 mN/m and another at near 30 mN/m. The low-pressure inflection is present in both the compression and expansion curves, indicating a reversible phenomenon that arises from altered DHP packing constraints resulting directly from bound PLL chains disrupting lipid organization within the layer. The upper inflection appears to be due to expulsion of PLL from the DHP interface as the compression, recompression and pure

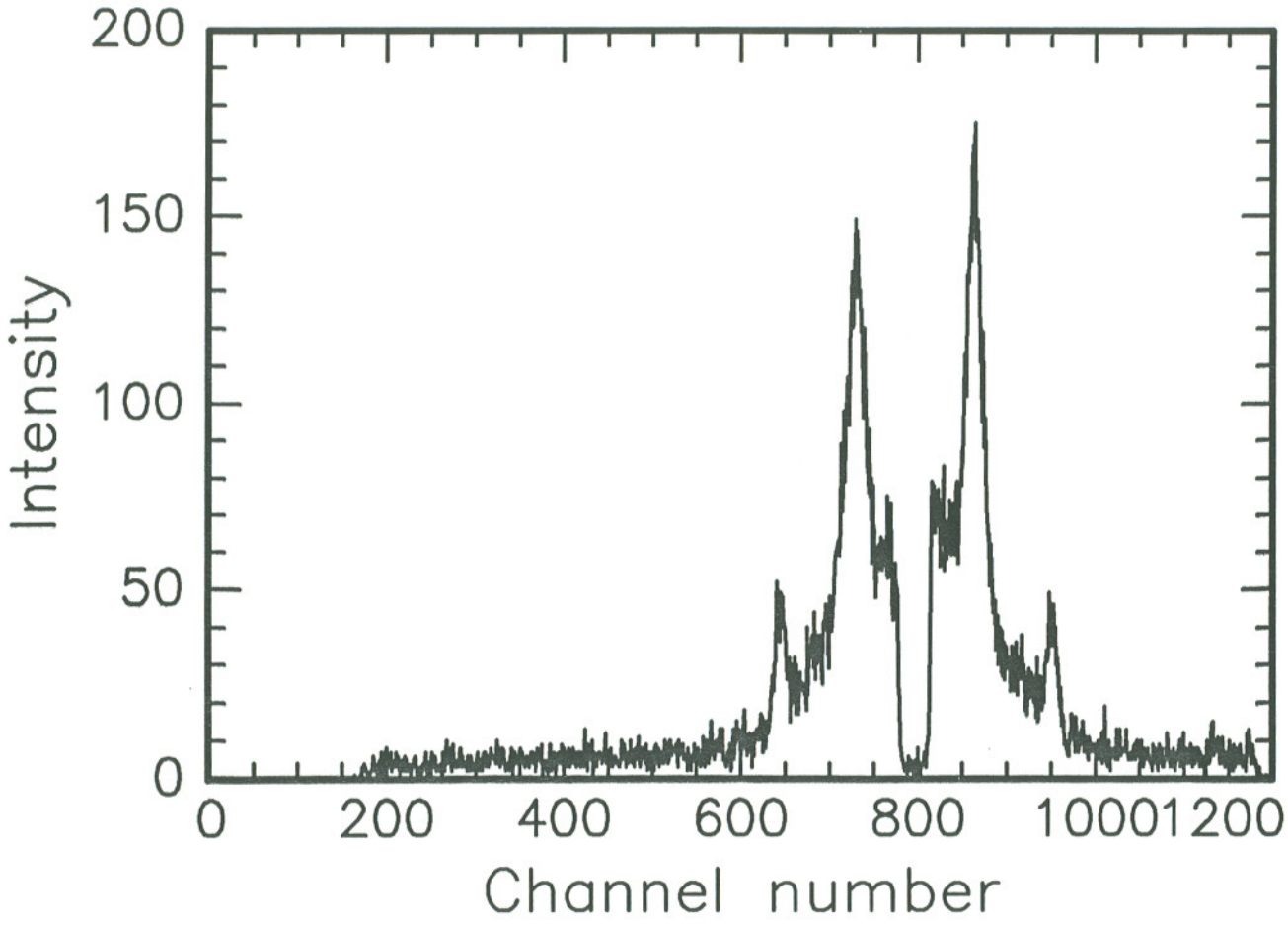

Fig. 3.18 Diagram of the small-angle X-ray diffraction for 67.7% DMPC-3.4% DMPA-5.2% PLL-24.9% (wt) H_2O lyotropic liquid crystalline lamellar phase at 25 °C.

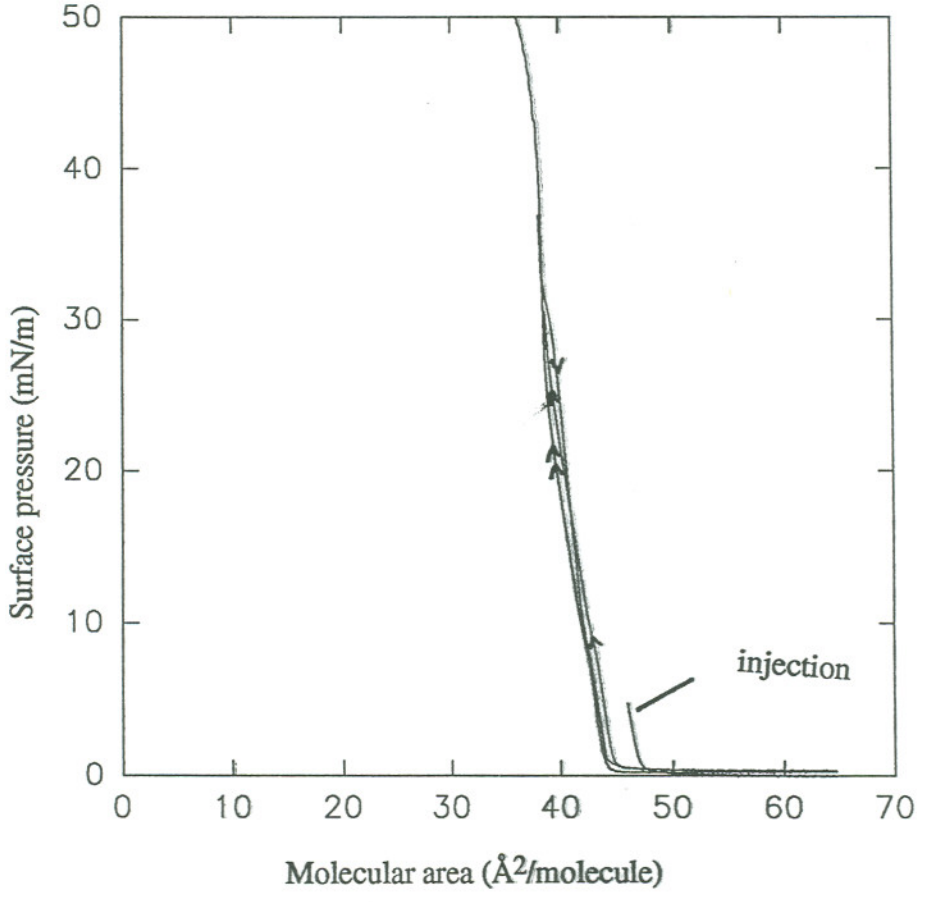

Fig. 3.19 Monolayer hysteresis of DHP with PLL injected at 5mN/m on a subphase of Tris buffer, pH 8.4 at 20°C.

isotherm curves follow similar routes to collapse after this point. The expansion curve following compression lies on the greater molecular area side of the compression curves, that is, expanding molecular area does not result in a rapid fall in surface pressure as observed for the other lipid hysteresis experiments. This is due to a failure of PLL to reattach/readsorb to the DHP monolayer to rapidly neutralize DHP-DHP repulsive interactions at a rate proportional to layer expansion.

Fig. 3.20 shows DHP behavior on subphases containing MBP C-1, injected again after monolayer compression to 5 mN/m. In contrast to PLL condensation, injection for MBP C-1 under DHP at 5 mN/m causes significant layer expansion resulting in the monolayer surface pressure increase to nearly 10 mN/m while incubating at constant area.

3.6 Circular Dichroism Analysis of MBP C-1 and PLL

Both PLL and MBP C-1 show random coil structures when they are in Tris buffer solution (pH=8.4). After adding the DHP SUV vesicles to each polypeptide solution, different effects are noted. Strong electrostatic attraction between PLL and DHP changes the PLL circular dichroism (CD) spectrum, indicating formation of some ß sheet structure. MBP C-1 however maintains its random structure despite its cationic nature (Fig. 3.21). The different positive charge densities in MBP C-1 and PLL may be the reason for their observed differences in secondary structural changes.

3.7 Discussion

The high affinity of MBP for acidic lipids was first demonstrated by Palmer and Dawson [84], using a biphasic solvent system to detect complex formation. The interaction of MBP is stronger with phosphatidylethanolamine (PE) than with PC, but it is much weaker with these two lipids than with acidic lipids. The distinguishing feature between PLL and MBP C-1 lies in the hydrophobic MBP C-1 sequences which can

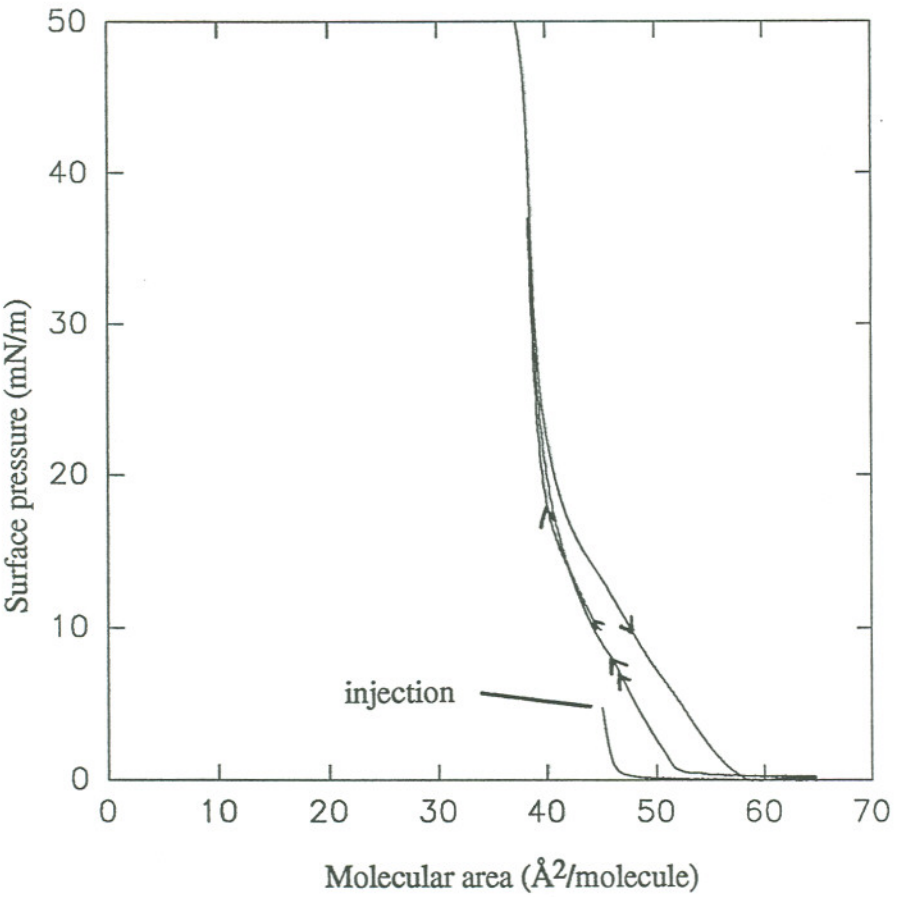

Fig. 3.20 Monolayer hysteresis of DHP with MBP C-1 injected at 5mN/m on a subphase of Tris buffer, pH 8.4 at 20°C.

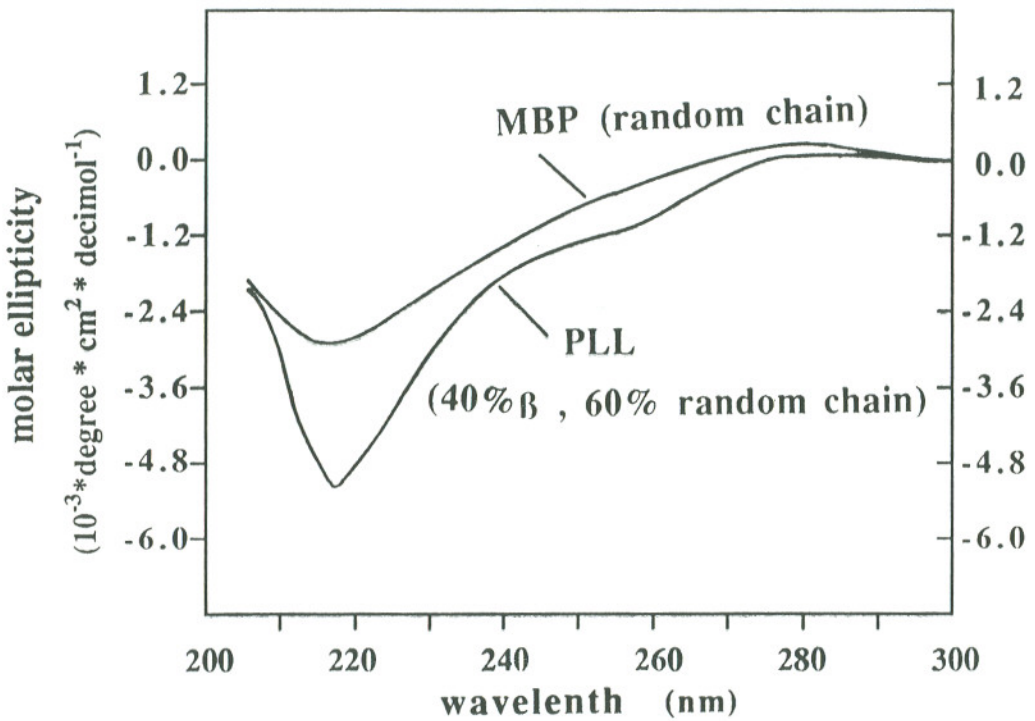

Fig. 3.21 Circular dichroism spectrum of PLL and MBP C-1 after interaction with DHP vesicles at room temperature. Buffer : 5mM Tris (pH= 8.4 ± 0.1).

insert into the lipid head group regions or perhaps further into the acyl region of the membrane. MBP C-1 has substantial intrinsic surface activity because of these hydrophobic sequences, indicating its tendency to perturb the hydrophobic core regions of lipid monolayers. PLL, lacking the hydrophobic drive, binds only electrostatically to acidic head group regions. Although PA is not present in myelin, its use allows the polar head group to be varied further to help understand the polar head group contribution in the interaction with protein [7]. DMPA-PLL interaction shows larger condensing effects than DMPA-MBP C-1 (Fig. 3.7). Charge neutralization which is a function of head group chemistry can explain differences in this monolayer binding behavior .

It has been suggested that PA, along with PE, PS (phosphatidylserine) and cerebroside sulfate are capable of intermolecular hydrogen bonding through their head groups [85]. In the absence of salt, the DMPA head group is surrounded by water molecules which prevent PLL from approaching. In order for PLL to interact with DMPA, some water molecules must first be displaced from the membrane interfacial phase. Removal of water molecules by PLL strengthens the intermolecular hydrogen bonding, causing the monolayer molecular area to condense. This effect prevails until a subphase salt concentration of 0.1 M. At higher concentrations, Na^+ ions break the intermolecular hydrogen bonds between phosphate head groups, allowing PLL to adsorb more readily onto the DMPA head groups. This results in stronger electrostatic interaction between DMPA and PLL.

Although PLL and MBP C-1 both interact with DMPA to a similar degree, charge differences between PLL and MBP C-1 distinguish the modes of interactions. Binding of MBP C-1, like PLL, can also utilize the ionized DMPA phosphate head group and diminish intermolecular hydrogen bonding, thus allowing the protein to interact both electrostatically and hydrophobically with PA [85]. These two interactions begin to show differences with increasing salt concentrations. On 0.3 M subphases,

injection of MBP C-1 expands the molecular area while PLL still has some condensing effect. On 1.5M salt subphases, MBP C-1 begins to penetrate into the DMPA monolayer, causing surface pressure to increase from 0 mN/m to 1.13 mN/m with a 28.9 $Å^2$ molecular area expansion (Fig. 3.22). At this salt concentration, the protein may be dehydrated, indicating a strong hydrophobic effect with the DMPA monolayer via a lipid/protein salting-out mechanism. The interaction of DMPA with PLL causes the phase transition region of PA to disappear, but with MBP C-1, an inflection at 12 mN/m replaces the high phase transition plateau (Fig. 3.2, 3.5), indicating that protein binding significantly perturbs the lipid organization.

With regard to the importance of ganglioside GM1, more than 2000 articles on gangliosides have been published during the past decade, many with special interest in the large hydrophilic sugar head group moiety and its great potential for hydrogen bonding. These reports give clear evidence that the polar head group determines both the physical and chemical properties of gangliosides in membranes.

A comparison of GM1-PLL and GM1-MBP C-1 hysteresis indicates some notable differences in their monolayer interactions. First, PLL condenses the lipid film while the GM1-MBP C-1 isotherm surface pressure takes off at relatively increased molecular area. Secondly, the recompression curve of GM1-MBP C-1 shows reduced molecular area than the expansion curve at surface pressures above 8 mN/m. The interaction obviously modifies the lipid properties at the interface [37]. The large head group region of GM1 is substantially different from the other phospholipids studied and allows both significant electrostatic and hydrophobic interactions. Depending on the direction of the effective local dipole moment of the head group of GM1, the head group potential of GM1 is sufficiently large enough to influence conformational changes in membrane proteins [47]. This may hinder the hydrophobic segments of MBP C-1 to penetrate deep into the GM1 head group region to interact hydrophobically with the monolayer interior.

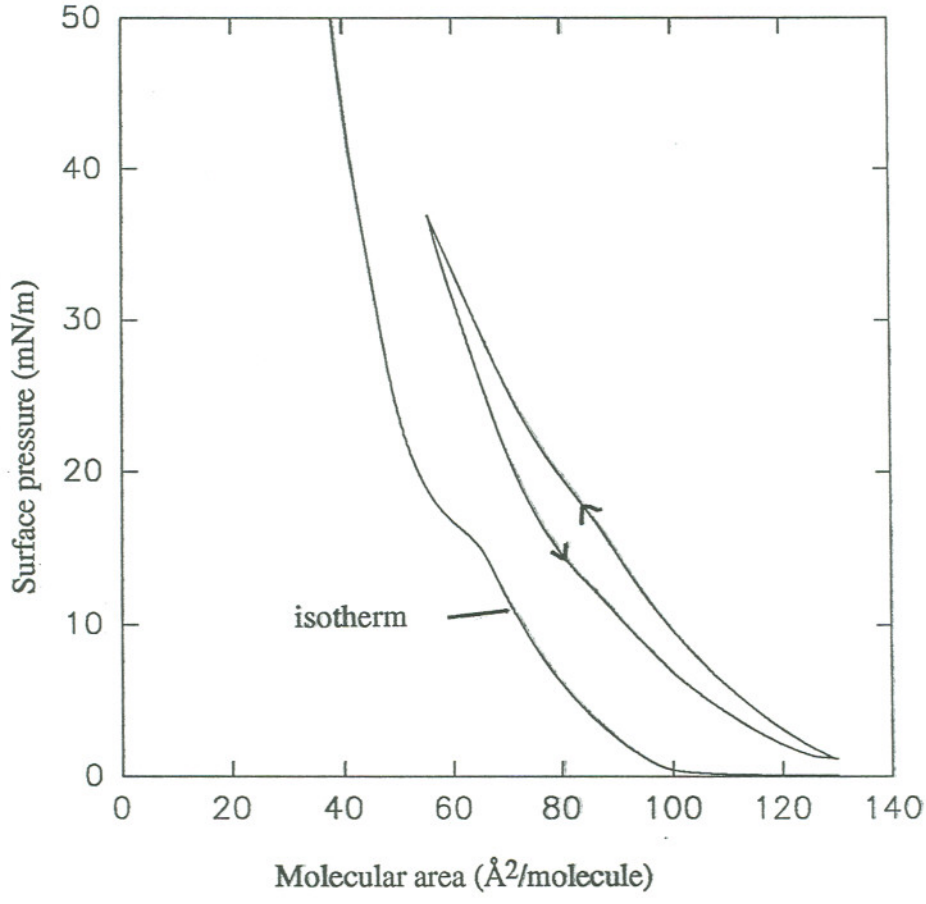

Fig. 3.22 Monolayer hysteresis of DMPA with MBP C-1 on 5mM Tris buffer and 1.5M NaCl subphase (pH=7.4 ± 0.1).

The hysteresis observed for GM1-MBP C-1 is much larger than that for GM1-PLL, indicating MBP C-1 has a strong interaction with GM1. As the negative charge on GM1 is located about 1nm from the surface and the head groups are assumed to project 2.5nm from the bilayer [86-87], PLL, which only has positive charge groups that can interact with GM1 electrostatically, associates with GM1 at a place far from the interface, without interfering much with the head group region. However, besides its positive charge groups, apolar regions on MBP C-1 are more likely to penetrate deep into the head group or even the hydrophobic region of GM1. This produces a much larger interaction between GM1 and MBP C-1 and greatly perturbs the monolayer packing structure.

Increasing the salt concentration in the study of lipid-protein interaction is used to distinguish proteins that interact only electrostatically with lipid interfaces [2]. However, with the existence of lipid intermolecular hydrogen bonds within the membrane plane, the results can become much more complicated to interpret. The GM1-PLL interaction increases as more salt are added to the subphase. The head group charges of GM1 are located deeper into the aqueous phase [86]. This makes it difficult for NaCl to effectively shield the charges. On the other hand, five sugar groups in GM1 head group form a complicated intermolecular hydrogen bonding network. The addition of NaCl helps to break this bonding and increases the negative surface charge density of GM1, so that more PLL can access and bind to the GM1 monolayer. This effect was also observed in PS-PC monolayers with PLL [2].

Although the existence of NaCl can promote GM1-MBP C-1 interaction, GM1-MBP C-1 interaction remains relatively steady at salt concentrations greater than 0.1M, indicating that the interaction is quite different from PLL. The positive charges in MBP C-1 are limited and the apolar regions of this protein can block the effective charge of GM1 by surrounding around the GM1 head group. This prevents some of the effects of NaCl. The result also shows that the hydrophobic interaction between GM1-MBP

C-1 is saturated since increasing ionic strength only slightly enhances the interaction (Fig. 3.12).

In the lipid-polypeptide interactions discussed above, the interaction in the liquid expanded phase is greater than in the liquid condensed phase. Because of the size of the polypeptides, at high surface pressure, the macromolecules are probably ejected out of the monolayer as the repulsion forces between adsorbed proteins increase. However, these ejected polypeptides still influence the features of the lipid monolayer where the shape of the interaction curve is different from the pure lipid isotherm. While they may not choose to penetrate the expanded monolayer, these polypeptides may associate with the monolayer interface.

The contrast in DHP's interactions with PLL and MBP C-1 makes the different natures of their respective behaviors quite clear. Fig. 3.19 demonstrates the case where adsorption of PLL lacks subsequent penetration events. The monolayer condenses as charge group repulsion is overcome. At surface pressures greater than 30 mN/m, there is little compression-expansion hysteresis. At this pressure, the lipid is in a solid-condensed state where PLL may not directly access the anionic phosphate group. The expansion curve lies to the larger molecular area side of both compression curves. This supports high charge-charge repulsion between head groups due to incomplete charge neutralization by PLL (monolayer expelled) at increased surface pressure. A second compression lies to the left of the first compression curve, indicating that expansion of the layer to zero surface pressure between both compressions expedites monolayer condensation.

DHP-MBP C-1 interaction (Fig. 3.20) shows expansion of all curves due to MBP C-1 insertion into DHP. Most significant is the very large area increase of the second compression curve after expansion to zero surface pressure. MBP C-1, in contrast to PLL, exhibits maximum surface activity to occupy the interface while binding electrostatically to DHP phosphate anions.

3.8 Stern Double Layer Model Analysis

When the lipid is at the air-water interface, its head group can be treated as a limited negatively charged surface, attracting ions of opposite charge, and thus, an electric double layer is established near the head group. In the following section, the Stern model will be applied to analyze the salt effect in the lipid-protein monolayer studies.

3.8.1 Stern Double Layer Model

Because of the charge at lipid interfaces, a layer of counterions would be immobilized at the interface by electrostatic attraction, called the "inner Helmholtz layer". However, these ions are not enough to exactly neutralize the surface charge. The remainder of the charge is neutralized by a diffuse atmosphere of ions located beyond the inner Helmholtz layer in solution. This diffuse region, comprised of both co- and counter- ions, is subject to random thermal motion and thus will be mobile near the interface. The ions in this double layer neutralize the surface charge and are spread throughout solution, forming a diffuse double layer (called the Gouy-Chapman layer) [83].

3.8.2 The Debye Length for Subphases of Different Ionic Strengths

The thickness of the ionic atmosphere at a charged interface, called the Debye length, can be calculated by [37],

$$\kappa = [\, \varepsilon\varepsilon_0 RT / F^2 I \,]^{1/2}$$

where, κ = Debye length (nm)

ε = dielectric constant of the medium

ε_0 = permittivity of free space = $8.854*10^{-12}\ C^2J^{-1}m^{-1}$

R = gas constant = 8.316 $JK^{-1}mol^{-1}$

T = temperature, in the unit of K = 293K

F = Faraday constant = 96500 C^2mol^{-2}

I = ionic strength

The calculated Debye length on different ionic strength subphases is shown in Table 3.2. When the ionic strength increases, the Debye length decreases. At 0.3 M ionic strength, distance (7.6nm) is within the effective range of van der Waals forces, where the "salt-out" effect dominate the interaction.

Table 3.2 The Debye Length for Different Salt Concentrations

dielectric constant [a]	concentration (M)	buffer strength	Debye length (nm)
78.54	0	0	0
78	0.02	0.02	3.0
77.1	0.1	0.1	1.3
75.7	0.3	0.3	0.76
73.7	0.5	0.5	0.58
64.3	1.5	1.5	0.32

[a] see reference 80 for explanation

Chapter 4

Results of Adsorption Kinetics of Albumin onto Supported Lipid Films

4.1 Adsorption Kinetics of Albumin onto Supported DMPG Films

The adsorption profiles at different bulk protein concentrations are shown in Fig. 4.1. At a protein bulk concentration of 0.0249 mg/ml, no fluorescence signal is observed. As the protein concentration increases, the fluorescence signal increases. A "overshoot" occurs at a concentration of 0.0498 mg/ml. Buffer flowing starts at 11th minute. After the buffer flows into the cell, the fluorescence intensity barely changes, indicating that most protein remains on the lipid surface. This obviously shows that most proteins have undergone conformational changes upon adsorbing onto the lipid layer.

4.2 Adsorption Kinetics of Albumin onto Supported DMPC Films

Supported DMPC films show larger protein adsorption amounts than DMPG films. At 0.0249 mg/ml, some proteins are detected on DMPC surfaces compared to no protein adsorption on DMPG (Fig. 4.2). After buffer flows into the cell for 2 minutes, desorption occurs and eventually all protein is desorbed. At higher protein concentrations, the adsorption amount increases. Though the buffer rinse causes some loosely bound protein to desorb, most proteins remain on the lipid surface.

Under experimental conditions (pH=7.), the protein has net negative charge as its isoelectric point is 5. Compared to the negative charge DMPG surface, it is more

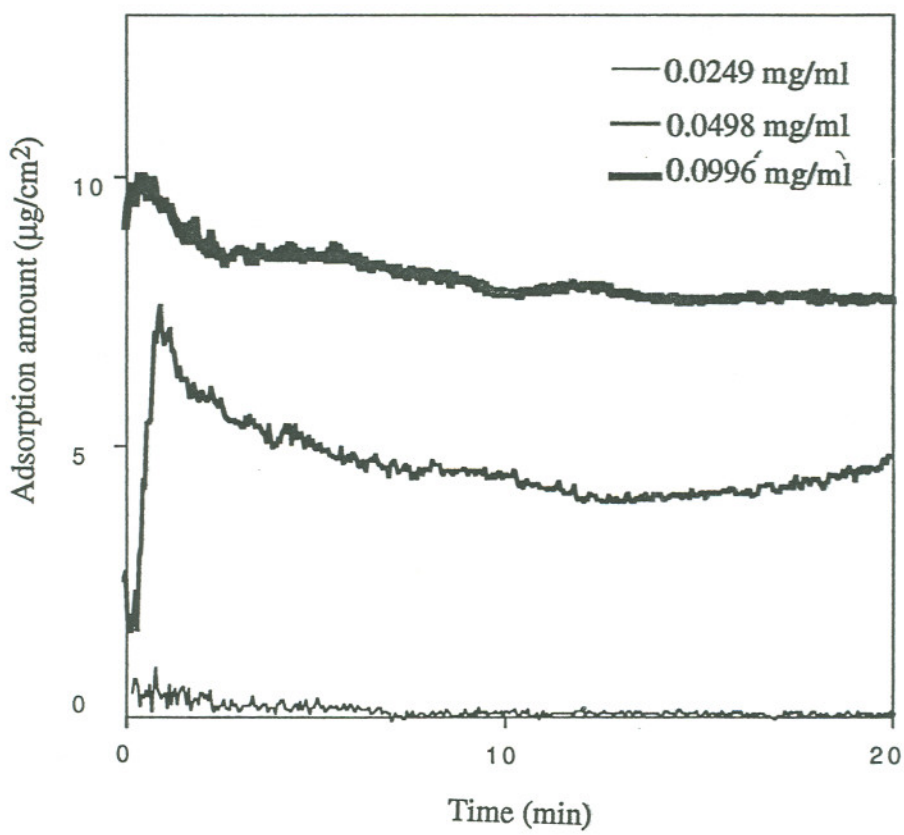

Fig. 4.1 Adsortion kinetics of albumin onto supported DMPG films on 50mM PBS buffer.

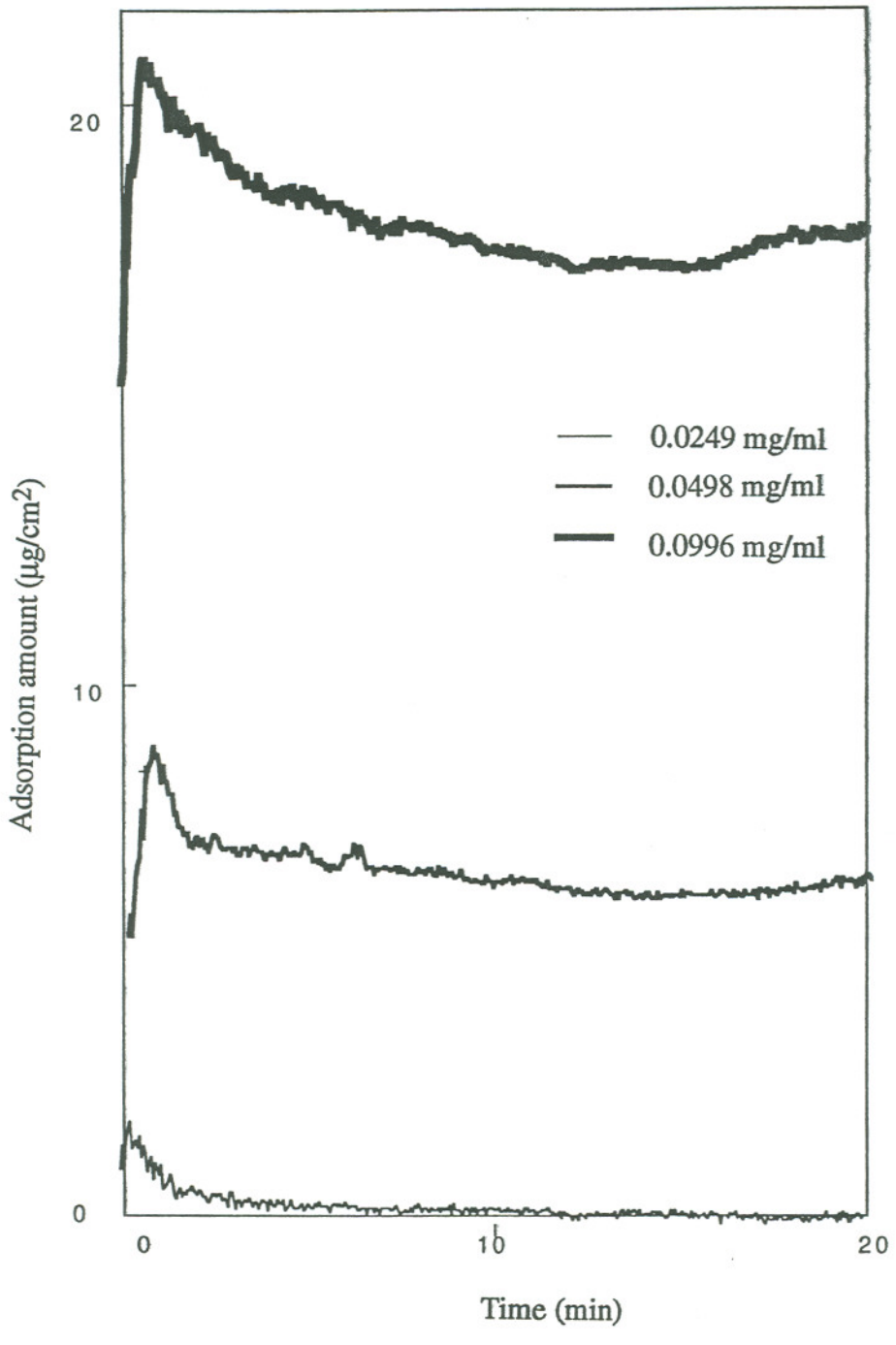

Fig. 4.2 Adsorption kinetics of albumin onto supported DMPC films on 50mM PBS buffer.

likely for protein to adsorb on DMPC surface than on DMPG, indicating that the electric charge attraction dominates the adsorption process.

4.3 Analysis of Adsorption Isotherm

Adsorption isotherms are plotted in the amount of protein adsorbed (expressed in μg/cm) versus protein bulk concentrations. Protein adsorption isotherms on supported DMPG lipid layers before and after buffer rinse appear to fit the Langmuir isotherm model (Fig. 4.3). The protein adsorption amount after buffer rinse is due to tightly bound protein layer on the surface. The surface prior to rinsing is composed of both tightly and loosely bound protein. After subtracting these two and plotting the protein amount versus protein bulk concentration, this isotherm can be classified as a loosely bound protein isotherm (Fig. 4.4). At 0.0996 mg/ml, the protein amount nearly reaches the saturation point. In contrast to DMPG, isotherms of tightly bound protein on supported DMPC layers exhibit linear behavior (Fig. 4.5). The loosely bound proteins which have been removed from supported DMPC layers fit the Langmuir type isotherm (Fig. 4.6).

Isotherm analysis of protein adsorption on both DMPC and supported DMPG layer indicates two adsorption mechanisms. Surface charge plays a important role in the albumin adsorption studies. Overshoot in the adsorption kinetics curve may be due to the instability of the supported lipid bilayer in the existence of albumin. High surface activity of albumin may extract some lipid from the surface and cause fluorescent probe quenching by internal energy transfer.

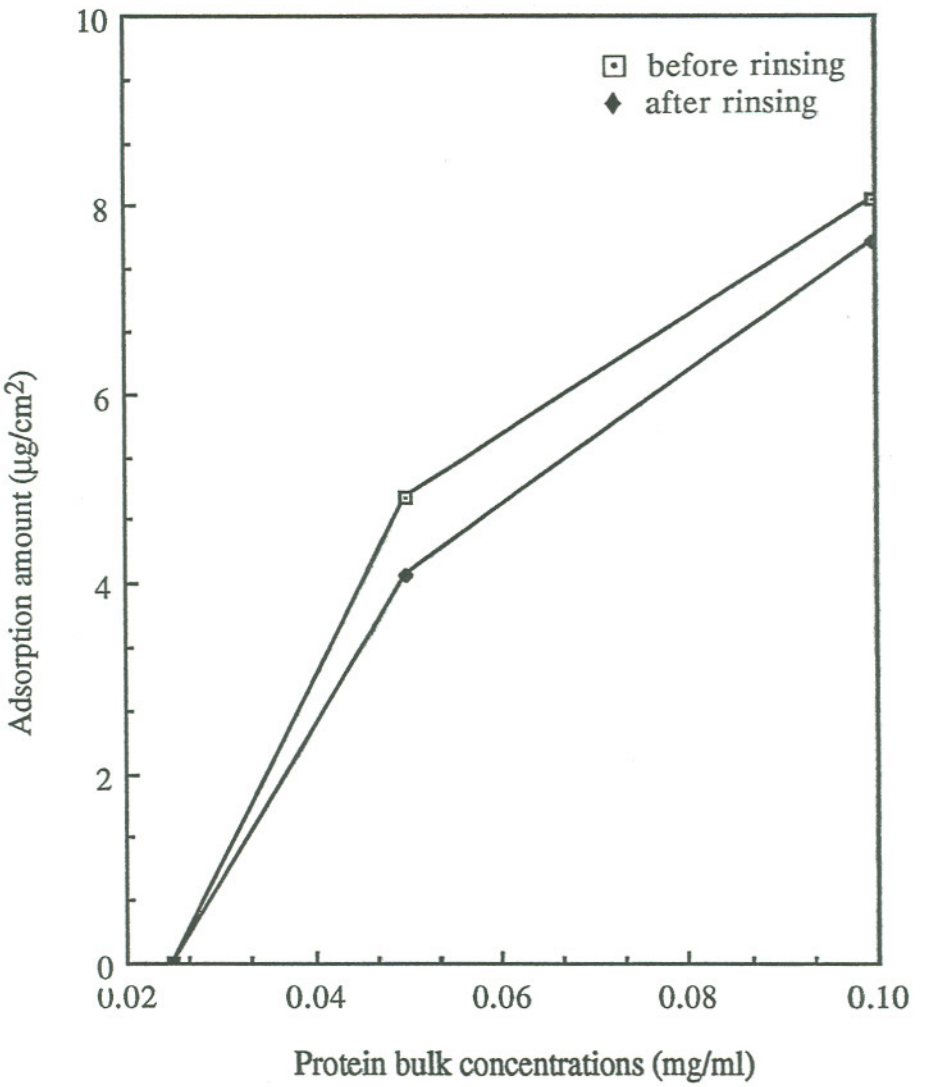

Fig. 4.3 Protein adsoption isotherm on supported DMPG films before and after buffer rinse.

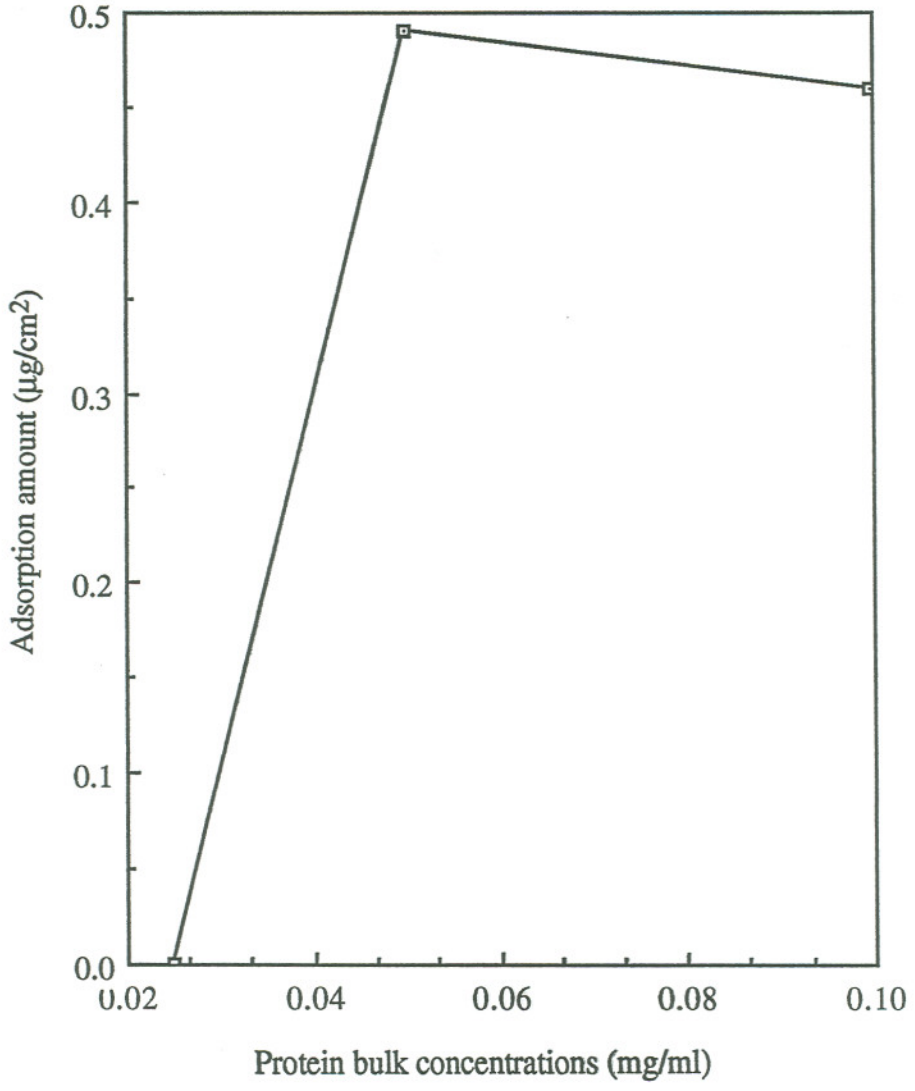

Fig. 4.4 Protein adsorption isotherm of loosely bound protein on supported DMPG films.

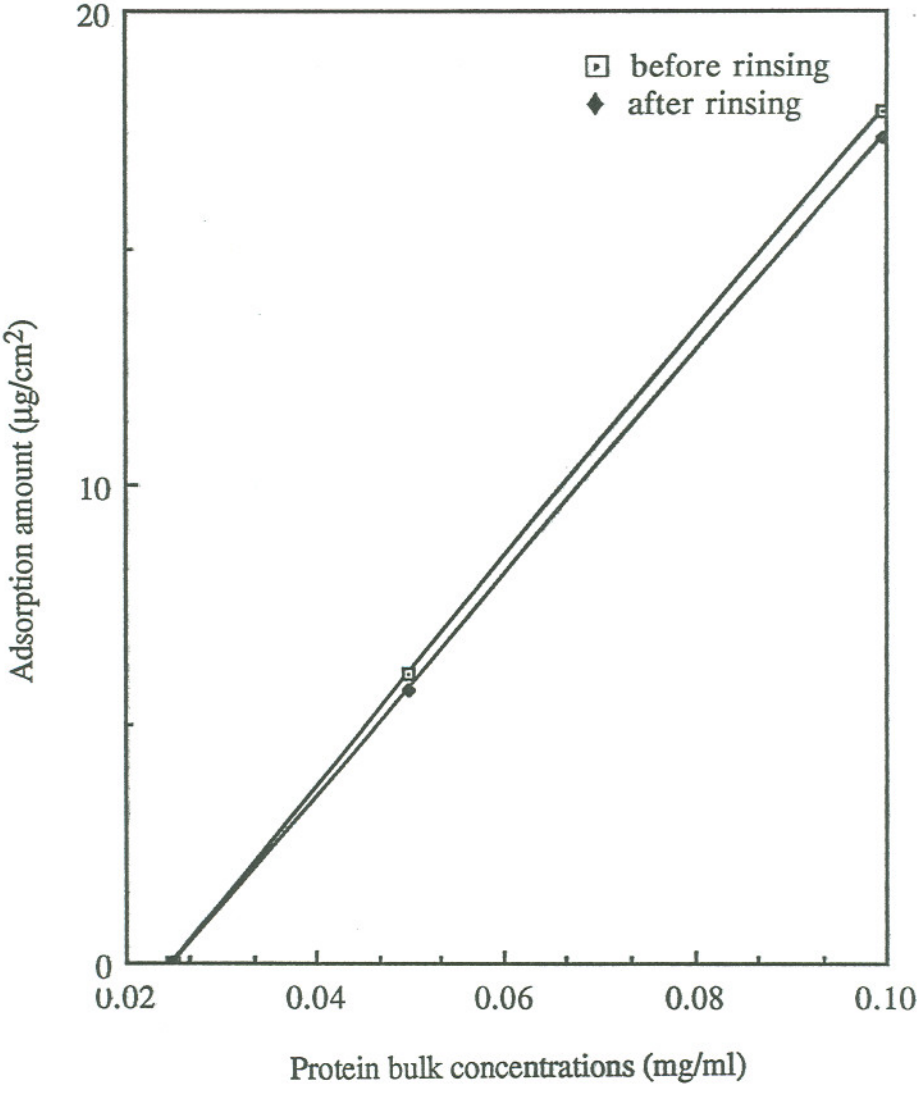

Fig. 4.5 Protein adsorption isotherm of tightly bound protein on supported DMPC films.

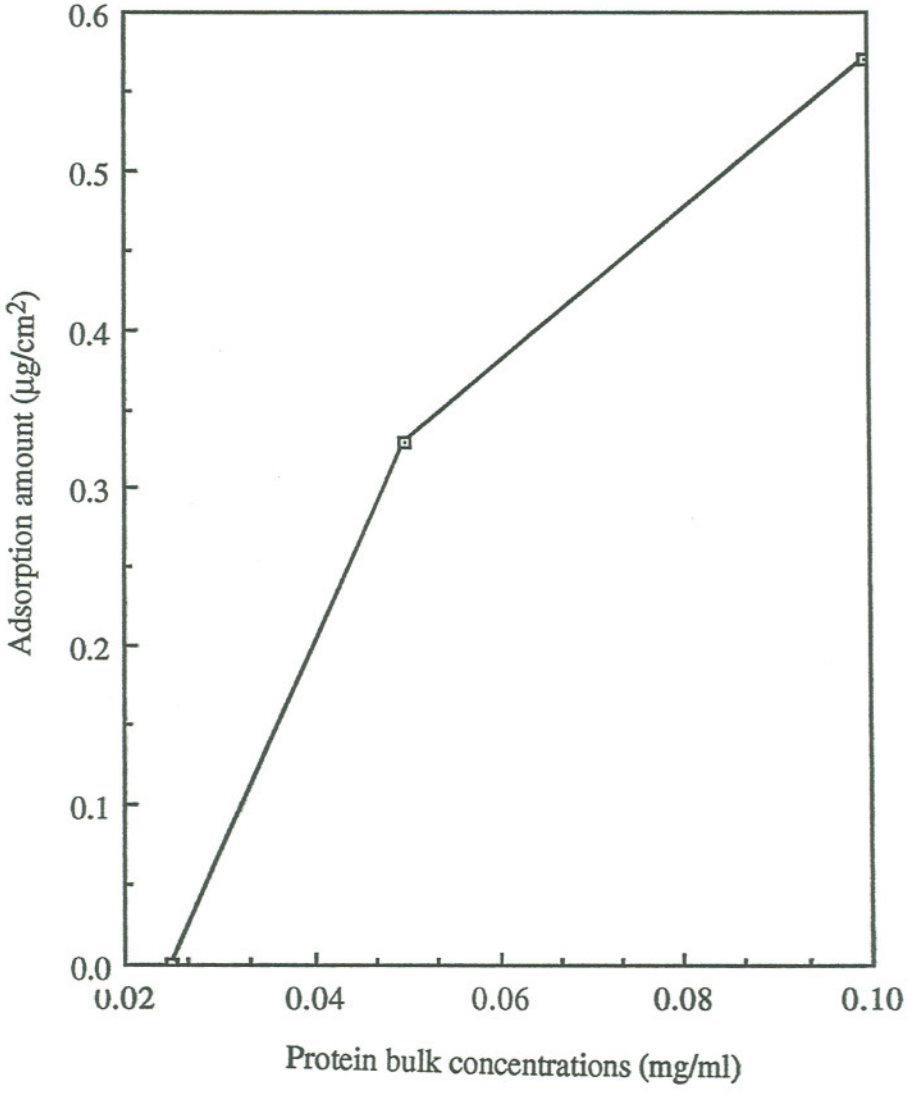

Fig. 4.6 Protein adsorption isotherm of loosely bound protein on supported DMPC films.

Chapter 5

Conclusions

The cationic polypeptide, PLL, exhibits strong electrostatic interactions with acidic lipids DMPA , DHP and GM1. No detectable interaction betwenn PLL and zwitterionic DMPC, both in the monolayer and lipid lyotropic liquid crystal systems is observed. The cationic protein, MBP C-1, interacts both with zwitterionic (DMPC) and anionic lipids (DMPA, GM1, DHP), indicating the dual hydrophobic and electrostatic nature of the protein in the model membrane systems.

Increasing ionic strength in the aqueous solution does screen the charge of the lipid head groups in the membrane. However, because of the competitive influence of intermolecular hydrogen bonding in the head group region, the interaction mechanism becomes complicated. At low ionic strength, the existence of Na^+ ions breaks the intermolecular hydrogen bonding between lipids and increases the lipid-protein interaction. Increasing the ionic strength also decreases the Debye length of the ionic double-layer (shown in Table 3.2). Short Debye lengths at high ionic strength enhance an apparent protein "salting-out" effects, allowing van der Waals attractive interactions over a short range between protein and lipid membrane. Additionally, a new technique -- Total Internal Reflection Fluorescence (TIRF) -- has been used to probe model lipid membrane-protein interactions at model surfaces with evanescent wave spectroscopy. Adsorption and desorption kinetics of the serum albumin have been investigated on supported bilayers of acidic and zwitterionic lipids.

References

1. C.K. Mathews and K.E. van Holde (1990) Biochemistry, The Benjamin/Cummings Publishing Company, Inc., New York, NY.
2. J.M. Boggs, M.A. Moscarello and D. Papahadjopoulos (1982) in: O.H. Griffith and P. Jost (Ed.), Lipid-Protein Interactions Vol.2, Wiley-Interscience/New York, pp. 1-51.
3. F.O. Schmitt, R.S. Bear and K.J. Palmer (1941) J. Cell. Comp. Physio. 18, 31-42.
4. A.E. Blaurock, M.B. Genter St. Clair and D.G. Graham (1991) Neuropath. App. Neurobiol. 17,309-321.
5. W. Stoffel (1990) Angew. Chem. Int. Ed. Engl. 29, 958-976.
6. J.F. Goodrum (1991) J. Neurochem. 56, 2082-2086.
7. D. Papahajopoulos, M. Cowden and H. Kimelberg (1973) Biochim. Biophys. Acta 330, 8-26.
8. J.F. Goodrum (1991) J. Neurochem. 54, 1709-1715.
9. Y.Uda and Y. Nakazawa (1976) Bull. Tokyo Med. Dent. Univ. 23, 135-140.
10. I.W. Levin, T.E. Thompson, Y. Barenholz and C. Huang (1985) Biochemistry 24, 6282-6286.
11. M. Busquets, C. Mestres, S. Bordas, F. Reig, M.A. Alsina and J.M. Garcia-Anton (1991) Thermochimica Acta 185, 99-109.
12. Y. Imanishi and S. Kimura (1991) Polymer J. 23, 593-601.
13. F. Castelli and G. Raciti (1991) Thermochimica Acta 186, 205-215.
14. S. Puvvada and D. Blankschtein (1990) J. Chem. Phys. 92, 3710-3724.
15. H. Akutsu and T. Nagamori (1991) Biochemistry 30, 4510-4516.
16. J.R. Silvius and P.M. Brown (1986) Biochemistry 25, 4249-4258.
17. G. Cevc (1987) Biochemistry 26, 6305-6310 .

18. H. Beitinger, V. Vogel, D. Mobius and H. Rahmann, (1989) Biochim. Biophys. Acta 984, 293-300.

19. G.D. Fidelio, B. Maggio and F.A. Cumar (1987) Biochim. Biophys. Acta 854, 231-239.

20. M. Ollmann, G. Schwarzmann, K. Sandhoff and H. Galla (1987) Biochemistry 26, 5943-5952.

21. B.A. Sela and D.Bach (1984) Biochim. Biophysica Acta 771, 177-182.

22. B. Maggio, T. Ariga, J.M. Sturtevant and R.K. Yu (1985) Biochemistry 24, 1084-1092.

23. B. Maggio, F.A. Cumar and R. Caputto (1981) Biochim. Biophys. Acta 650, 69-87.

24. M. Masserini and E. Freire (1986) Biochemistry 25, 1043-1049.

25. D. Voet and J.G. Voet (1990) Biochemistry, John Wiley &Sons, New York.

26. L. Horvath, P.J. Brophy and D. Marsh (1988) Biochemistry 27, 5296-5304.

27. B.H. Waksman, S.C. Reingold and W.E. Reynolds (1987) Research on Multiple Sclerosis, Demmos Publications, New York, NY.

28. P.E. Fraser, R.P. Rand and C.M. Deber (1989) Biochim. Biophys. Acta 983 (1989), 23-29.

29. C.M. Deber, D.W. Hughes, P.E. Fraser, A.B. Pawagi and M.A. Moscarello (1986) Arch. of Biochem. and Biophys. 245, 455-463.

30. L. Ginsberg and N.L. Gershfeld (1991) Neurosci. Lett. 130, 133-136.

31. M.B. Sankaram, P.J. Brophy and D. Marsh (1989) Biochemistry 28, 9699-9707.

32. R.A. Demel, Y. London, W.S.M. Geurts van Kessel, F.G.A. Vossenberg and L.L.M. van Deenen (1973) Biochim. Biophys. Acta 311, 507-519.

33. R. Persaud, J.M. Boggs, D.D. Wood and M.A. Moscarello (1989) Biochemistry 28, 4209-4216.

34. J.M. Boggs, L.S. Chia, G. Rangaraj and M.A. Moscarello (1986) Chem. Phys. Lipids 39, 165-184.

35. J.G. Stollery, J.M. Boggs, M.A. Moscarello and C.M. Deber (1980) Biochemistry 19, 2391-2396.

36. W.K. Surewicz, M.A. Moscarello, H.H. Mantsch (1987) Biochemistry 26 , 3881-3886.

37. G.D. Fidelio, B. Maggio and F.A. Cumar (1982) Biochem. J. 203, 717-725.

38. B. Maggio, J.M. Sturterant, M.A. Moscarello and C.M. Deber (1987) J. Biological Chemistry 262, 2652-2659.

39. D.W. Hughes, J.G. Stollery, M.A. Moscarello and C.M. Deber (1982) J. Biol. Chem. 257, 4698-4700.

40. D. Papahadjopoulos, M.A. Moscarello, E.H. Eylar and T. Isac (1975) Biochim.Biophys.Acta 401, 317-335.

41. J.M. Boggs, M.A. Moscarello and D. Papahadjopoulos (1977) Biochemistry 16, 5420-5426.

42. J.M. Boggs and M.A. Moscarello (1978) J.Membr.Biol. 39, 75-96.

43. F. Sixl, P.J. Brophy and A. Watts (1985) Biochemistry 23, 2032-2039.

44. F.M. Harold (1986) The Vital Force: A Study of Bioenergetics, W. H. Freeman and Company, New York, NY.

45. D.B. Datta (1987) A Comprehensive Introduction to Membrane Biochemistry, Floral Publishing, Madison, Wiscosin.

46. S.J. Singer and G.L. Nicolson (1972) Science 175, 720-731.

47. A.J. Verkleij, R.F.A. Zwaal, B. Roelofsen, P. Comfurius, D. Kastelijn and L.L.M. van Deenen (1973) Biochim. Biophys. Acta 323, 178-193.

48. H. Ringsdorf, B. Schlarb and J. Venzmer, (1988) Angew. Chem. Intl. Ed. Engl. 27, 113-158.

49. J.H. Fendler (1982) Membrane Mimetic Chemistry, A Wiley-Interscience Publication, New York.

50. M. Aoudia, W.H. Nade and M.A.J. Rodgers (1991) J. Colloid and Interface Science (145), 493-501.

51. J. Castresana, J.M. Valpuesta, J.L.R. Arrondo and F.M. Goni (1991) Biochim. Biophys. Acta 1065, 29-34.

52. E.J. Dufourc, I.C.P. Smith, J. Dufourcq (1986) Biochemistry 25, 6448-6455.

53. P.W. Holloway and T.C. Markello (1982) biophys. J. 37, 63-64.

54. M.D. Bazzi and G.L. Nelsestuen (1991) Biochemistry 30, 7970-7977.

55. R.A. Demel, C.C. Yin, B.Z. Lin and H. Hauser (1992) Chem. Phys. Lipids 60, 209-223.

56. N.L. Thompson and A.G. Palmer III (1988) Comments Mol. Cell. Biophys 5, 39-56.

57. R.M. Swart (1990) in: G. Roberts (Ed.), Langmuir-Blodgett Films.

58. G.L. Gaines,Jr (1966) Insoluble monolayers at liquid-gas interfaces, Interscience Publishers, New York.

59. F. Machrite (1990) Chemistry at Interfaces, Academic Press Inc., San Diego. Plenum Press, New York, pp. 273-316.

60. R. Blankenburg, P. Meller, H. Ringsdorf and C. Salesse (1989) Biochemistry 28, 8214-8221.

61. C. Salesse, F. Lamarche and R.M. Leblanc (1989) Biochem. Cell. Biol. 67, 422-427.

62. G.W. Brady, D.B. Fein, D.D. Wood and M.A. Moscarello (1985) Biochem. Biophys. Res. Comm. 126, 1161-1165.

63. J.J. Ramwani, R.M. Epand and M.A. Moscarello (1989) Biochemistry 28, 6538-6543.

64. J.M. Boggs (1984) in: M.Kates and L.A. Manson (Ed.), Intermolecular hydrogen

bonding between membrane lipids Vol.12, Plenum Press, New York, pp. 3-53.

65. J.D. Andrade (1985) in J.D. Andrade (Ed.), Principles of Protein Adsorption Vol.2, Plenum Press, New York, NY, pp. 1-80.
66. T.A. Horbett and J.L. Brash (1987) in J.L. Brash and T.A. Horbett (Ed.), Protein at Interfaces: current Issues and future Prospects, American Chemical Society, Washinton,DC, pp. 1-33.
67. P.A. Cuyer, G.M. Willems, J.M.M. Kop, J.W. Corsel, M.P. Janssen and W.T. Hermens (1987) in J.L. Brash and T.A. Horbett (Ed.), Kinetics of Protein Sorption on Phospholipid Membranes Measured by Ellipsometry, American Chemical Society, Washinton, DC, pp. 208-221.
68. K. Ishihara, S. Ohta, T. Yoshikawa and N. Nakabayashi (1992) J. Polym. Sci. Part A: Polym. Chem. 30, 929-932.
69. V. Hlady, R.A. Van Wagenen and J.D. Andrade (1985) in J.D. Andrade (Ed.), Total Internal Reflection Intrinsic Fluorescence (TIRF) Spectroscopy Applied to Protein Adsorption Vol.2, Plenum Press, New York, NY, pp.81-119.
70. S. Cheifetz, M.A. Moscarello and C.M. Deber (1984) Arch. Biochem. Biophys. 233, 151-160.
71. F.C.H. Chou, C.H. Chou, R. Shapira and R.F. Kibler (1976) J. Biol. Chem. 251, 2671-2676.
72. M.J. Janiak, D.M. Small and G.G. Shipley (1979) J. Biol. Chem., 254, 6068-6078.
73. D.H. Thompson, K.F. Wong, R. Humphry-Baker, J. Wheeler, J-M. Kim and S.B. Rananavare, J. Amer. Chem. Soc., in press, 1992.
74. E.P. Bertin (1970) Principles and practice of X-ray spectrometric analysis, Plenum Press, New York, pp. 127.
75. D. Marsh (1990) CRC Handbook of Lipid Bilayers, CRC Press, Boca Raton, Fla., pp. 87.

76. G.H. Stout and L.H. Jensen (1968) X-ray Structure Determination, the Macmillan Company Collier-Macmillan Ltd., London, pp. 23.

77. P. Silberzan, L. Leger, D. Ausserre and J.J. Benattar (1991) Langmuir 7, 1647-1651.

78. V. Hlady (1991) Applied Spectroscopy 45, 246-252.

79. G. Cevc (1990) Biochim. Biophys. Acta 1031, 311-382.

80. H. Trauble and H. Eibl (1974) Proc. Natl. Acad. Sci. U.S.A., 214-219.

81. F. Jahnig, K. Harlòo, H. Vogel, and H. Eibl (1979), Biochemistry 18, 1459-1468.

82. A. Blume and H. Eibl (1979) Biochim. Biophys. Acta 558, 13-21.

83. P.H. Riegler (1987) Electrochemistry, Prentice-Hall Inc. Englewood Cliff, Ca, pp. 75.

84. F.B. Palmer, R.M.C. Dawson (1969) Biochem. J. 111, 629-636.

85. J.M. Boggs (1980) Can. J. Biochem. 58, 755-770.

86. R.V. McDaniel, A. McLaughlin, A.P. Winiski, M. Eisenberg and S. McLaughlin (1984) Biochemistry 23, 4618-4624.

87. A.P. Winiski, M. Eisenberg, M. Langner and S. McLaughlin (1988) Biochemistry 27, 386-392.

88. J.O'M. Bockris and A.K.N. Reddy (1970) Modern Electrochemistry, Plenum Press, New York, p. 157.